2038-5625

# Italian Journal of Agrometeorology

## Rivista Italiana di Agrometeorologia

n. 1 – 2025

# Italian Journal of Agrometeorology

**n. 1 - 2025**

Firenze University Press

The ***Italian Journal of Agrometeorology*** (***IJAm - Rivista Italiana di Agrometeorologia***) is the official periodical of the Italian Association of Agrometeorology (AIAM) and aims to publish original scientific contributions in English on agrometerology, as a science that studies the interactions of hydrological and meteorological factors with the agricultural and forest ecosystems, and with agriculture in its broadest sense (including livestock and fisheries).

https://riviste.fupress.net/index.php/IJAm
ISSN 2038-5625 (print) | ISSN 3103-1722 (online)

**Italian Association of Agrometeorology (AIAM)**
*Presidente:* Simone Orlandini (simone.orlandini@unifi.it)
*Vicepresidente:* Gabriele Cola
*Consiglieri:* Marina Baldi, Claudio Cassardo, Carmelo Maucieri, Federico Spanna, Danilo Tognetti, Leonardo Verdi
*Revisori dei conti:* Andrea Cicogna, Marco Secondo Gerardi, Emanuele Scalcione
*Segreteria:* Simone Falzoi, Emanuela Forni, Tiziana La Iacona, Mattia Sanna, Irene Vercellino
*e-mail AIAM:* segreteria@agrometeorologia.it
*Sede legale:* via Caproni, 8 - 50144 Firenze
*web:* www.agrometeorologia.it
*e-mail Italian Journal of Agrometeorology:* ijagrometeorology@agrometeorologia.it

**SUBSCRIPTION INFORMATION**
*IJAm* articles are freely available online, but print editions are available to paying subscribers. Subscription rates are in Eur and are applicable worldwide.
Annual Subscription: € 50,00 Single Issue: € 25,00

**CONTACT INFORMATION**
Please contact ordini@fupress.com, if you have any questions about your subscription or if you would like to place an order for the print edition. Information on payment methods will be provided after your initial correspondence.



Published by Firenze University Press

Firenze University Press
Università degli Studi di Firenze
via Cittadella, 7, 50144 Firenze, Italy
www.fupress.com

Italian Journal of Agrometeorology
Rivista Italiana di Agrometeorologia

Firenze University Press
https://riviste.fupress.net/index.php/IJAm

OPEN ACCESS

**Citation:** Deveci, H. (2025). Modeling the impact of climate change on the climatic suitability of some horticultural crops. *Italian Journal of Agrometeorology* (1): 3-17. doi: 10.36253/ijam-3064

**Received:** October 29, 2024

**Accepted:** June 20, 2025

**Published:** August 27, 2025



**Data Availability Statement:** All relevant data are within the paper and its Supporting Information files.

**Competing Interests:** The Author(s) declare(s) no conflict of interest.

**ORCID:**
HD: 0000-0002-0143-2185

# Modeling the impact of climate change on the climatic suitability of some horticultural crops

Huzur Deveci

*Tekirdağ Namık Kemal University, Vocational School of Technical Sciences, Tekirdağ, Türkiye*
Email: huzurdeveci@nku.edu.tr

**Abstract.** Summer and winter vegetable cultivation is widely practiced in Türkiye. Therefore, when unexpected situations such as wars and epidemics occur with climate change, it is important to accurately determine how the cultivation areas of vegetables, which have an important place in the food sector and agriculture, will change due to climate change. This study aimed to estimate how climate change would affect the geographical distribution of tomato, watermelon, onion, and cucumber to be planted in Türkiye in the future by using a climatic suitability model. For this purpose, climatic suitability estimation was done using the EcoCrop module included in the DIVA-GIS program for tomato, watermelon, onion, and cucumber under the results of the HADGEM2_ES model RCP4.5 and RCP8.5 scenarios in the future period (2050s) and the reference period (1950-2000) in Türkiye. The results of the research were evaluated, and it was determined that the climatic suitability for watermelon would be positively affected, while the climatic suitability for tomato, onion, and cucumber would be negatively affected in Türkiye. It is estimated that in the 2050s, climatically suitable areas for tomato (13–16%), onion (3–7%), and cucumber (4–12%) cultivation will decrease, while suitable areas for watermelon (26–35%) cultivation will increase. While it is estimated that Türkiye will fall further behind in tomato and onion production in the world rankings in the 2050s, the rankings for watermelon and cucumber will not change. The changes in production due to the decrease in climatic suitability for tomatoes and cucumbers and the increase in climatic suitability for watermelon will impact the economy. It is recommended that production be based on these estimates to maintain the diversity of vegetables on our tables in the future and to ensure the sustainability of these products.

**Keywords:** EcoCrop Model, DIVA-GIS, Türkiye, suitability, sustainability.

## 1. INTRODUCTION

Climate change is considered the biggest environmental disaster today, and its effects are increasing in the current period. Many studies conducted on a global and regional scale show that the adverse effects of climate change and variability on water, soil, and agricultural resources may become stronger in the future (Çaltı and Somuncu, 2019). Türkiye is among the risk group countries in terms of the effects of global warming (WBG, 2022). The nega-

tive impacts of climate change on the agricultural sector will indirectly affect the national economy. Therefore, the importance of mitigation and adaptation policies emerges once again (Temur, 2017).

Türkiye ranks fourth in the world in vegetable production (26.6 million tons), third in tomato production (13.0 million tons), second in watermelon (3.4 million tons) and cucumber (1.9 million tons) production, and sixth in onion production (2.4 million tons) (Table 1). When the data in Table 1 is evaluated, it is seen that tomato, watermelon, onion, and cucumber are among the vegetables with significant production amounts in the world. Additionally, Türkiye ranks high in the world in terms of cultivation. Therefore, it is very important to determine how vegetables, which have an important place in human nutrition, will be affected by climate change in the future.

Climate change affects cucumber and watermelon cultivation (Oyediran et al., 2018; Melo et al., 2020; Aparna et al., 2023). Litskas et al. (2019) stated that tomato cultivation will be negatively affected by climate change in Türkiye. Biratu (2018) expects that possible changes in the context of climate change, such as increased air temperature, changes in precipitation, long-term water scarcity, etc., will have a significant impact on tomato performance, which in turn will have a serious impact on food security. Hancı and Cebeci (2015) stated that the importance of abiotic stress factors emerged distinctively with global warming and that the most important abiotic factors in onion cultivation were salinity and drought. When these and other studies investigating the effects of climate change on these plants are evaluated, it is seen that precautions should be taken to adapt these plants to climate change.

The EcoCrop model was used to determine climatic suitability in the study. Initially, the EcoCrop database was created by the Food and Agriculture Organization (FAO) as a database containing plant characteristics and crop environmental requirements for more than 2000 plants (FAO, 2023). This database was integrated into DIVA-GIS by Hijmans et al. (2001) and named EcoCrop. The reason for choosing this model is primarily its high accuracy (Jarvis et al., 2012; Ramirez-Villegas et al., 2013). In addition, it can perform suitability analysis for many plant species in large areas over a long period. It is a great advantage that it can determine climatic suitability with high accuracy with limited data and contribute to agricultural production by providing important predictions. Ignoring other environmental factors can be considered a disadvantage. However, it is possible to diversify and develop studies by integrating environmental factors into these results.

Climatic suitability has been determined for various vegetables around the world (Egbebiyi et al., 2019; Egbebiyi et al., 2020; Gardner et al., 2021; Møller et al., 2021; Zagaria et al., 2023). In Türkiye, climatic suitability has been investigated in plants such as safflower, corn, millet, canola, wheat, cotton, spinach, and sunflower (Aydın and Sarptaş, 2018; Deveci, 2023; Deveci, 2024; Şen et al., 2024). Studies on climatic suitability estimation in Türkiye are quite limited. Therefore, to reduce the negative effects of climate change, such studies should be supported and increased by conducting trials in different regions with various models, especially with strategic plants. One of the most important features that distinguishes this study from other studies is that tomato, watermelon, onion, and cucumber, the most widely cultivated vegetables in Türkiye and the world, and occupy an important place in human nutrition, were selected and evaluated for climatic suitability. In recent years, research on the effects of climate change on horticultural crops has been frequently conducted in Türkiye, including the species examined in this study. However, this study is the first to address the spatio-temporal distribution of climatic suitability for these vegetables at the Türkiye level through modeling using climate change projections. It is also very significant in terms of ensuring diversity and sustainability.

**Table 1.** Vegetable and tomato, watermelon, cucumber, and onion production amounts and rankings in the world and Türkiye (2022) (WPR, 2024a; WPR, 2024b; WPR, 2024c; WPR, 2024d; WPR, 2024e).

| Vegetable Production (million tons) | Tomato (million tons) | Watermelon (million tons) | Onion (million tons) | Cucumber (million tons) |
|---|---|---|---|---|
| China (616) | China (68.2) | China (60.4) | India (31.7) | China (77.3) |
| India (145) | India (20.7) | Türkiye (3.4) | China (24.5) | Türkiye (1.9) |
| United States (27.1) | Türkiye (13.0) | India (3.3) | Egypt (3.7) | Russia (1.6) |
| Türkiye (26.6) | United States (10.2) | Algeria (2.0) | United States (2.9) | Mexico (1.1) |
| Vietnam (17.8) | Egypt (6.3) | Brazil (1.9) | Bangladesh (2.5) | Uzbekistan (0.9) |
| Nigeria (16.1) | Italy (6.1) | Russia (1.6) | Türkiye (2.4) | Ukraine (0.8) |

This study aims to estimate climatic suitability for tomato, watermelon, onion, and cucumber in Türkiye for the reference period (1950-2000) and future (2050s) according to the outputs of the HADGEM2_ES model RCP4.5 and RCP8.5 scenarios with the EcoCrop module in the DIVA-GIS program. In this context, the effects of temperature and precipitation, which are the most important factors for plant cultivation, on the areas where these vegetables can be planted have been tried to be revealed. When unforeseen situations arise with climate change, accurately estimating the areas where these vegetables, which have an important place in the agriculture and food sector, can be planted will guide producers and those working in this field while planning.

## 2. MATERIAL AND METHODS

### *2.1 Research area*

Türkiye is located between 26°-45° E longitude and in 36°-42° N latitude in the Northern Hemisphere. Its surface area is approximately 780000 km$^2$. 3% of Türkiye's surface area is in the European continent (Thrace) and 97% is in the Asian continent (Anatolia). Türkiye is bordered to the west by Bulgaria and Greece, to the east by Iran, Georgia, Armenia, Azerbaijan/Nahcivan, and to the south by Iraq and Syria (GDSHW, 2023). The research area and seven geographical regions in Türkiye are shown in Figure 1. According to the 2022 data of the Turkish Statistical Institute, Türkiye's total utilized agricultural land is 38501 thousand hectares. Cereals and other plant products are 16529 thousand hectares, vegetable gardens are 718 thousand hectares, ornamental plants are 6 thousand hectares, and fruits, beverages, and spice crops are 3671 thousand hectares. While meadow and pasture lands cover an area of 14617 thousand hectares, 2960 thousand hectares of land are left fallow (TurkStat, 2024a).

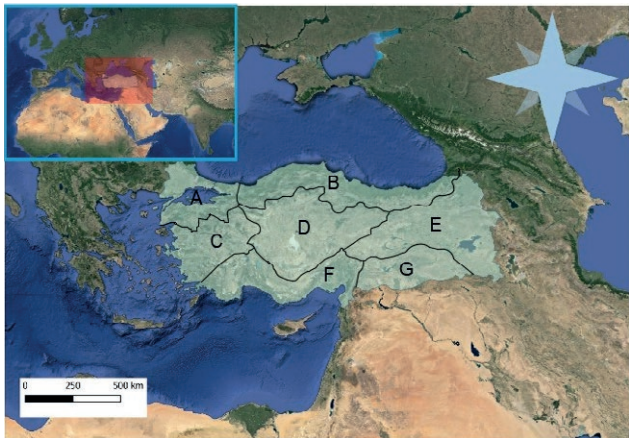


**Figure 1.** Türkiye map (A-Marmara Region, B-Black Sea Region, C-Aegean Region, D-Central Anatolia Region, E-Eastern Anatolia Region, F-Mediterranean Region, G- Southeastern Anatolia Region).

### *2.2 Climate of the research area*

Türkiye is located between the temperate zone and the subtropical zone. The fact that Türkiye is surrounded by seas on three sides, the extension of the mountains, and the diversity of landforms have led to the emergence of climate types with different characteristics. In the coastal regions of Türkiye, milder climate characteristics are observed with the effect of the seas. Continental climate characteristics are observed in the interior of Türkiye. Based on the criteria used in worldwide climate classifications, Türkiye has continental climate (Southeastern Anatolia Continental Climate, Eastern Anatolia Continental Climate, Central Anatolia Continental Climate, Thrace Continental Climate), Mediterranean climate, Marmara (transition) climate, and Black Sea climate (Atalay, 1997). According to long-term (1970-2024) climate data averages for Türkiye, average maximum temperature is 19.2 °C (TSMS, 2023a), average minimum temperature is 7.9 °C (TSMS, 2023b), average mean temperature is 13.3 °C (TSMS, 2023c), average annual total precipitation is 593.3 mm (TSMS, 2023d), average relative humidity is 63.5% (TSMS, 2023e).

### *2.3 Climate model and scenarios used in the research*

HadGEM2 is a second-generation global model developed by the Hadley Center, a research organization of the United Kingdom Meteorological Service, and stands for Global Environment Model Version 2. There are many versions of this model with similar physical properties but in different configurations. The HadGEM2 series includes a coupled atmosphere-ocean configuration and an Earth system configuration that includes dynamic vegetation, ocean biology, and atmospheric chemistry (Collins et al., 2011; Gündoğan et al., 2017), while the HadGEM2-ES version includes terrestrial carbon cycle, chemistry, ocean biochemistry, ocean and sea ice, troposphere, aerosols, land surface, and hydrology configuration(Martin et al., 2011).

In 2007, the Intergovernmental Panel on Climate Change (IPCC) Experts Meeting in the Netherlands defined four Representative Concentration Pathways (RCPs) for characteristics and radiative forcing levels and pathways. RCP4.5 used in the study is the medi-

um stabilization path and assumes that radiative forcing stabilizes at 4.5 W/m$^2$ between 2100 and 2150. The other scenario in the study, RCP8.5, is the high radiative forcing and concentration path (Moss et al., 2008; Gündoğan et al., 2017).

### *2.4 Crop suitability model: EcoCrop*

EcoCrop within DIVA-GIS only considers monthly precipitation and temperature to determine plant suitability (Hijmans et al., 2001; Hijmans et al., 2005). The parameters used by EcoCrop are minimum length of growing season (Gmin), maximum length of growing season (Gmax), killing temperature during rest (KTmp), minimum temperature (Tmin), the maximum optimum temperature (TOPmax), minimum optimum temperature (TOPmn), maximum temperature (Tmax), minimum precipitation (Rmin), maximum precipitation (Rmx), minimum optimum precipitation (ROPmn), and maximum optimum precipitation (ROPmx). The model gives suitability maps according to suitability index values as output. The suitability index varies between 0 and 100 in EcoCrop (Ramirez-Villegas et al., 2013). EcoCrop's working logic and the method of calculating the suitability index have been explained in detail with formulas and graphs by many researchers (Ramirez-Villegas et al., 2013; Wichern et al., 2019; Joshi, 2021; Labaioui and Bouchoufi, 2021). The classifications are as follows in EcoCrop: 0% is not-suited, 1–20% is very marginal, 21–40% is marginal, 41–60% is suitable, 61–80% is very suitable, and 81–100% is excellent. The EcoCrop parameters for tomato, watermelon, onion, and cucumber are shown in Table 2 (FAO, 2023).

### *2.5 Method*

In this study, climatic suitability maps were generated for four different vegetables (tomato, watermelon, onion, and cucumber), which play a significant role in human nutrition. Since the climatic suitability maps were modeled for four crops, it was thought that it would be more appropriate to use only one climate model (HadGEM2_ES model, the most comprehensive version of the HadGEM2 series) and two scenarios (RCP4.5 and RCP8.5) due to the high plant diversity. There are many reasons why the HadGEM2_ES model RCP4.5 and RCP8.5 scenarios are preferred. Firstly, climate predictions have been made using these models and scenarios in Türkiye (Akçakaya et al., 2013; Akçakaya et al., 2015; GDWM, 2016). This is very important in terms of comparability. Moreover, it was also determined that the HadGEM2_ES model produced highly accurate estimates of temperature data (Deveci, 2025). The scenarios used in this research were RCP scenarios within the scope of AR5. As is well known, RCP scenarios directly consider radiative forcing and are classified according to the energy balance that will be achieved by 2100. These scenarios are simple to implement and are compatible with the contents of CMIP5 (Coupled Model Intercomparison Project Phase 5) and CMIP6 (Coupled Model Intercomparison Project Phase 6). RCP scenarios are currently employed by many researchers, particularly in conjunction with SSP (Deveci et al., 2025; Dokuyucu et al., 2025; Duvan et al., 2025; Khazaei, 2025; Zhang et al., 2025).

The schematic representation of the method applied in the research is given in Figure 2. The climate data file, consisting of climate data covering the reference period (1950-2000), was obtained from the DIVA-GIS website (DIVAGIS, 2023). Future period (2050s) data obtained

**Table 2.** Growth threshold for tomato, watermelon, onion, and cucumber crops according to the EcoCrop model (FAO, 2023).

| Crop growth thresholds | Units | EcoCrop Parameters | | | |
|---|---|---|---|---|---|
| | | Tomato | Watermelon | Onion | Cucumber |
| Killing temperature (KTmp) | °C | 0 | 0 | 0 | 0 |
| Minimum temperature (Tmin) | °C | 7 | 15 | 4 | 6 |
| Minimum optimum temperature (TOPmn) | °C | 20 | 20 | 12 | 18 |
| Maximum optimum temperature (TOPmax) | °C | 27 | 30 | 25 | 32 |
| Maximum temperature (Tmax) | °C | 35 | 35 | 30 | 38 |
| Minimum length of the growing season (Gmin) | days | 70 | 80 | 85 | 40 |
| Maximum length of the growing season (Gmax) | days | 150 | 160 | 175 | 180 |
| Minimum precipitation (Rmin) | mm | 400 | 400 | 300 | 400 |
| Minimum optimum precipitation (ROPmn) | mm | 600 | 500 | 350 | 1000 |
| Maximum optimum precipitation (ROPmx) | mm | 1300 | 750 | 600 | 1200 |
| Maximum precipitation (Rmx) | mm | 1800 | 1800 | 2800 | 4300 |

from HADGEM2_ES global climate model RCP4.5 and RCP8.5 scenario outputs were downloaded from the GCM Downscaled Data Portal website (CCAFS, 2023). In this study, crop growth thresholds were obtained from EcoCrop (Table 2). Climatic suitability indexes for tomato, watermelon, onion, and cucumber in Türkiye for the reference and future periods were calculated with the EcoCrop module in DIVA-GIS 7.5 software. The working principle of the EcoCrop model is explained below (Ramirez-Villegas et al., 2013).

- The duration of the crop's growing season is defined. The length of the growing season is the average of the minimum and maximum days specified in the crop cycle. Here, the calculation is made by assuming that each month is potentially the first month of the crop's growing season for 12 months separately.
- The temperature suitability percentage is found. It is calculated for each month. It is the minimum value of all 12 potential growing seasons ($T_{SUIT}$).
- The rainfall suitability percentage is found. It is calculated for each growing season ($R_{SUIT}$).
- After calculating temperature and precipitation suitability, total suitability is obtained by multiplying these two values (Equation 1).

$$SUIT = T_{SUIT} * R_{SUIT} \quad (1)$$

SUIT: Suitability
$T_{SUIT}$: Temperature suitability
$R_{SUIT}$: Rainfall suitability

Then, reference and future period maps were created in DIVA-GIS 7.5 according to the calculated suitability indices. In the last stage, these maps were transferred to QGIS version 3.28, analyzed, and evaluated. QGIS, also known as Quantum GIS, was preferred because it is an open-access, free, and continuously updated software. With this software, mapping, data analysis, and editing layers can be done, and vector and raster data types can be used and processed. It is also possible to find many details, such as geographic coordinate systems, symbols, labels, and data analysis tools in this software (QGIS, 2023).

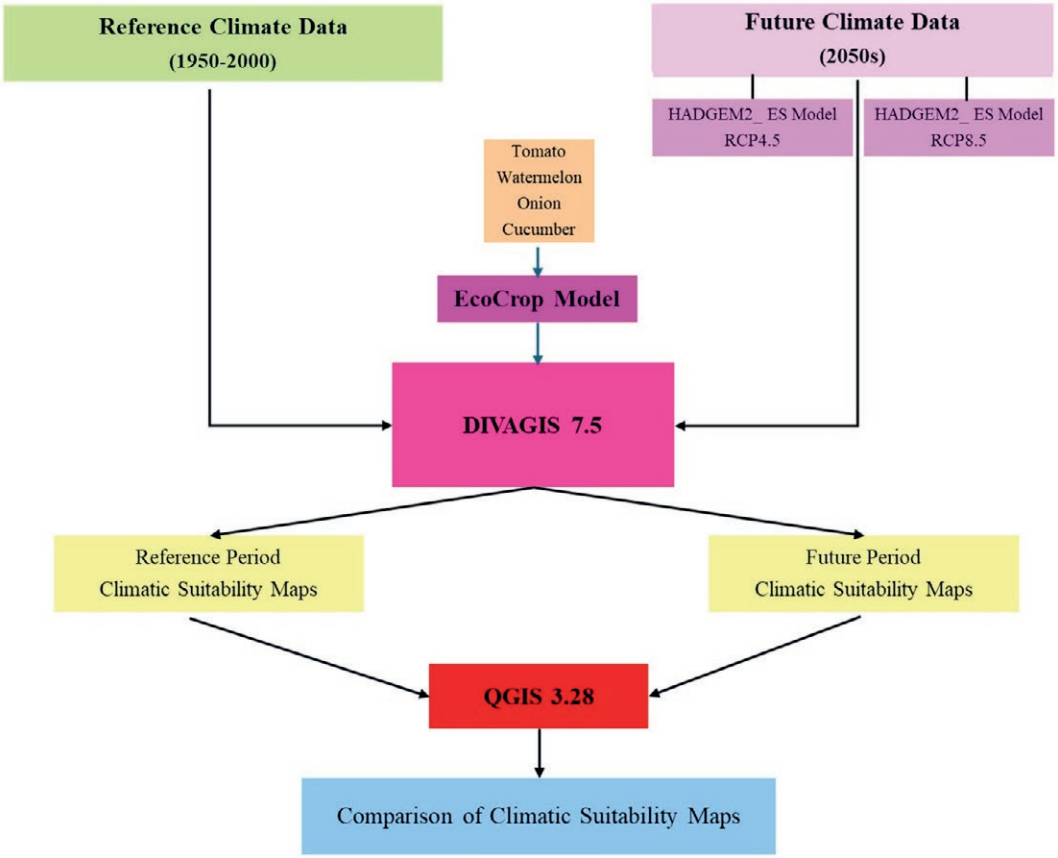


**Figure 2.** Schematic representation of the method applied in the research.

## 3. RESULTS

The climatic suitability obtained for reference and future periods for tomato, watermelon, onion, and cucumber is presented in Figure 3. When reference and future period climatic suitability results for tomato were evaluated, it was determined that not suited and marginal areas increased in both scenarios, and suitable, very suitable, and excellent areas decreased in both scenarios according to the reference period. In the 2050s, very marginal areas increased in the HADGEM2_ES model RCP8.5 and decreased in RCP4.5. In watermelon, in both scenarios, very suitable and excellent areas increased, while unsuitable, very marginal, and marginal areas decreased. Suitable areas increased to RCP8.5 and decreased to RCP4.5 compared to the reference period. When the climatic suitability results for onion were evaluated in the 2050s, it was determined that the excellent areas decreased in both scenarios compared to the reference period, while all other areas (unsuitable, very marginal, marginal, suitable, and very suitable areas) increased. In the future, in cucumber, while not suited and excellent areas increased in both scenarios, marginal, suitable, and very suitable areas decreased. Very marginal areas decreased to RCP4.5 and increased to RCP8.5 compared to the reference period.

Climatical suitable and unsuitable areas for tomato, watermelon, onion, and cucumber cultivation in Türkiye are shown in Figure 4. It is estimated that the areas suitable for tomato cultivation in Türkiye will decrease in RCP4.5 and RCP8.5. This decrease will be greater in the RCP4.5 scenario. For watermelon, it is estimated that suitable areas will increase, and unsuitable areas will decrease in RCP4.5 and RCP8.5, respectively. In contrast, the opposite is true for onions. In other words, in the RCP4.5 and RCP8.5 scenarios, climatic unsuitable areas are expected to increase while suitable areas are expected to decrease, respectively. It can also be said that these increasing and decreasing rates will not change much. For cucumber, it is predicted that suitable areas will decrease, with a further decrease in RCP4.5.

HADGEM2_ES model reference period (1950-2000) and future period (2050s) climatic suitability maps for tomato, watermelon, onion, and cucumber cultivation in Türkiye are given in Figure 5. When the climatic suitability maps for tomato cultivation in Türkiye were evaluated, it was seen that the unsuitable areas in the Central Anatolia Region increased in the 2050s. This increase was estimated to be greater at RCP4.5. According to the reference period, it has been determined that tomato

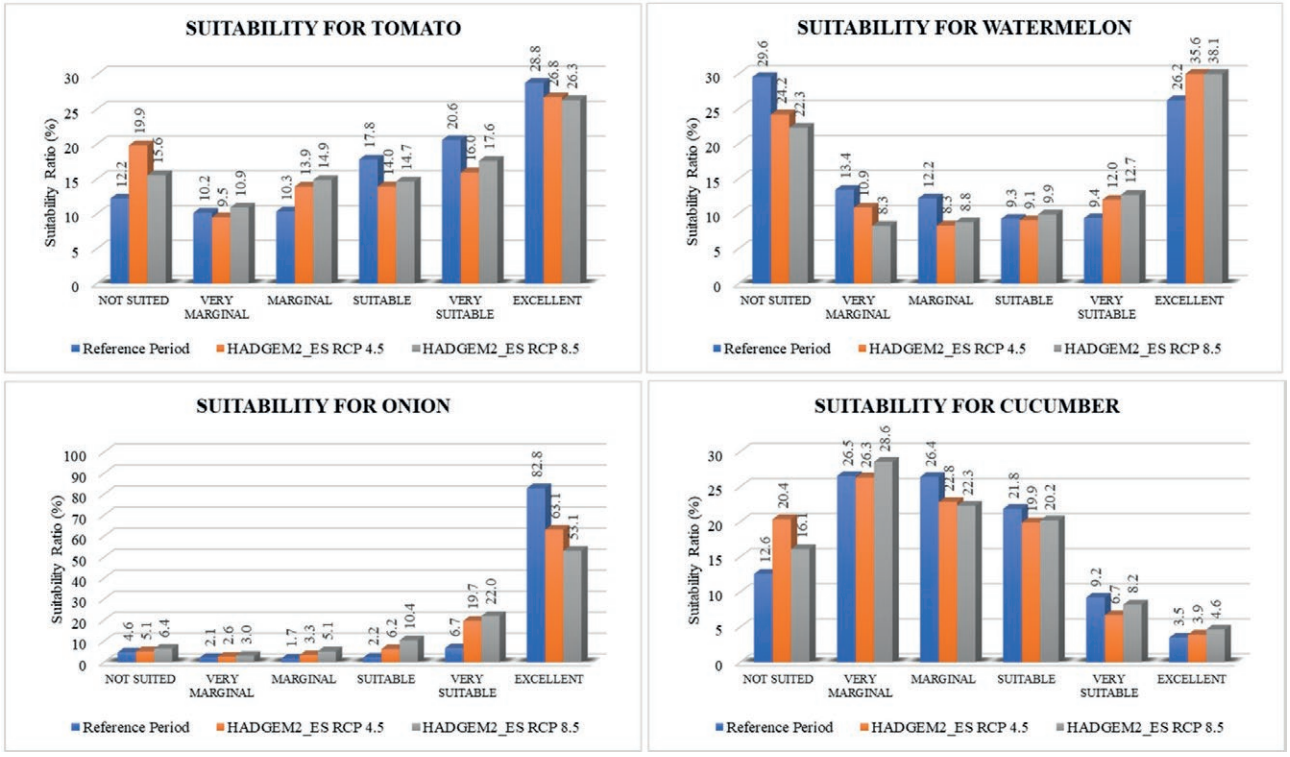


**Figure 3.** Climatic suitability of tomato, watermelon, onion, and cucumber under the RCP4.5 and RCP8.5 according to the HADGEM2_ES model for the reference period (1950-2000) and the future period (2050s).

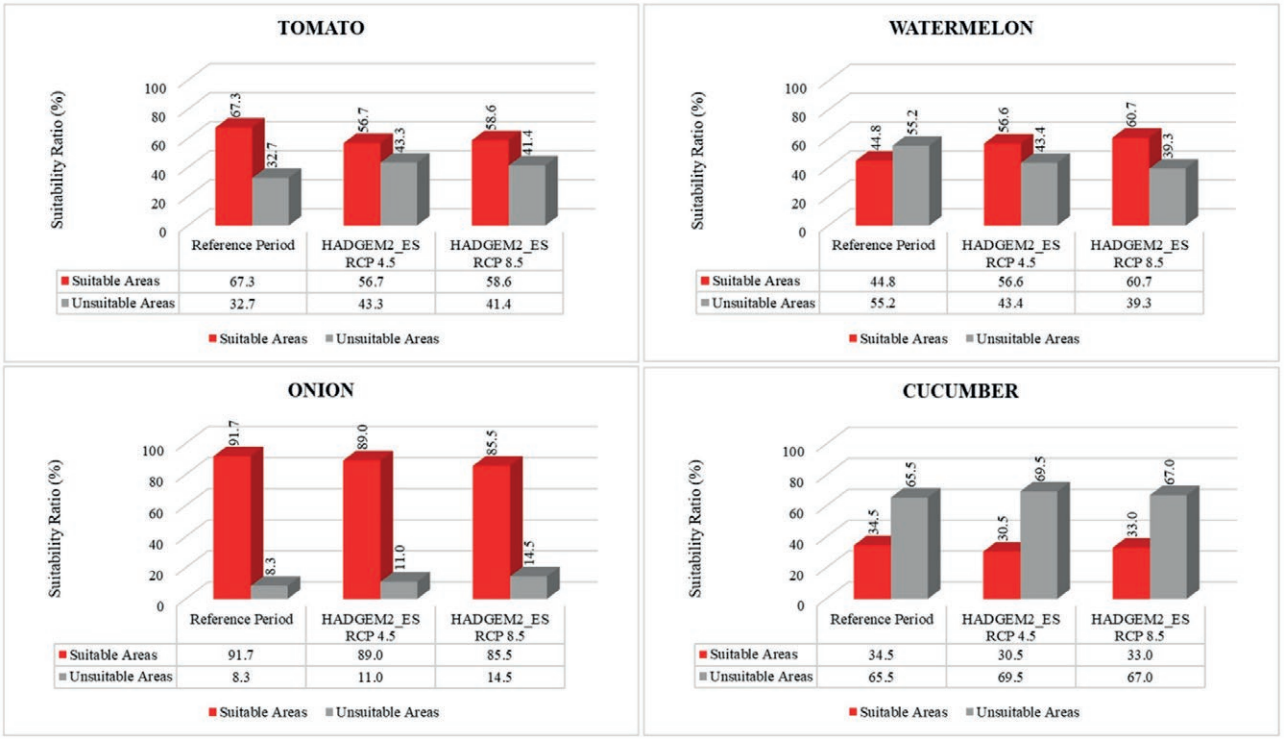


**Figure 4.** Comparison of climatic suitable and unsuitable areas for tomato, watermelon, onion, and cucumber under the RCP4.5 and RCP8.5 according to the HADGEM2_ES model for the reference period (1950-2000) and future period (2050s).

cultivation areas in the Black Sea Region will expand and become more suitable areas in the future. While unsuitable areas in the northeast of Türkiye turn into more suitable areas in the future, on the contrary, it was understood that the suitability of suitable areas in the southeast of Türkiye will decrease in future estimates. Another important change is that while tomato cultivation could be done in southern latitudes in the reference period, there will be a shift towards northern latitudes in 2050 due to the effect of climate change.

When the climatic suitability maps for watermelon cultivation in Figure 5 are evaluated, it is determined that the unsuitable areas in the north of Türkiye will become more suitable in the RCP4.5 and RCP8.5 scenarios, respectively. In the southeast, it is estimated that the suitable areas will gradually become unsuitable, and this situation will be more pronounced in RCP8.5. It is understood that the suitable areas will expand in the west of Türkiye. Here, the transformation of watermelon cultivation, which can be done intensively in the Southeastern Anatolia Region, into unsuitable areas in the 2050s has emerged as an important change.

In Türkiye, it is estimated that the areas that were not suitable for onion cultivation in the reference period will become more suitable in the future in both scenarios (Figure 5). In Figure 5A, it is determined that while a small area in the Central Anatolia Region is marginal, these areas will turn into unsuitable areas in the future in both scenarios. It is estimated that a part of the southeastern side, which was suitable in the reference period, will turn into marginal, very marginal, and unsuitable areas in the future. A particularly striking situation is that the onion, whose homeland is Western Asia, has shown excellent climatic suitability in most parts of Türkiye and has adapted well.

Climatic suitability maps for cucumber cultivation are evaluated in Figure 5. In the reference period, there are unsuitable areas in Central Anatolia, Northeastern Anatolia, and Southeastern Anatolia, which are shown as gray. These unsuitable areas are predicted to expand further in the future in the HADGEM2_ES model RCP4.5 and RCP8.5 scenarios (Figure 5B, Figure 5C). In the RCP8.5 scenario, it is determined that climatic suitability for cucumber cultivation will increase in the Black Sea Region compared to the reference period. In the reference period, it is predicted that the unsuitable gray areas in the north will shift to the east of Türkiye in the 2050s.

The change of suitable and unsuitable areas for tomato, watermelon, onion, and cucumber cultivation in Türkiye in the 2050s compared to the reference

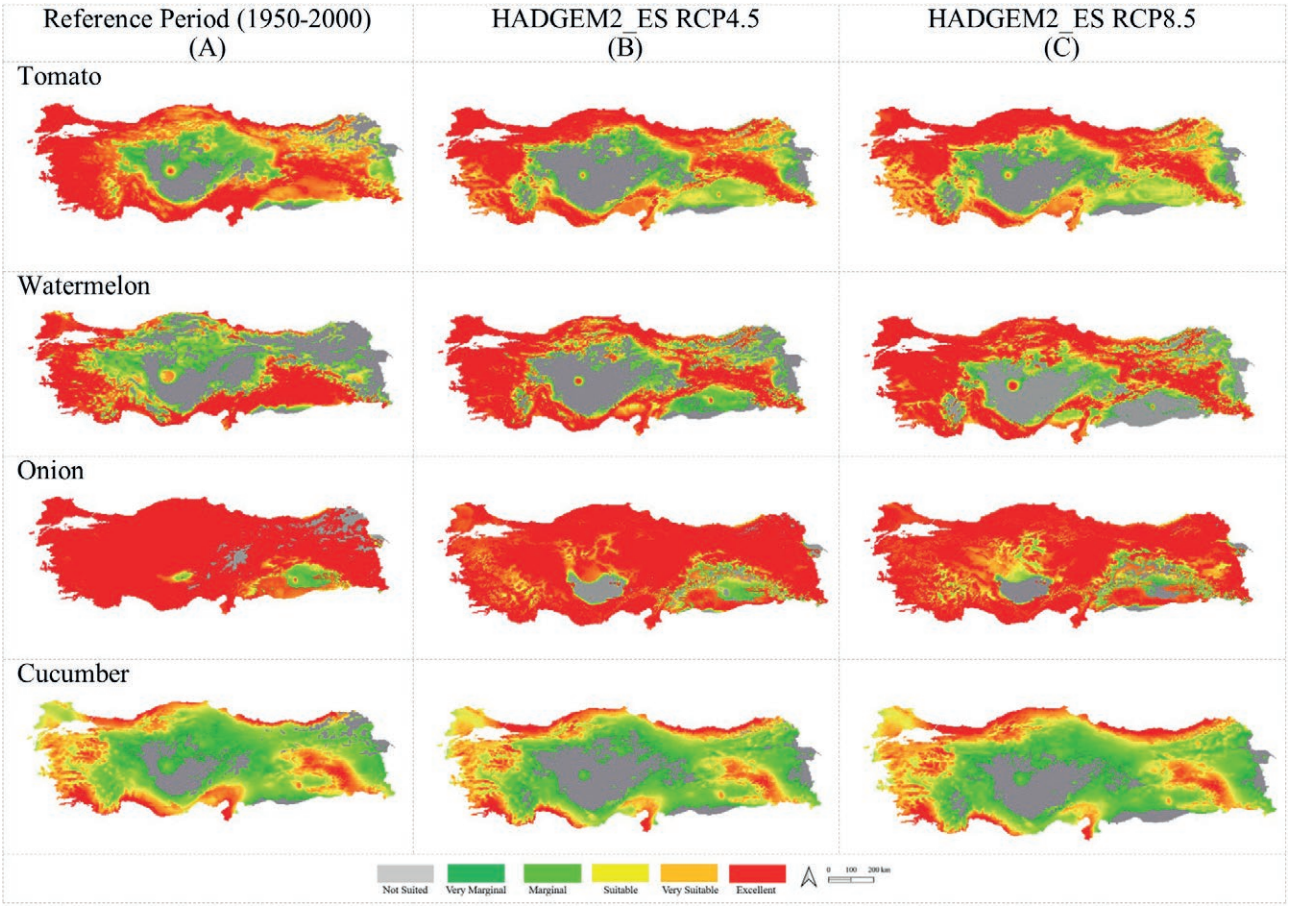


**Figure 5.** Climatic suitability maps for the reference period (A), HADGEM2_ES RCP4.5 scenario (B), and HADGEM2_ES RCP8.5 scenario (C).

**Table 3.** Change in suitable and unsuitable areas in the reference period (1950-2000) and future periods (HADGEM2_ES model RCP4.5 and HADGEM2_ES model RCP8.5 in the 2050s).

| Areas | Vegetables | Reference Period | HADGEM2_ES Model | | Deviation from Reference Period | |
|---|---|---|---|---|---|---|
| | | | RCP 4.5 | RCP 8.5 | RCP 4.5 (%) | RCP 8.5 (%) |
| Suitable Areas | Tomato | 67.3 | 56.7 | 58.6 | -16 | -13 |
| | Watermelon | 44.8 | 56.6 | 60.7 | 26 | 35 |
| | Onion | 91.7 | 89.0 | 85.5 | -3 | -7 |
| | Cucumber | 34.5 | 30.5 | 33.0 | -12 | -4 |
| Unsuitable Areas | Tomato | 32.7 | 43.3 | 41.4 | 32 | 26 |
| | Watermelon | 55.2 | 43.4 | 39.3 | -21 | -29 |
| | Onion | 8.3 | 11.0 | 14.5 | 32 | 74 |
| | Cucumber | 65.5 | 69.5 | 67.0 | 6 | 2 |

period in line with the HADGEM2_ES model RCP4.5 and RCP8.5 scenarios is summarized in Table 3. In the 2050s, suitable areas for tomato cultivation are projected to decrease by (13%-16%) and unsuitable areas are projected to increase by (26%-32%); suitable areas for onion cultivation are projected to decrease by (3%-7%) and unsuitable areas are projected to increase by (32%-74%); suitable areas for cucumber cultivation are projected to decrease by (4%-12%) and unsuitable areas are projected to increase by (2%-6%); suitable areas for watermelon cultivation are projected to increase by (26%-35%) and unsuitable areas are projected to decrease by (21%-29%). In general, it is estimated that watermelon cultivated areas will be positively affected, and tomato, onion, and cucumber cultivated areas will be negatively affected by the possible climate change in the 2050s.

## 4. DISCUSSION

In this study, when comparing the change in climatic suitability for tomato, watermelon, onion, and cucumber growing areas in Türkiye during the 2050s with the reference period (1950-2000), it was determined that cli-

matic suitability for tomato, onion, and cucumber would be negatively impacted, while climatic suitability for watermelon would be positively impacted. It is estimated that in the 2050s, climatically suitable areas for tomato (13%-16%), onion (3%-7%), and cucumber (4%-12%) cultivation will decrease, while suitable areas for watermelon (26%-35%) cultivation will increase.

Türkiye is among the countries that will be affected by climate change (WBG, 2022). Therefore, there are important studies on climate change prediction in the research area (Dalfes et al., 2008; GDWM, 2016). Deveci (2023) modeled climate change in Türkiye during the 2050s with the HADGEM2_ES model under the RCP4.5 and RCP8.5 scenarios. This study overlaps with the current research in terms of the model used, scenarios, and selected period range. According to Deveci (2023), while the average temperature data was 10.8 °C for the reference period (1950-2000), it was estimated to be 13.9 °C in the HADGEM2_ES model RCP4.5 scenario and 14.8 °C in the HADGEM2_ES model RCP8.5 scenario in the 2050s. While the average annual precipitation data was 594 mm for the reference period (1950-2000), it was estimated to be 560 mm in the HADGEM2_ES model RCP4.5 scenario and 573 mm in the HADGEM2_ES model RCP8.5 scenario in the 2050s. In the HADGEM2_ES model RCP4.5 scenario, the temperature increase was 3.1 °C, and the highest precipitation decrease reached 34 mm. In the RCP8.5 scenario, although the temperature increase was 4 °C, precipitation throughout Türkiye did not decrease as much as in the RCP4.5 scenario (only 21 mm) (Deveci, 2023). This situation was interpreted as the temperatures will increase and precipitation will decrease in the research area in the 2050s.

In Türkiye, temperature increases have negatively affected tomato cultivation and caused tomato planting areas to decrease. Rhiney et al. (2018) found that tomatoes would be negatively affected by a 1.5 °C temperature increase on the Caribbean Island of Jamaica, while Egbebiyi et al. (2019) determined that tomatoes would be negatively impacted by decreased rainfall associated with a 1-4.5 °C temperature increase in West Africa. In Türkiye, tomato cultivation was possible in the southern latitudes during the reference period, but with the impact of climate change, there is a shift to northern latitudes. Both studies were conducted in a region in the south, which was hot according to the climate of Türkiye. As the region in the south gets even hotter, the appropriate temperatures for tomato are exceeded, and tomato cultivation areas are negatively influenced by the temperature. The reason for the increase in tomato cultivation areas in the north of Türkiye (Black Sea Region) in the future is that the region, which is currently cool in terms of tomato cultivation, will become more suitable for tomato cultivation with the increase in temperature averages in the future. Similarly, it was observed that the south of Türkiye (Southeastern Region) is very suitable for tomato cultivation currently. In the forecasts for the future, it was estimated that the areas suitable for tomato cultivation would decrease in both scenarios due to the further increase in temperature and decrease in precipitation in these regions, which are already the hottest in the country, and would turn into not suited, marginal, and very marginal areas. The occurrence of this situation is considered normal. The results of this study are consistent with Rhiney et al. (2018) and Egbebiyi et al. (2019) show similar results. Saadi et al. (2015) found in their study in the Mediterranean that changes in precipitation will affect tomato cultivation less. Therefore, since it was observed that temperature changed more than precipitation in the research area, this study also confirms the results.

Climate change affects watermelon cultivation (Stewart and Ahmed, 2020; Walters et al., 2021). Watermelon does not like cool temperatures and is extremely sensitive to frost (Şalk et al., 2008; Kumar and Reddy, 2021). Watermelon is a plant species that can adapt to arid conditions and is suitable for tolerating the water it contains, as well as being a high-yielding species under irrigated conditions (Yokota et al., 2002). There is a positive relationship between the climate requirements required to cultivate watermelon and the climate change estimation results given by the climate change estimation model in the study. In the Inner Aegean Region and Central Anatolia Region of Türkiye, the higher temperatures compared reference period caused more suitable conditions for watermelon cultivation, and it was estimated that watermelon cultivation areas in these regions would be positively impacted by possible climate change. Contrary to this situation, in the future, watermelon production will decrease or even become impossible in regions where the optimum temperature required for watermelon cultivation is exceeded (Southeast Anatolia Region) due to increasing temperatures. This situation is slightly different in the Black Sea Region. In this region, the reference period is cool and very rainy. It is estimated that watermelon cultivation will be more significantly positively affected by climate change in the HADGEM2_ES RCP8.5 map. The reason for this is that the temperature has increased more in the HADGEM2_ES model RCP8.5 scenario than in the HADGEM2_ES model RCP4.5 scenario. It is estimated that the climatic suitability for watermelon will increase, although it varies regionally in Türkiye.

In the research, it was predicted that there would be changes in suitable areas in the climatic suitability maps for onion, that is, they would turn into unsuitable areas. It is thought that this is because the necessary climatic growing conditions for onion in Türkiye have been exceeded. Simões et al. (2022) stated that an increase in temperature may cause a decrease in the production of onion varieties, and Brewster (2018) stated that temperature is an important determinant of onion growth duration and yield. Additionally, according to Rao (2016), water is the primary limiting factor in reducing onion yield. Therefore, the results of this study on estimating the effect of climate change on onion cultivation showed that onion, as a cool climate vegetable, was negatively affected by the increase in temperature and decrease in precipitation, by the results given by the above researchers for onion cultivation conditions. In the HADGEM2_ES RCP4.5 and RCP8.5 scenarios, the increase in temperature created not suited areas, especially in the Central Anatolia region, while it caused the areas to become suitable in the Eastern Black Sea Region. Wurr et al. (1998) suggested that a warmer climate would be advantageous for producing onions in Britain. This result contrasts with the results of the study estimated for Türkiye. This situation can be explained as follows. Because Türkiye is located further south, the climate is more suitable for onion cultivation. With the increase in temperature, onion cultivation will be disrupted as cool climate conditions will turn to hot climate, while more favorable conditions will be created for onion seed production.

Cucumber is one of the oldest cultivated and most widely grown vegetable species and is grown in almost all countries of the temperate belts (Tatlıoglu, 1993). Temperature, relative humidity, and radiation are the main climatic parameters that significantly impact cucumber growth and yield (Singh et al., 2017). Constantly changing temperature is an important factor for the growth, development, and yield of cucumber. Higher temperature in both air and soil reduces overall growth by affecting various physiological processes, such as reduced rate of photosynthesis and increased transpiration rate (Li et al., 2014; Ding et al., 2016). The annual water consumption of the cucumber plant is 400-650 mm. Cucumber is very sensitive to water. It is desired that the root area is always moist (Cemek et al., 2005). When these conditions are evaluated, it is understood that cucumber is negatively impacted by temperature increase and is sensitive to water. The fact that cucumber will be negatively influenced by the increase in temperatures and decrease in precipitation in the 2050s in Türkiye is in line with these studies. According to the results of this study, it was concluded that cucumber would be negatively impacted in the 2050s due to changes in growing temperature and water requirement, according to possible climate change prediction results. The change in cucumber cultivation in the future with climate change is less affected than the other vegetables (tomato, watermelon, onion), according to the research. Because when Table 3 is analyzed, it is estimated that there will be changes in both unsuitable areas (6%-2%) and suitable areas (12%-4%) in the HADGEM2_ES model future periods compared to reference periods. Therefore, the lowest rates of change are observed in cucumber.

In the research, the decrease in suitable areas with the effect of possible climate change on tomato cultivation in Türkiye also shows that its contribution to the country's economy will decrease in economic terms. There will be deficiencies in human nutrition in terms of the nutritional values given by tomato after the decrease in the cultivation areas of tomato, which is very common on the tables. Tomatoes, which are easily accessible and found on every table today, will become difficult to purchase and obtain due to geographical and climatic reasons. According to TurkStat (2024b), Türkiye's tomato production, which exceeds 85 million population by 2024, ranks third in the world (Table 1). With the possible climate change in the 2050s, it is estimated that Türkiye will fall further in the world ranking. This will have a negative economic impact not only on the Turkish economy but also on the tomato market in the countries where Türkiye produces and exports tomatoes. Türkiye ranks second after China in watermelon production. It is estimated that watermelon production in Türkiye will increase further with the positive effect of climatic suitability. However, it is estimated that this increase will not cause a significant change in the ranking since there is a huge difference in production between China (60.4 million tons) and Türkiye (3.4 million tons) (Table 1). It is thought that this expected increase in watermelon production will have a positive impact first in Türkiye and then in the world regarding both the economy and human nutrition. It is estimated that Türkiye, which ranks sixth in the world in onion production in Table 1, will remain in the same rank or fall to a lower rank. This is because it is predicted to be adversely affected by climate change (especially temperature increases), likely to occur in the 2050s. Since the production amount of onion, which has a large place in food preparation in the world and Türkiye and is in high demand, will decrease due to the negative impact on its cultivation in Türkiye, it will be used less in human nutrition and the onion market will be impacted economically, as in the case of tomatoes. As the climatic suitability of cucumber in Türkiye decreases, the amount of production will decrease,

and the economy of Türkiye will be negatively affected by this situation. Türkiye, which ranks second in the world in terms of cucumber production, is expected to maintain its position between China and Russia in the world ranking since it is estimated that there will not be a dramatic increase in unsuitable areas.

There may be some possible limitations in this study. One of these limitations is the lack of previous research studies on this topic. This study is the first to address the spatio-temporal distribution of climatic suitability for these vegetables at the level of Türkiye through modelling using climate change projections. Therefore, it has been difficult to compare and consider all aspects of the research. The EcoCrop model only takes into account the effects of temperature and precipitation when modeling climate suitability. However, there are many environmental factors that affect cultivation. Determining climatic suitability by considering the effects of climate change, topography of the land, soil temperature and soil type, soil quality, and water availability, etc., will provide a more comprehensive picture. Perhaps, in a region that is climatically suitable, it will be difficult to cultivate that plant because there is no water, or it will not be possible to cultivate that plant. In addition, even if it is not suitable for that region to cultivate any plant due to the structure of the land, it may be classified as very suitable on maps. Diversifying research with current scenarios will be useful in understanding the effects of climate change. If similar maps can be obtained with different scenarios, the predictions can be verified, and if other results are obtained, the reasons for the differences can be investigated and evaluated. In addition, the lack of a recent suitability classification study for these plants to calibrate the model is another limitation of the study.

## 5. CONCLUSIONS

The research predicts that, in the future, watermelon and tomato cultivation areas are predicted to decrease in the south and increase in the north of Türkiye, while cucumber and onion cultivation areas are expected to vary regionally. Alternative crops should be encouraged instead of these crops in regions where production decreases due to climate change. There is a generally negative trend in tomato, onion, and cucumber cultivation in Türkiye. It was observed that especially the increase in temperatures and the decrease in precipitation, even if slightly, were effective in this negative trend. The differentiated impact of climate change on the cultivation areas (positively affecting watermelon, while negatively impacting tomato, onion, and cucumber) highlights the complex nature of climate change effects on agriculture. To understand this complex structure, such studies need to be diversified with different models, different scenarios, and different periods. While it is estimated that Türkiye will fall further behind in tomato and onion production in the world rankings in the 2050s, the rankings for watermelon and cucumber will not change. The changes in production due to the decrease in climatic suitability for tomatoes and cucumbers and the increase in climatic suitability for watermelon will impact the economy. It is important to estimate and evaluate the future cultivation areas of these plants, which have a very important place in nutrition in the world and Türkiye, and to direct the future.

## AUTHOR CONTRIBUTIONS

Huzur Deveci: Conceptualization, Methodology, Software, Investigation, Resources, Data curation, Writing – original draft, Writing – review & editing, Visualization.

## REFERENCES

Akçakaya A., Eskioğlu O., Atay H., Demir Ö., 2013. Climate Change Projections for Türkiye With New Scenarios. Meteorology General Directorate Printing House, Türkiye. https://mgm.gov.tr/FILES/iklim/IKLIM_DEGISIKLIGI_PROJEKSIYONLARI.pdf

Akçakaya A., Sümer U.M., Demircan M., Demir Ö., Atay H., Eskioğlu O., Gürkan H., Yazıcı B., Kocatürk A., Şensoy S., Bölük E., Arabaci H., Açar Y., Ekici M., Yağan S., Çukurçayir F., 2015. Türkiye Climate Projections with New Scenarios and Climate Change TR2015-CC. https://www.mgm.gov.tr/FILES/iklim/iklim-degisikligi-projeksiyon2015.pdf

Aparna A.S., Pląder W., Pawełkowicz M., 2023. Impact of climate change on regulation of genes involved in sex determination and fruit production in cucumber. Plants, 12 (14): 2651. https://doi.org/https://doi.org/10.3390/plants12142651

Atalay İ., 1997. Geography of Türkiye. Ege University Publications, İzmir, Türkiye.

Aydın F., Sarptaş H., 2018. The impact of the climate change to crop cultivation: the case study with model crops for Turkey. Pamukkale University Journal of Engineering Sciences, 24 (3): 512-521. https://doi.org/10.5505/pajes.2017.37880

Biratu W., 2018. Review on the effect of climate change on tomato (Solanum Lycopersicon) production in

Africa and mitigation strategies. Journal of Natural Sciences Research, 8 (5): 2225-0921.

Brewster J.L., 2018. Physiology of Crop Growth and Bulbing, Onions and Allied Crops, CRC press. pp. 53-88. https://doi.org/https://doi.org/10.1201/9781351075169-3

CCAFS 2023. GCM Downscaled Data Portal. Climate change agriculture and food security. https://www.ccafs-climate.org/

Cemek B., Apan M., Demir Y., Kara T., 2005. Effects of different irrigatin water applications on growth, development and yield of cucumber grown in greenhouse. Anadolu Journal of Agricultural Sciences, 20 (3): 27-33.

Collins W.J., Bellouin N., Doutriaux-Boucher M., Gedney N., Halloran P., Hinton T., Hughes J., Jones C.D., Joshi M., Liddicoat S., Martin G., O'Connor F., Rae J., Senior C., Sitch S., Totterdell I., Wiltshire A., Woodward S., 2011. Development and evaluation of an Earth-System model – HadGEM2. Geoscientific Model Development, 4 (4): 1051-1075. https://doi.org/https://doi.org/10.5194/gmd-4-1051-2011

Çaltı N., Somuncu M., 2019. The impact of climate change on agriculture in Turkey and farmers' ttitudes to climate change, 1st Istanbul International Geography Congress Proceedings Book, İstanbul, Türkiye. pp. 890-912. https://doi.org/https://doi.org/10.26650/PB/PS12.2019.002.084

Dalfes N., Karaca M., Şen Ö.L., Kindap T., Önol B., Turunçoğlu U., Bozkurt D., Fer I., Akın H.S., Çankur R., Ural D., Kılıç G., Coşkun M., Demir İ. (2008) Climate scenarios for Türkiye, TÜBİTAK. Proje No:105G015.

Deveci H., 2023. Estimation of the impact of climate change on spinach cultivation areas in Türkiye. Sustainability, 15 (21): 15395. https://doi.org/10.3390/su152115395

Deveci H., 2024. Modeling the impact of climate change on cotton cultivation. COMU Journal of Agriculture Faculty, 12 (1): 96-107. https://doi.org/10.33202/comuagri.1449471

Deveci H., 2025.Determination of the accuracy of average temperature values obtained from different climate models in TR21 Thrace Region. In: 9th International Conference on Global Practice of Multidisciplinary Scientific Studies, Havana, Cuba. https://www.izdas.org/_files/ugd/614b1f_c300ca6abbdf45db9aed0060cde06741.pdf

Deveci H., Önler B., Erdem T., 2025. Modeling the effects of climate change on the irrigation water requirements of wheat and canola in the TR21 Thrace Region using CROPWAT 8.0. Frontiers in Sustainable Food Systems, 9. https://doi.org/10.3389/fsufs.2025.1563048

Ding X., Jiang Y., He L., Zhou Q., Yu J., Hui D., Huang D., 2016. Exogenous glutathione improves high root-zone temperature tolerance by modulating photosynthesis, antioxidant and osmolytes systems in cucumber seedlings. Scientific reports, 6 (1): 35424. https://doi.org/https://doi.org/10.1038/srep35424

DIVAGIS 2023. DIVA-GIS. https://www.diva-gis.org/climate

Dokuyucu Ö., Eskioğlu O., Özgökçe M.S., Ülgentürk S., 2025. Predicting future distribution and generation number of mulberry scale, Pseudaulacapis pentagona under climate change scenarios in Turkiye. Phytoparasitica, 53 (3): 41. https://doi.org/10.1007/s12600-025-01261-y

Duvan A., Aktürk G., Yıldız O., 2025. Assessing spatiotemporal characteristics of meteorological droughts in the Marmara Basin using HadGEM2-ES global climate model data. Environmental Monitoring and Assessment, 197 (4): 436. https://doi.org/10.1007/s10661-025-13884-z

Egbebiyi T.S., Crespo O., Lennard C., 2019. Defining crop–climate departure in West Africa: improved understanding of the timing of future changes in crop cuitability. Climate, 7 (9): 101. https://doi.org/10.3390/cli7090101

Egbebiyi T.S., Crespo O., Lennard C., Zaroug M., Nikulin G., Harris I., Price J., Forstenhausler N., Warren R., 2020. Investigating the potential impact of 1.5, 2 and 3 degrees C global warming levels on crop suitability and planting season over West Africa. PeerJ, 8: e8851. https://doi.org/10.7717/peerj.8851

FAO 2023. Food and Agriculture Organization of the United Nations. Database of crop constraints and characteristics. https://gaez.fao.org/pages/ecocrop

Gardner A.S., Gaston K.J., Maclean I.M.D., Scheiter S., 2021. Accounting for inter-annual variability alters long-term estimates of climate suitability. Journal of Biogeography, 48 (8): 1960-1971. https://doi.org/10.1111/jbi.14125

GDSHW 2023. General Directorate of State Hydraulic Works. Türkiye's Location. https://dsi.gov.tr/Sayfa/Detay/754

GDWM 2016. General Directorate of Water Management. Impact of climate change on water resources project project final report. ttps://www.tarimorman.gov.tr/SYGM/Belgeler/iklim%20de%C4%9Fi%C5%9Fikli%C4%9Finin%20su%20kaynaklar%C4%B1na%20etkisi/Iklim_NihaiRapor.pdf

Gündoğan A.C., Aydın C.İ., Voyvoda E., Turhan E., Özen İ.C., 2017. The Price of Inertia: An Assessment of

the Costs to Turkey of Failing to Achieve Climate Change Targets through Common Socioeconomic Pathways. Earth Association Publications, Ankara, Türkiye. https://wwftr.awsassets.panda.org/downloads/ataletin_bedeli_rapor___yeryuzu_dernegi___ab.pdf?7180/ataletinbedeli

Hancı F., Cebeci E., 2015. The effects of salinity and drought on onion production. Bahçe, 44 (1): 23-29.

Hijmans R.J., Cameron S.E., Parra J.L., Jones P.G., Jarvis A., 2005. Very high resolution interpolated climate surfaces for global land areas. International Journal of Climatology: A Journal of the Royal Meteorological Society, 25 (15): 1965-1978. https://doi.org/https://doi.org/10.1002/joc.1276

Hijmans R.J., Guarino L., Cruz M., Rojas E., 2001. Computer tools for spatial analysis of plant genetic resources data: 1. DIVA-GIS. Plant genetic resources newsletter, 127: 15-19.

Jarvis A., Ramirez-Villegas J., Herrera Campo B.V., Navarro-Racines C., 2012. Is cassava the answer to African climate change adaptation? Tropical Plant Biology, 5 (1): 9-29. https://doi.org/10.1007/s12042-012-9096-7

Joshi N., 2021. Future crop suitability assessment and the integration of Orphan crops into Kenya's food systems. MSc. Thesis. University of Cape Town, South Africa.

Khazaei M.R., 2025. Projected changes to drought characteristics in Tehran under CMIP6 SSP-RCP climate change scenarios. Heliyon, 11 (2). https://doi.org/10.1016/j.heliyon.2025.e41811

Kumar R., Reddy K.M., 2021. Impact of Climate Change on Cucurbitaceous Vegetables in Relation to Increasing Temperature and Drought, in: S. S. Solankey, et al. (Eds.), Advances in Research on Vegetable Production Under a Changing Climate Vol. 1, Springer International Publishing, Cham. pp. 175-195. https://doi.org/https://doi.org/10.1007/978-3-030-63497-1_9

Labaioui A., Bouchoufi K., 2021. Assessing the impact of climate change on land suitability for crops in El Hajeb province Morocco. African and Mediterranean Agricultural Journal Al Awamia, 132: 65-90.

Li H., Liu S.S., Yi C.Y., Wang F., Zhou J., Xia X.J., Shi K., Zhou Y.H., Yu J.Q., 2014. Hydrogen peroxide mediates abscisic acid-induced HSP 70 accumulation and heat tolerance in grafted cucumber plants. Plant Cell Environment, 37 (12): 2768-2780. https://doi.org/https://doi.org/10.1111/pce.12360

Litskas V.D., Migeon A., Navajas M., Tixier M.-S., Stavrinides M.C., 2019. Impacts of climate change on tomato, a notorious pest and its natural enemy: small scale agriculture at higher risk. Environmental Research Letters, 14 (8): 084041. https://doi.org/https://doi.org/10.1088/1748-9326/ab3313

Martin G.M., Bellouin N., Collins W.J., Culverwell I.D., Halloran P.R., Hardiman S.C., Hinton T.J., Jones C.D., McDonald R.E., McLaren A.J., O'Connor F.M., Roberts M.J., Rodriguez J.M., Woodward S., Best M.J., Brooks M.E., Brown A.R., Butchart N., Dearden C., Derbyshire S.H., Dharssi I., Doutriaux-Boucher M., Edwards J.M., Falloon P.D., Gedney N., Gray L.J., Hewitt H.T., Hobson M., Huddleston M.R., Hughes J., Ineson S., Ingram W.J., James P.M., Johns T.C., Johnson C.E., Jones A., Jones C.P., Joshi M.M., Keen A.B., Liddicoat S., Lock A.P., Maidens A.V., Manners J.C., Milton S.F., Rae J.G.L., Ridley J.K., Sellar A., Senior C.A., Totterdell I.J., Verhoef A., Vidale P.L., Wiltshire A., 2011. The HadGEM2 family of Met Office Unified Model climate configurations. Geosci. Model Dev., 4 (3): 723-757. https://doi.org/https://doi.org/10.5194/gmd-4-723-2011

Melo T.K., Sobrinho J.E., Medeiros J.F., Figueiredo B.V., Silva J.S., SÁ F.V.S., 2020. Impacts of cimate change scenarios in the Brazilian Semiarid Region on watermelon cultivars. Revista Caatinga, 33 (3): 794-802. https://doi.org/10.1590/1983-21252020v33n323rc

Møller A.B., Mulder V.L., Heuvelink G.B.M., Jacobsen N.M., Greve M.H., 2021. Can we use machine learning for agricultural land suitability assessment? Agronomy, 11 (4): 703. https://doi.org/10.3390/agronomy11040703

Moss R.H., Babiker M., Brinkman S., Calvo E., Carter T., Edmonds J.A., Elgizouli I., Emori S., Lin E., Hibbard K., 2008. Towards new scenarios for analysis of emissions, climate change, impacts, and response strategies. Intergovernmental Panel on Climate Change.

Oyediran W.O., Omoare A.M., Alaka F.A., Shobowale A.A., Oladoyinbo O.B., 2018. Rural Farmers' Coping Strategies to Effects of Climate Change on Watermelon Production in Igboora, Oyo State, Nigeria. International Journal of Sustainable Agricultural Research, 5 (2): 19-26. https://doi.org/10.18488/journal.70.2018.52.19.26

Ramirez-Villegas J., Jarvis A., Läderach P., 2013. Empirical approaches for assessing impacts of climate change on agriculture: The EcoCrop model and a case study with grain sorghum. Agricultural and Forest Meteorology, 170: 67-78. https://doi.org/10.1016/j.agrformet.2011.09.005

Rao N.K.S., 2016. Onion, in: N. K. S. Rao, et al. (Eds.), Abiotic Stress Physiology of Horticultural Crops, Springer India, New Delhi. pp. 133-149. https://doi.org/https://doi.org/10.1007/978-81-322-2725-0_8

Rhiney K., Eitzinger A., Farrell A.D., Prager S.D., 2018. Assessing the implications of a 1.5 °C temperature limit for the Jamaican agriculture sector. Regional

Environmental Change, 18 (8): 2313-2327. https://doi.org/10.1007/s10113-018-1409-4

Saadi S., Todorovic M., Tanasijevic L., Pereira L.S., Pizzigalli C., Lionello P., 2015. Climate change and Mediterranean agriculture: Impacts on winter wheat and tomato crop evapotranspiration, irrigation requirements and yield. Agricultural water management, 147: 103-115. https://doi.org/https://doi.org/10.1016/j.agwat.2014.05.008

Simões W.L., Angelotti F., Guimarães M.J.M., Silva J.S.d., Silva R.M., Barros J.R.A., 2022. Water-use efficiency and onion quality in future climate scenarios. Pesquisa Agropecuária Tropical, 52: e72212.

Singh M.C., Singh J.P., Pandey S.K., Mahay D., Srivastava V., 2017. Factors affecting the performance of greenhouse cucumber cultivation-a review. International Journal of Current Microbiology and Applied Sciences, 6 (10): 2304-2323. https://doi.org/https://doi.org/10.20546/ijcmas.2017.610.273

Stewart A.L., Ahmed S., 2020. Effects of climate change on fruit nutrition, in: A.K. Srivastava and Chengxiao Hu (Eds.), Fruit crops, Elsevier, Amsterdam, The Netherlands. pp. 77-93. https://doi.org/https://doi.org/10.1016/B978-0-12-818732-6.00007-1

Şalk A., Arın L., Deveci M., Polat S., 2008. Special Vegetables. Onur Graphics, Printing and Advertising, Tekirdağ, Türkiye.

Şen A.S., Deveci H., Konukcu F., 2024. Modelling the adaptation of some cultural plants produced in Thrace Region to climate change. Journal of Tekirdag Agricultural Faculty, 21 (2): 501-516. https://doi.org/10.33462/jotaf.1312707

Tatlıoglu T., 1993. Cucumber, in: G. Kalloo and B. O. Bergh (Eds.), Genetic Improvement of Vegetable Crops, Pergamon, Amsterdam. pp. 197-234. https://doi.org/10.1016/b978-0-08-040826-2.50017-5

Temur B., 2017. The impact of global warming on agricultural sector in Turkey: An application of the ARDL model. MSc. Thesis. Anadolu University, Türkiye.

TSMS 2023a. Türkiye State Meteorological Service. Türkiye maximum temperature average. https://www.mgm.gov.tr/FILES/resmi-istatistikler/parametreAnalizi/2024-maksimum-sicaklik.pdf

TSMS 2023b. Türkiye State Meteorological Service. Türkiye minimum temperature average. https://www.mgm.gov.tr/FILES/resmi-istatistikler/parametreAnalizi/2024-minimum-sicaklik.pdf

TSMS 2023c. Türkiye State Meteorological Service. Türkiye Average Temperature. https://www.mgm.gov.tr/FILES/resmi-istatistikler/parametreAnalizi/2024-ortalama-sicaklik.pdf

TSMS 2023d. Türkiye State Meteorological Service. Annual total precipitation average in Türkiye. https://www.mgm.gov.tr/FILES/resmi-istatistikler/parametreAnalizi/2024-yagis.pdf

TSMS 2023e. Türkiye State Meteorological Service. Türkiye average humidity. https://www.mgm.gov.tr/FILES/resmi-istatistikler/parametreAnalizi/2024-ortalama-nem.pdf

TurkStat 2024a. Turkish Statistical Institute. Statistical Tables of Agricultural Areas. https://data.tuik.gov.tr/Search/Search?text=tar%C4%B1m%20alanlar%C4%B1

TurkStat 2024b. Turkish Statistical Institute. World Population Day. https://data.tuik.gov.tr/Bulten/Index?p=Dunya-Nufus-Gunu-2024-53680#:~:text=T%C3%BCrkiye%2C%2085%20milyon%20372%20bin,1%2C1'ini%20olu%C5%9Fturdu.

Walters S.A., Abdelaziz M., Bouharroud R., 2021. Local melon and watermelon crop populations to moderate yield responses to climate change in North Africa. Climate, 9 (8): 129. https://doi.org/https://doi.org/10.3390/cli9080129

WBG 2022. World Bank. Group. Türkiye Country Climate and Development Report, CCDR Series; World Bank: Washington, DC, USA. https://openknowledge.worldbank.org/entities/publication/01826a0c-059f-5a0c-91b7-2a6b8ec5de2f

Wichern J., Descheemaeker K., Giller K.E., Ebanyat P., Taulya G., van Wijk M.T., 2019. Vulnerability and adaptation options to climate change for rural livelihoods – A country-wide analysis for Uganda. Agricultural Systems, 176: 102663. https://doi.org/https://doi.org/10.1016/j.agsy.2019.102663

WPR 2024a. World Population Review, Vegetable production by Country 2022. https://worldpopulationreview.com/country-rankings/vegetable-production-by-country

WPR 2024b. World Population Review, Tomato Production by Country 2022. https://worldpopulationreview.com/country-rankings/tomato-production-by-country

WPR 2024c. World Population Review, Watermelon Production by Country 2022. https://worldpopulationreview.com/country-rankings/watermelon-production-by-country

WPR 2024d. World Population Review, Onion Production by Country 2022. https://worldpopulationreview.com/country-rankings/onion-production-by-country

WPR 2024e. World Population Review, Cucumber Production by Country 2022. https://worldpopulationreview.com/country-rankings/cucumber-production-by-country

Wurr D.C.E., Hand D.W., Edmondson R.N., Fellows J.R., Hannah M.A., Cribb D.M., 1998. Climate change: a response surface study of the effects of CO2 and temperature on the growth of beetroot, carrots and onions. The Journal of Agricultural Science, 131 (2): 125-133. https://doi.org/https://doi.org/10.1017/S0021859698005681

Yokota A., Kawasaki S., Iwano M., Nakamura C., Miyake C., Akashi K., 2002. Citrulline and DRIP-1 protein (ArgE homologue) in drought tolerance of wild watermelon. Annals of Botany, 89 (7): 825-32. https://doi.org/10.1093/aob/mcf074

Zagaria C., Schulp C.J.E., Malek Ž., Verburg P.H., 2023. Potential for land and water management adaptations in Mediterranean croplands under climate change. Agricultural Systems, 205: 103586. https://doi.org/10.1016/j.agsy.2022.103586

Zhang Y., Lv J., Wang T., Zhang K., Wu Y., 2025. Assessment of ecological risk under different SSP-RCP scenarios of the Xinjiang province in China. Scientific reports, 15 (1): 8345. https://doi.org/10.1038/s41598-024-81879-w

Italian Journal of Agrometeorology
Rivista Italiana di Agrometeorologia

Firenze University Press
https://riviste.fupress.net/index.php/IJAm

OPEN ACCESS

**Citation:** Mota, M.C., Candido, L.A., Cuadra, S.V., Marenco, R.A., Tomé, A.M., Lopes, A.B.A., Lima, F.L., Reis, J., Brizolla, R.M. & Lopes, A.B.D.A. (2025). Validation of the leaf area index estimated using the extinction coefficient of photosynthetically active radiation in soybean. *Italian Journal of Agrometeorology* (1): 19-29. doi: 10.36253/ijam-2770

**Received:** May 17, 2024

**Accepted:** June 27, 2025

**Published:** August 27, 2025



**Data Availability Statement:** All relevant data are within the paper and its Supporting Information files.

**Competing Interests:** The Author(s) declare(s) no conflict of interest.

# Validation of the leaf area index estimated using the extinction coefficient of photosynthetically active radiation in soybean

Marcelo Crestani Mota[1,*], Luiz Antonio Candido[2], Santiago Vianna Cuadra[3], Ricardo Antonio Marenco[4], Adriano Maito Tomé[5], Andressa Back De Andrade Lopes[5], Francinei Lopes De Lima[5], Juliana Reis[5], Rafael Morbeque Brizolla[5]

[1] *Researcher, Agronomy Course Coordination, Faculdade Marechal Rondon (FARON), Vilhena, RO, Brazil*
[2] *Researcher, Climate and Water Resources Coordination, Instituto Nacional de Pesquisas da Amazônia (INPA), Manaus, AM, Brazil*
[3] *Researcher, Brazilian Agricultural Research Corporation (EMBRAPA Agricultura Digital), Campinas, SP, Brazil*
[4] *Researcher, Environmental Dynamics Coordination, Instituto Nacional de Pesquisas da Amazônia (INPA), Manaus, AM, Brazil*
[5] *Undergraduate student, Agronomy Course, Faculdade Marechal Rondon (FARON), Vilhena, RO, Brazil*
*Corresponding author. E-mail: crestanimota@gmail.com

**Abstract.** Techniques to monitor vegetation cover have been used to track the biomass and yield of agricultural crops. Quantifying the leaf area index (LAI) and its variation throughout the production cycle of soybean is important because this data can be used as an input variable in growth and productivity models. Field experiments were carried out during the 2017/2018 and 2018/2019 growing season in soybean crops at the Faculdade Marechal Rondon (FARON) in Vilhena, RO, Brazil, to measure the LAI of cultivar 75I77 RSF IPRO from the estimated extinction coefficient of photosynthetically active radiation (PAR). LAI measurements were performed weekly in the 2018/2019 crop season. The PAR data were collected using the PAR Apogee® SQ-316-S linear sensor. The light extinction coefficient (Kc) was calculated using LAI and solar radiation interception data. A Kc value of 0.687 was found for this crop, indicating that more than 68% of the light was intercepted by the plant structure. In addition, the LAI data estimated via Kc were compared with LAI values estimated with the CROPGRO-Soybean model. The first method estimated the LAI values better than the second, as the $r^2$ increased from 0.738 to 0.882, the difference was reduced from 19.9 to 13.3%, and the d-value changed from 0.815 to 0.952. Thus, the extinction coefficient method of PAR can efficiently estimate the LAI parameter in soybean.

**Keywords:** shortwave radiation, light extinction coefficient, photosynthetic efficiency, crop parameterization, yield improvement.

## 1. INTRODUCTION

During the development cycle of agricultural crops, the variation of the vegetation cover fraction (fc) and the leaf area index (LAI) are biophysical parameters considered fundamental in vegetation dynamics (Chechi et al., 2021). They provide a better understanding of the partitioning of crop evapotranspiration in plant transpiration and soil water evaporation coefficients (Paredes et al., 2017; Allen and Pereira, 2009). Also, LAI is useful to infer about the fraction of the photosynthetically active solar radiation (PAR) intercepted by the plant canopy (Purcell et al., 2002), and the dry matter of crops (Li et al., 2010). Chechi et al. (2021) highlighted that $f_c$ and LAI are often used as mandatory variables in agricultural models, including AquaCrop (Foster et al., 2017), SIMDualKc (Paredes et al., 2017), CSM-CROPGRO (Cuadra et al., 2021; Crestani Mota et al., 2024), and Agro-IBIS (Moreira et al., 2023).

The radiation impinging on the canopy can be reflected, absorbed or transmitted. The radiation flux that is transmitted to the soil decreases exponentially as the leaf area increases in the canopy (Jones, 2014). According to Adeboye et al. (2016), under optimal environmental conditions, the accumulation of biomass through the photosynthetic process is strongly correlated with the radiation absorbed by plants in the spectral range of the PAR, which corresponds to visible wavelengths (400 to 700 nm).

The absorbed PAR is a fundamental parameter in the modeling of soybean growth and yield, because as the plant foliage increases (and so LAI), the use efficiency of this radiation increases, and improves the accumulation of plant dry matter, especially in grains (Fontana et al., 2012). However, the characterization of the internal distribution of the PAR to the plant canopy is not uniform, considering the canopy architecture (spatial orientation) and the spectral properties of the leaves (Plénet et al., 2000; Jones, 2014).

Monsi and Saeki (1953) were the first to analyze the modification of the Lambert-Beer radiation extinction law through a model of light energy distribution along the plant canopy for homogeneous areas of agricultural cultivation with dense leaf development. In this model, the exponential reduction of radiation with increasing LAI is associated with an extinction coefficient (Kc; dimensionless) of the PAR (Bréda, 2003).

Hence, the proportion of intercepted PAR is directly related to the LAI of the crop and the Kc characteristic of the species (Shibles and Weber, 1965; Pengelly et al., 1999; Schöffel and Volpe, 2001). These factors influence leaf area production (leaf mass ratio), duration of the leaf area, and the potential of phytomass production (Mayers et al., 1991ab). Therefore, the biomass production is a function of the integrated PAR intercepted by the culture ($f_{IPAR}$), where the angular coefficient of the regression curve between biomass (dry matter) and PAR defines the light use efficiency for phytomass production (Shibles and Weber, 1966).

However, the light use efficiency for biomass production is not constant, as it varies during the plant cycle (Steinmetz and Siqueira, 1995). For instance, it can vary between cultivars and with the development phases of irrigated rice, reaching the highest values between the differentiation of the floral primordium and flowering (Steinmetz and Siqueira, 2001). Also, light use efficiency can vary between the subperiods of crop development. In maize, it was 1.71 g $MJ^{-1}$ from emergence to the ninth expanded leaf and 3.58 g $MJ^{-1}$ from the end of the vegetative subperiod to grain filling (Müller et al., 2001).

Soybean biomass yield can also be analyzed in terms of interception efficiency and conversion of the PAR to phytomass (Mayers et al., 1991ab). During the first 42 days of the vegetative stage, the light use efficiency (conversion of the PAR to phytomass) of two soybean cultivars was 1.2 and 1.32 g $MJ^{-1}$ (Muchow, 1985). The light use efficiency of the aerial part accumulated from the emergence to initial flowering can be linear. For example, in ten soybean cultivars light use efficiency was linear during the dry season (1.15 g $MJ^{-1}$); however, there was a large dispersion of the data during the flowering phase (Mayers et al., 1991a).

Most soybean growth models use a constant Kc value (fixed average) throughout the crop cycle and for the complete canopy. However, the timing of a specific phenological stage can vary in different locations and years due to factors such as sowing season, soil moisture, air temperature, and management practices (Sakamoto et al., 2010), as well as structural conditions, leaf age, and photosynthetic and respiratory characteristics of plants (Costa et al., 1996). Thus, the on-site observation of dates and values of these variables limits the use of many agricultural models because conducting observations requires time and resources.

This study aimed to evaluate the accuracy and consistency of LAI estimation in soybean based on the Kc of PAR. For this purpose, both observed and Kc-estimated LAI values were computed throughout the crop's phenological cycle, enabling a detailed comparison with simulations generated by the CROPGRO-Soybean model.

## 2. MATERIALS AND METHODS

### *2.1 Characterization of the experimental area*

The experiment was conducted during the 2017/2018 and 2018/2019 crop seasons at the Faculdade Marechal Rondon (FARON), in the municipality of Vilhena, RO, Brazil, whose geographical coordinates are 60°05´ W and 12°46´ S, at 600 m altitude (Figure 1). The field plots were located in the mesoregion known as the Southern Cone of Rondônia (SCRO), where soybean is normally sown in the no-tillage system as a succession crop with maize (Nóia Júnior and Sentelhas, 2019). The predominant soil of the region is classified as dystrophic Red-Yellow Latosol, characterized by a flat relief (Crestani Mota et al., 2024). The climate is the Am type, defined as rainy tropical with a well-defined dry season (Alvares et al., 2013). The average annual rainfall and temperatures are 2,200.0 mm and 24.6 °C, respectively.

### *2.2 Determination of the Leaf Area Index (LAI)*

#### 2.2.1 Field sampling method and Leaf Area Index estimation

The LAI was obtained every two weeks during the 2017/2018 crop season and every week during the 2018/2019 crop by employing the software Digital Area Determiner (DDA – *Determinador Digital de Áreas*) version 20.0 (Ferreira et al., 2008). Beginning 35 days after sowing (DAS), three plants from the soybean plot were randomly collected until full maturation. The leaves of each plant collected in the field were separated and placed in a tabletop scanner connected to a microcomputer. The leaves were digitized on a monochrome scale, generating a file of single images or several BITMAP files (.bmp) of images with the areas to be measured. Then the files were processed in the DDA to directly obtain the mean LAI, from the scans of the leaves from the three plants. To reduce the experimental error during the collections, the plants of the external lines and the plants present in the initial and final 0.5 m of the plot were not collected.

The variation in sampling frequency between the 2017/2018 (biweekly) and 2018/2019 (weekly) crop seasons reflects a methodological refinement intended to improve the temporal resolution and accuracy of LAI estimation. Although the biweekly sampling was sufficient to characterize overall canopy development, we decided to improve the accuracy of the output by increasing the sampling frequency in the second season (to weekly intervals) in to order to more accurately capture the rapid changes in leaf area during key phenological stages, particularly the vegetative and early reproductive phases.

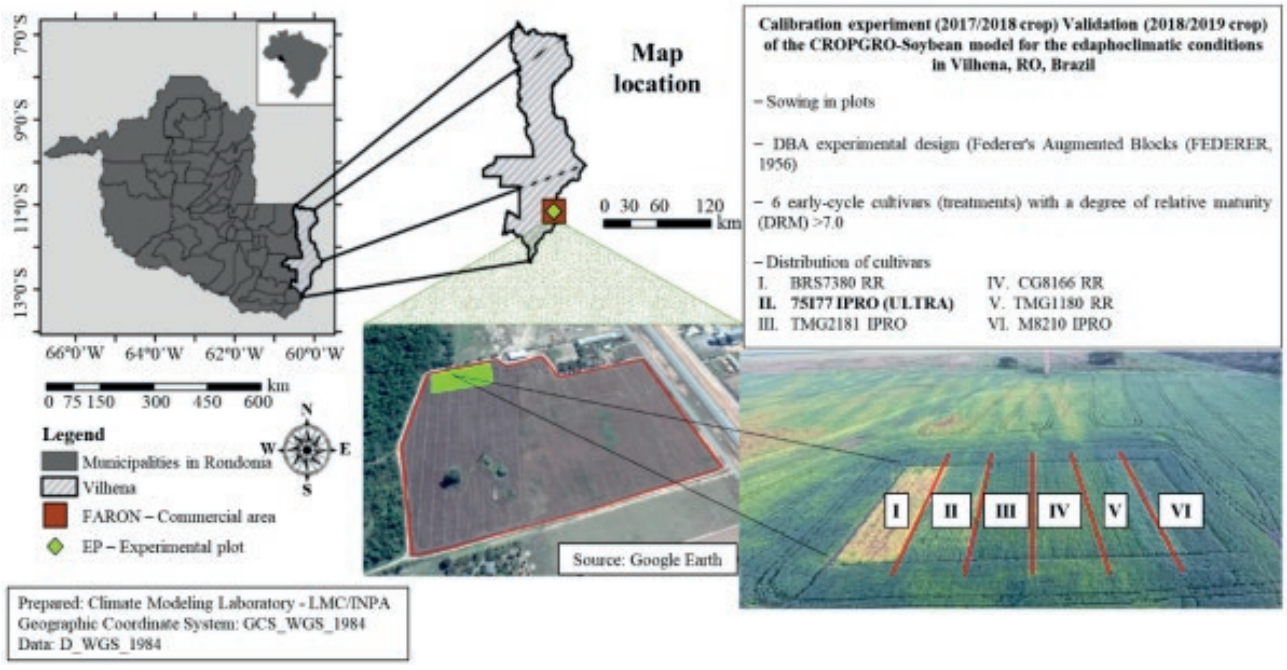


**Figure 1.** Location map of the experimental area at the Faculdade Marechal Rondon in Vilhena, RO, Brazil (2018).

*2.2.2 Leaf Area Index Estimated from the Extinction Coefficient of the Photosynthetically Active Radiation*

To determine the Kc of the PAR on the canopy of the cultivar sown in the present study and, to obtain LAI measurements for the complete development cycle of the cultivar, measurements of the incident PAR ($PAR_{in}$) and intercepted PAR ($PAR_{int}$) were performed for both crop season, using the PAR Apogee® SQ-316-S bar sensor (Figure 2).

The sensor was installed in the plot sown with the 75I77 RSF IPRO (ULTRA) cultivar positioned in the row line and fixed 0.1 m from the ground. Measurements were taken until the reproductive stage of soybean when green leaves were still present. As described by Zdziarski et al. (2018), this soybean cultivar is technically recommended for macro-region 4 and edaphoclimatic zone 402, particularly in areas situated at elevations above 400 m. Thus, LAI of this cultivar was monitored under field conditions in the municipality of Vilhena, within the recommended sowing window from October 10 to November 15, to ensure alignment with its optimal agronomic performance. In addition, this medium-cycle cultivar was estimated at 104 days and small size, with a low branching index but high productive potential, and its population ranges from 320 to 380 thousand plants per hectare (www.brasmaxgenetica.com.br).

Equations 1 and 2 were used to obtain the fraction of the PAR intercepted ($f_{IPAR}$; dimensionless) by the canopy. The seasonal average Kc of the PAR was determined through destructive measurements of LAI (performed at seven-day intervals throughout the 2018/2019 crop season, from 35 DAS) and $f_{IPAR}$ (initiated four DAS during the 2018/2019 crop), using Equation 3. The estimated LAI, $f_{IPAR}$, and Kc values are presented in Table 1.

$$PAR_{int} = PAR_{in} * \left[1 - exp^{(-LAI * K_c)}\right] \quad (1)$$

$$f_{IPAR} = \frac{PAR_{int}}{PAR_{in}} = 1 - exp^{(-LAI * K_c)} \quad (2)$$

$$K_c = \frac{-ln(1-f_{IPAR})}{LAI} \therefore LAI_{estimated} = \frac{-ln(1-f_{IPAR})}{K_c} \quad (3)$$

**Figure 2.** The PAR Apogee® SQ-316-S bar sensor (Apogee Instruments, Inc., Logan, Utah, USA) installed on the cultivation line of 75I77 RSF IPRO (ULTRA) cultivar in an experimental area at the Faculdade Marechal Rondon, in Vilhena, RO, Brazil (2018).

Where $PAR_{in}$ is the incident photosynthetically active radiation (μmol $m^{-2}$ $s^{-1}$); $PAR_{int}$ is the intercepted photosynthetically active radiation (μmol $m^{-2}$ $s^{-1}$); *LAI* is the leaf area index (dimensionless); *Kc* is the PAR extinction coefficient (dimensionless); and $f_{IPAR}$ is the fraction of the PAR intercepted by the canopy (dimensionless). For comparison, the data were transformed into MJ $m^{-2}$ $day^{-1}$, using the conversion value developed by Thimijan and Heins (1983), by Equation 4:

$$\sum_{daily} \frac{PAR(\mu mol\ m^{-2}s^{-1}) * \frac{t(s)}{4.57}}{10^6} \quad (4)$$

Where *t* is the time between collections (300 s) and 4.57 is the conversion factor. All values were integrated for a 24 h period.

2.2.3 Leaf Area Index simulated by the Cropgro-Soybean agricultural model

The CROPGRO-Soybean agricultural model (Boote et al., 1996) in version 4.7.5 of the DSSAT (dssat.net) was used to simulate the LAI throughout the development cycle of cultivar 75I77 RSF IPRO (ULTRA). This mechanistic model considers all soybean development processes, from photosynthesis to the partition of photoassimilates, through the growth of leaves, stems, and roots, soil water extraction, and transpiration, in response to meteorological variations (Hoogenboom et al., 2012). The model can simulate the performance components (soil moisture and evapotranspiration; dry biomass – leaves, pods, stem, and petiole; leaf expansion through the LAI; and grain yield), quantifying and tracing the daily growth of the crop to the stages of physiological maturity and harvest (Confalone et al., 2016).

*2.3 Calibration and validation of the Cropgro-Soybean agricultural model*

The CROPGRO-Soybean model was calibrated for the experimental conditions of the 2017/2018 crop season and validated in the 2018/2019 crop season, following the recommendations of Hoogenboom et al. (2003) and Jones et al. (2003) through the method of sensitive adjustments and minimization of variable error (Fensterseifer et al., 2017). First, the following sets of phenological information were established: dates of sowing, emergence, flowering, and physiological maturation, weight of one thousand grains (PMG), and yield of cultivars (kg $ha^{-1}$) under field conditions. Then, the genetic-specific parameters of the cultivar 75I77 RSF IPRO (ULTRA) were adjusted based on growth data (maximum leaf

**Table 1.** Estimated leaf area index (LAI estimated), photosynthetically active radiation interception fraction (fIPAR), and extinction coefficient of the photosynthetically active radiation (Kc estimated).

| Cultivar | Year | DAS | Day | Month | $LAI_{estimated}$ | - ln (1 - $f_{IPAR}$) | $Kc_{estimated}$ |
|---|---|---|---|---|---|---|---|
| 75I77 RSF IPRO (ULTRA) | 2018 | 31 | 1 | Dec | 1.5 | 0.838 | 0.555 |
| | 2018 | 38 | 8 | Dec | 2.1 | 1.296 | 0.617 |
| | 2018 | 46 | 16 | Dec | 3.4 | 1.847 | 0.546 |
| | 2018 | 52 | 22 | Dec | 3.6 | 2.710 | 0.753 |
| | 2018 | 59 | 29 | Dec | 4.2 | 3.225 | 0.770 |
| | 2019 | 66 | 5 | Jan | 3.6 | 3.151 | 0.868 |
| | 2019 | 73 | 12 | Jan | 3.3 | 2.186 | 0.843 |
| | 2019 | 80 | 19 | Jan | 3.0 | 2.079 | 0.702 |
| | 2019 | 87 | 26 | Jan | 2.3 | 1.215 | 0.528 |
| | | | | | | Mean | 0.687 |

area, maximum photosynthetic rate, and specific leaf area), development (number of nodes, date of emergence, and reproductive stages R1 – beginning of flowering, R3 – beginning of pod formation, R5 – beginning of grain filling, and R7 – beginning of maturation) and yield components (number of grains per square meter and average weight of a grain) (Cera et al., 2017). Data were collected in the experimental field at the FARON during the two harvests. The phenological development of the crops was monitored according to the scale of Fehr and Caviness (1977), and the counting of data in days followed the Julian calendar, starting on the date of emergence.

### *2.4 Statistical analysis*

To evaluate the performance of the LAI estimated from the Kc of the PAR in comparison with the CROPGRO-Soybean model, the following statistical indices were used: coefficient of determination ($r^2$) (Equation 5), percentage deviation ($P_d$) (Equation 6), root mean square error (RMSE) (Equation 7), and the agreement index (d-value) of Willmott (1982) (Equation 8).

$$r^2 = \left( \frac{\sum_{i=1}^{n} \left(O_i - \bar{O}_i\right) * \left(P_i - \bar{P}_i\right)}{\sqrt{\sum_{i=1}^{n} \left(O_i - \bar{O}_i\right)^2} * \sqrt{\sum_{i=1}^{n} \left(P_i - \bar{P}_i\right)^2}} \right)^2 \quad (5)$$

$$P_d = \left[ \frac{P_i - O_i}{O_i} \right] * 100 \quad (6)$$

$$RMSE = \sqrt{\frac{\sum_{i=1}^{n} (P_i - O_i)^2}{n}} \quad (7)$$

$$d = 1 - \left[ \frac{\sum_{i=1}^{n} (P_i - O_i)^2}{\sum_{i=1}^{n} \left( \left| P_i - \bar{O}_i \right| + \left| O_i - \bar{O}_i \right| \right)^2} \right], \; 0 \leq d \leq 1 \quad (8)$$

Where $n$ is the number of observations; $P_i$ is the simulated values; $\bar{P}_i$ is the mean of the simulated values; $O_i$ is the observed values; and $\bar{O}_i$ is the mean of the observed values.

## 3. RESULTS AND DISCUSSION

On a ground area basis, at the beginning of the plant cycle, until approximately 48 DAS, the crop used the PAR that reached the plant less efficiently. The observed measurements indicated that the maximum intercepted PAR was 4.3 MJ $m^{-2}$ $day^{-1}$ (60 DAS) when the fraction of leaf cover in the canopy projected over the area of 1 $m^2$ of soil reached 98.3% in the R5 stage. While the simulated intercepted PAR reached the maximum light use efficiency of 8.9 MJ $m^{-2}$ $day^{-1}$ (at 55 DAS), when the leaf cover fraction reached 97.3%, also during the R5 stage (Figure 3). The decline in the intercepted PAR, both observed and estimated, began with leaf senescence in R6, either at around 72 DAS for the field conditions or at 65 DAS for the CROPGRO-Soybean model, respectively. The anticipated drop in simulated interception was due to the overestimates of the LAI at the beginning of the cycle of this cultivar when the model anticipated the emission of leaves favoring maximum growth (4.6 $cm^2$ $cm^{-2}$) seven days before the greatest leaf expansion was observed.

For field conditions, the 75I77 RSF IPRO (ULTRA) cultivar achieved 96% of PAR interception, between 60 and 70 DAS, and approximately 95%, between 50 and 63 DAS in the CROPGRO-Soybean simulation (Figure 3). Results follow those obtained by Confalone and Dujmovich (1999) for the edaphoclimate of the central-eastern region of the province of Buenos Aires, Argentina, where the 1998/1999 crop exhibited a 95% level of

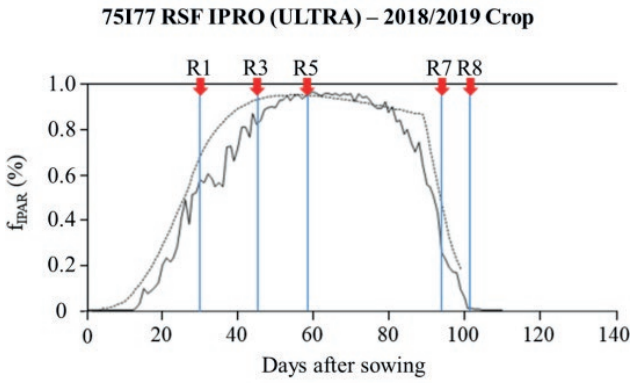


**Figure 3.** Fraction of intercepted PAR (fIPAR) observed in the field (—) using the PAR Apogee® SQ-316-S line sensor and simulated by the CROPGRO-Soybean model (....) throughout the development cycle of cultivar 75I77 RSF IPRO (ULTRA) during the 2018/2019 crop cycle.

radiation interception 78 days after emergence, when the indeterminate growth cultivar Asgrow 4656 presented a maximum LAI of 5.3 in R4. Souza et al. (2009) during field experiments carried out in the municipality of Paragominas, PA, Brazil, found for the cultivar BRS Tracajá (indeterminate cycle) 99% interception of the PAR between 70 and 96 DAS (R4 and R5), when the maximum Kc and LAI were 0.717/4.1 and 0.715/6.5 for the 2007/2008 and 2008/2009 crops, respectively. Similarly, Costa et al. (1999) found values of maximum radiation interception (99%) occurring between 70 and 96 DAS for soybeans grown under different irrigation conditions throughout the cycle in the Southeastern region of Brazil.

According to Souza et al. (2009), the increased efficiency in the use of the PAR found during the reproductive phase of soybean is reflected in most of the results found for this crop (Confalone and Dujmovich, 1999; Schöffel and Volpe, 2001; Santos et al., 2003; Adeboye et al., 2016). The same authors reported that this increase is closely linked to the progressive accumulation of vegetative and reproductive biomass, becoming markedly significant from the V5 vegetative stage onward. This elevated efficiency persists through subsequent phenological phases and remains pronounced until the onset of the R5 reproductive stage, a critical period when the physiological transition toward reproductive phase occurs, marked by the remobilization of photoassimilates from source tissues to developing sink organs, primarily for grain filling.

According to Figure 4, the calibrated CROPGRO-Soybean model simulated more accurate and robust values for the LAIs in the validation period, evidenced by the increases in $r^2$ (0.738) and d-value (0.815), as well as the decrease in RMSE (0.7 $cm^2\ cm^{-2}$) and $P_d$ amplitude (19.9%), compared to the 2017/2018 harvest and also with the model maintaining the original parameters during the 2018/2019 crop. However, when comparing the LAIs simulated by the CROPGRO-Soybean model with those estimated through the mean Kc calculated daily for the field conditions, the latter ones were closer to the observed LAIs due to increased $r^2$ (0.882) and d-value (0.952), as well as the reduced $P_d$ amplitude (13.3%).

The estimated LAIs obtained from Kc showed results similar to those that occurred under field conditions during most of the development cycle of cultivar 75I77 RSF IPRO (ULTRA), especially in the initial (up to 50 DAS) and final (90 DAS up to the stage R8) phases (Figure 4). Between 55 and 83 DAS, the LAIs estimated through Kc were, on average, 28.6% higher than those observed, with new growth of RMSE (1.3 $cm^2\ cm^{-2}$) and greater differences during senescence (R6), in which the new LAI values were about 1.4 and 1.2 $cm^2\ cm^{-2}$ higher than those observed 69 and 76 DAS, respectively. This was likely due to variations in plant density at the randomly selected sampling locations from which the plants used for LAI measurements were collected.

Together with the PAR Apogee® SQ-316-S bar sensor used to determine $f_{IPAR}$ and Kc, the population of plants per square meter was relatively higher than the three points sampled weekly, which were chosen randomly to determine the mean LAI of the cultivar. In addition, the cultivated area within the range of action of the PAR line sensor did not suffer, like other parts of the plot, from damage caused by fungal diseases between stages R5 and R7, which also contributed to higher LAI values estimated by the Kc methodology compared to the LAI measurements obtained by the leaf scanning process that depended on random sampling. In this context, Yokoyama et al. (2018) highlighted the importance of maintaining the LAI between the middle of the grain filling period until physiological maturity, as it positively impacts yield. The authors also emphasize that special care is necessary to avoid loss of LAI at this stage. Moreover, proper management of diseases and insect pests is indispensable, as Moreira et al. (2015) discussed.

As the cultivar developed, self-shading occurred due to the overlapping leaves from the high density of plants at the sensor location point, which resulted at 60 DAS in values very close to the incidence of PAR, providing greater than 96% interception. This was also observed by Petter et al. (2016), who demonstrated that a major benefit of increasing the number of plants per area is the increase of the LAI, influencing the use of light by the crop (greater than 90%). According to Cox and Cherney

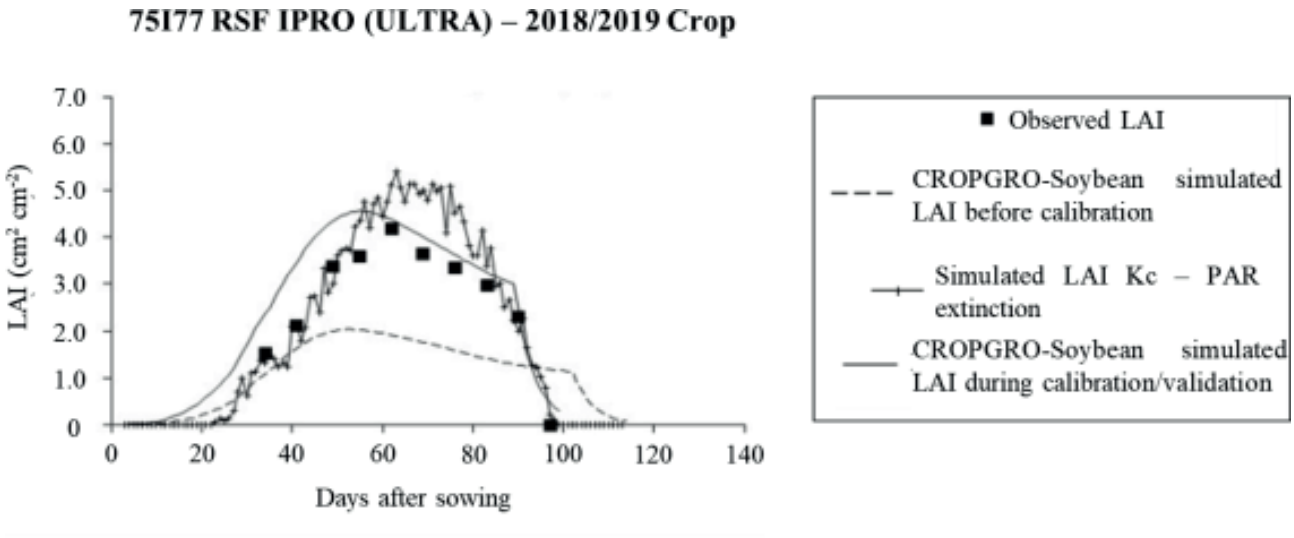


| Statistics of the Simulation | $r^2$ | $P_d$ (%) | RMSE ($cm^2$ $cm^{-2}$) | d-value |
|---|---|---|---|---|
| Before calibration of the CROPGRO-Soybean model | 0.661 | 45.7 | 1.5 | 0.517 |
| Validation of the CROPGRO-Soybean model | 0.738 | 19.9 | 0.7 | 0.815 |
| Estimated by Kc - PAR extinction | 0.882 | 13.3 | 1.3 | 0.952 |

**Figure 4.** Time variation of the observed LAI (▪), simulated with the original parameters of CROPGRO-Soybean (----), simulated in the validation (—), and from the extinction coefficient of the PAR (Kc) (+—+—+) throughout the development cycle of cultivar 75I77 RSF IPRO (ULTRA) during the 2018/2019 crop. Statistics applied to the LAI: coefficient of determination ($r^2$); percent deviation ($P_d$); root mean squares error (RMSE); and Willmott agreement index (d-value).

(2011), high leaf growth plasticity is a relevant mechanism of phenotypic plasticity of soybean.

The LAI estimated by Kc was significantly affected in an increasing linear manner by the plant population up to the R4 stage, with the maximum peak occurring at 63 DAS (5.4) (Figure 4). For the period between 55 and 83 DAS, the average LAI was established at 4.5 $cm^2$ $cm^{-2}$. According to Tagliapietra et al. (2018), these values are recommended between stages R3 and R5 for cultivars of indeterminate growth to obtain maximum yields (optimization of dry matter accumulation by plants). This is equivalent to LAI values (3.5-4.5) greater than those normally cited as ideal for soybean cultivation, which does not consider the growth habit, the degree of relative maturity (DRM), and the water inputs in the cultivated area (irrigated and rain-fed fields). Up to around 30 DAS, the accumulation of soybean dry matter was slow, but it became faster from 30 to 60 DAS. Subsequently, the slight drop after 75 DAS was mainly due to the senescence of the leaves near the ground and the redistribution of photoassimilates and nutrients from the leaves to the grains formation, as observed in the works of Petter et al. (2016) and Srinivasan et al. (2017).

The temporal changes in the dry matter biomass of the cultivar canopy and its distribution in pods and grains, together with the simulated values, are shown in Figure 5. The agricultural cultivation model can simulate with some precision changes in the dry weight of plant components (pods, stems, leaves, and grains). Boote et al. (1997) found that CROPGRO-Soybean can reasonably predict temporal changes in LAI and biomass for various locations in the USA. However, because of the anticipation of the maximum LAI and the excess of simulated leaf area, the model tends to overestimate the biomass of the pods, which directly interferes with the dry matter of grains (yield), as there is a greater demand and partitioning of photoassimilates during stages R4 and R5.3 (Borrás et al., 2004), a period in which grains are between 26 and 50% formed (Fehr and Caviness, 1977), for the development of pods and grains (Figure 5). This situation was also verified by Crestani Mota et al. (2024) for the cultivar TMG2181 IPRO, with a slightly later cycle but with less impact, as the overestimates of the LAI by the model at the beginning of the development of this genetic material were lower.

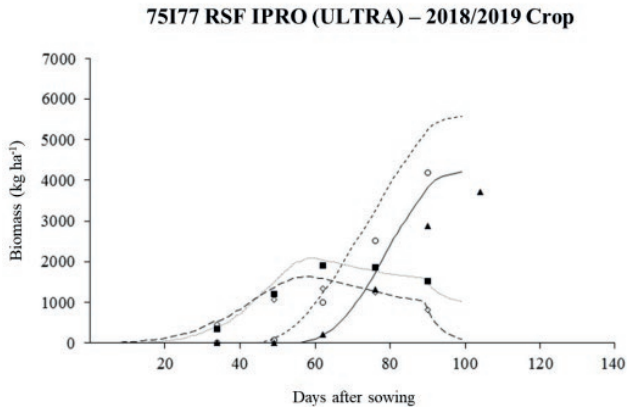


**Figure 5.** Dry biomasses measured (○ pods, ▪ stems, ◊ leaves, and ▲ grains) and simulated by the CROPGRO-Soybean model (----- pods, —– stems, – – – leaves, and —– grains) throughout the development cycle of cultivar 75I77 RSF IPRO (ULTRA) during the 2018/2019 crop season.

The minimum tillage is another important detail during the validation. According to Mota (2019), the increases in simulated LAIs may also be linked to the increased nitrogen accumulation, an essential nutrient in grain filling and a fundamental prerequisite for high grain yields and quality (Salvagiotti et al., 2008), especially in cultivars with undetermined growth habits, by incorporating maize straws into the soil. This indicates that CROPGRO-Soybean responds differently (systematic error) to this condition in shorter-cycle cultivars, such as 75I77 RSF IPRO (ULTRA). With the appearance of leaves earlier in CROPGRO-Soybean simulations, the period of filling pods coincides with the maximum LAI, in the same way as the redistribution of mineral nutrients, carbohydrates, and nitrogen compounds in grains, stems, branches, and senescent leaves during this phase (Mundstock and Thomas, 2005).

Thus, the results of air-dried matter for the 2018/2019 crop season demonstrated that the model has limitations in its estimation of leaf expansion and senescence. Therefore, finer adjustments are required to the parameters related to the parameterization of the LAI in the CROPGRO-Soybean model, which applies three functions in this process. The growth stage is initially characterized by an exponential logistic function (sigmoid model) from emergence to the maximum LAI. Then, there is a linear phase (Goudriaan and Monteith, 1990) as self-shading increases and plants invest more in the production of pods and grains, and other non-leaf structures. Finally, the phase extending from leaf senescence to physiological maturity (Taiz and Zeiger, 2004) is terminated by an exponential function. Therefore, to minimize the effects of overestimated LAI on biomass production by the CROPGRO-Soybean model, the methodology proposed by Moreira et al. (2018) should be adopted. Those authors developed for the Agro-IBIS agroecosystem model an equation with a dynamic exponent to reduce the simulated LAI, particularly between stages R5 and R7, because Kucharik and Twine (2007) and Webler et al. (2012) identified in this model, problems similar to CROPGRO-Soybean for LAI simulations.

## 4. CONCLUSIONS

The proposed methodology represents a robust and scalable solution with potential to be used in crop simulation models, decision support systems, and digital platforms dedicated to monitoring and managing agricultural production. The use of an estimated average crop coefficient (Kc) of 0.687, derived from measurements conducted throughout the entire phenological cycle of the soybean cultivar 75I77 RSF IPRO (ULTRA), proved to be an effective procedure for the daily estimation of LAI in soybean cultivars. This approach offers a viable, low-cost, and non-destructive alternative to direct field measurements, particularly advantageous for long-term experiments or under operational constraints. The main finding of this study lies in the close alignment between the estimated Kc and the fixed value of 0.67 used by the CROPGRO-Soybean model (parameter KCAN – canopy light extinction coefficient for the daily PAR, present in the SBGRO.047.ESP file), which governs the attenuation of PAR within the canopy across all phenological stages. This consistency validates the methodology used for Kc estimation, enhances the reliability of LAI modeling under tropical conditions, and provides a sound basis for calibrating and validating agrometeorological models. Moreover, the accurate estimation of LAI based on Kc broadens the scope for studies on radiation interception and biomass accumulation, supporting advancements in yield modeling, climate risk zoning, and optimized crop management strategies. Therefore, the methodology developed in this study emerges as a reliable and applicable tool for sustainable agricultural intensification and its integration into modern monitoring and decision-support frameworks.

## ACKNOWLEDGMENTS

The authors thank the Coordenação de Aperfeiçoamento de Pessoal de Nível Superior (CAPES) / Financing Code 001 for the doctoral fellowship for Marcelo Crestani Mota, as well as the Conselho Nacional de

Desenvolvimento Científico e Tecnológico (CNPq), the Fundação de Amparo à Pesquisa do Estado do Amazonas (FAPEAM), and the Fundação de Apoio à Pesquisa e ao Desenvolvimento (FAPED – EMBRAPA) for the assistance during the fieldwork in Vilhena, RO, Brazil. We are also grateful to the Instituto Nacional de Pesquisas da Amazônia (INPA), the Universidade do Estado do Amazonas (UEA), the Faculdade Marechal Rondon (FARON), and the Brazilian Agricultural Research Corporation – EMBRAPA Agricultura Digital (CNPTIA) for providing the infrastructure and materials used in this research.

## REFERENCES

Adeboye, O.B., Schultz, B., Adekalu, K.O., Prasad, K. (2016). Impact of water stress on radiation interception and radiation use efficiency of Soybeans (*Glycine max* L. Merr.) in Nigeria. *Brazilian Journal of Science and Technology*, 3(15), 2-21.

Allen, R.G., Pereira, L.S. (2009). Estimating crop coefficients from fraction of ground cover and height. *Irrigation Science*, 28(1), 17-34.

Alvares, C.A., Stape, J.L., Sentelhas, P.C., Gonçalves, J.L.M., Sparovek, G. (2013). Köppen climate classification map for Brazil. *Meteorologische Zeitschrift*, 22(6), 711-728

Boote, K.J., Jones, J.W., Hoogenboom, G., Wilkerson, G.G. (1997). Evaluation of the CROPGRO-Soybean model over a wide range of experiments. In: Kropff M.J. et al. (eds) Applications of systems approaches at the field level. Systems Approaches for Sustainable Agricultural Development, vol 6. Springer, Dordrecht.

Boote, K.J., Jones, J.W., Pickering, N.B. (1996). Potential uses and limitations of crop models. *Agronomy Journal*, 88(5), 704-716.

Borrás, L., Slafer, G.A., Otegui, M.E. (2004). Seed dry weight response to source-sink manipulations in wheat, maize and soybean: a quantitative reappraisal. *Field Crops Research*, 86(2-3), 131-146.

Bréda, N.J.J. (2003). Ground-based measurements of leaf area index: a review of methods, instruments and current controversies. *Journal of Experimental Botany*, 54(392), 2403-2417.

Cera, J.C., Streck, N.A., Fensterseifer, C.A.J., Ferraz, S.E.T., Bexaira, K.P., Silveira, W.B., Cardoso, Â.P. (2017). Soybean yield in future climate scenarios for the state of Rio Grande do Sul, Brazil. *Pesquisa Agropecuária Brasileira*, 52(6), 380-392.

Chechi, L., Petry, M.T., Oliveira, Z.B., Dantas, M.K.L., Silva, C.M., Gonçalves, A.F. (2021). Estimativa do índice de área foliar e da fração de cobertura do solo nas culturas de milho e soja usando NDVI. *Irriga*, 26(3), 620-637.

Confalone, A., Vilatte, C., Lázaro, L., Roca, N., Mestelan, S., Aguas, L., Navarro, M., Sal, F. (2016). Parametrización del modelo CROPGRO-soybean su uso como herramienta para evaluar el impacto del cambio climático sobre el cultivo de soja. *Revista de la Facultad de Ciencias Agrarias Uncuyo*, 48(1), 49-64.

Confalone, A., Djumovich, M.N. (1999). Influência do déficit hídrico sobre a eficiência da radiação solar em soja. *Revista Brasileira de Agrociência*, 5(3), 195-198.

Costa, L.C., Confalone, A., Pereira, C.R. (1999). Effect of water stress on the efficiency of capture of water and radiation by soybean. *Tropical Science*, 39, 91-97.

Costa, L.C., Morison, J., Dennett, M. (1996). Carbon balance of growing faba bean and its effect on crop growth: experimental and modelling approaches. *Revista Brasileira de Agrometeorologia*, 4(2), 11-17.

Cox, W.J., Cherney, J.H. (2011). Growth and yield responses of soybean to row spacing and seeding rate. *Agronomy Journal*, 103(1), 123-128.

Crestani Mota, M., Candido, L.A., Cuadra, S.V., Marenco, R.A., Souza, R.V.A., Tomé, A.M., Lopes, A.B.A., Lima, F.L., Reis, J., Brizolla, R.M. (2024). CROPGRO-soybean model – Validation and application for the southern Amazon, Brazil. *Computers and Electronics in Agriculture*, 216, 108478.

Cuadra, S.V., Kimball, B.A., Boote, K.J., Suyker, A.E., Pickering, Nigel. (2021). Energy balance in the DSSAT-CSM-CROPGRO model. *Agricultural and Forest Meteorology*, 297, 108241.

Fehr, W.R., Caviness, C.E. (1977). Stages of soybean development. Ames: Iowa State University of Science and Technology. (Special Report, 80)

Fensterseifer, C.A., Streck, N.A., Baigorria, G.A., Timilsina, A.P., Zanon, A.J., Cera, J.C., Rocha, T.S.M. (2017). On the number of experiments required to calibrate a cultivar in a crop model: the case of CROPGRO-Soybean. *Field Crop Research*, 204, 146-152.

Ferreira, O.G.L., Rossi, F.D., Andrighetto, C. (2008). DDA – Determinador Digital de Áreas: software para determinação de área foliar, índice de área foliar e área de olho de lombo. Versão 2.0. Santo Augusto: IFFarroupilha.

Fontana, D.C., Alves, G.M., Roberti, D., Moraes, O.L.L., Gerhardt, A. (2012). Estimativa da radiação fotossinteticamente ativa absorvida pela cultura da soja através de dados do sensor Modis. *Bragantia*, 71(4), 563-571.

Foster, T., Brozovic, N., Butler, A.P., Neale, C.M.U., Raes, D., Steduto, P., Fereres, E., Hsiaog, T.C. (2017).

AquaCrop-OS: An open source version of FAO's crop water productivity model. *Agricultural Water Management*, 181, 18-22.

Goudriaan, J., Monteith, J.L. (1990). A mathematical function for crop growth based on light interception and leaf area expansion. *Annals of Botany*, 66(6), 695-701.

Hoogenboom, G., Jones, J.W., Porter, C.H., Wilkens, P.W., Boote, K.J., Batchelor, W.D., Hunt, L.A., Tsuji, G.Y. (2003). Decision Suport System Agrotechnology Transfer (DSSAT) Version 4.0 [CD-ROM]. Honolulu, Hawaii: University of Hawaii.

Hoogenboom, G., Jones, J.W., Wilkens, P.W., Porter, C.H., Boote, K.J., Hunt, L.A., Singh, U., Lizaso, J.L., White, J.W., Uryasev, O., Royce, F.S., Ogoshi, R., Gijsman, A.J., Tsuji, G.Y., Koo, J. (2012). Decision Support System for Agrotechnology Transfer (DSSAT) Version 4.5 [CD-ROM]. Honolulu, Hawaii: University of Hawaii.

Jones, H.G. (2014). Plants and microclimate – A quantitative approach to environmental plant physiology. Third Edition. Cambridge University Press.

Jones, J.W., Hoogenboom, G., Porter, C.H., Boote, K.J., Batchelor, W.D., Hunt, L.A., Wilkens, P.W., Singh, U., Gijsman, A.J., Ritchie, J.T. (2003). The DSSAT cropping system model. European Journal Agronomy, 18, 235-265.

Kucharik, C.J., Twine, T.E. (2007). Residue, respiration, and residuals: Evaluation of a dynamic agroecosystem model using eddy flux measurements and biometric data. *Agricultural and Forest Meteorology*, 146(3-4), 134-158.

Li, Y., Chen, D., Walker, C.N., Angus, J.F. (2010). Estimating the nitrogen status of crops using a digital camera. *Field Crops Research*, 118(3), 221-227.

Mayers, J.D., Lawn, R.J., Byth, D.E. (1991a). Agronomic studies on soybean (*Glycine max* L. Merrill) in the dry seasons of the tropics. I. Limits to yield imposed by phenology. *Australian Journal of Agricultural Research*, 42(7), 1075-1092.

Mayers, J.D., Lawn, R.J., Byth, D.E. (1991b). Agronomic studies on soybean (*Glycine max* L. Merrill) in the dry seasons of the tropics. II. Interaction of sowing date and sowing density. *Australian Journal of Agricultural Research*, 42(7), 1093-1107.

Monsi, M., Saeki, T. (1953). Über den Lichtfaktor in den Pflanzengesellschaften und seine Bedeutung für die Stoffproduktion. *Japanese Journal of Botany*, 14, 22-52.

Moreira, E.N., Vale, F.X.R., Paul, P.A., Rodrigues, F.A., Jesus Júnior, W.C. (2015). Temporal dynamics of soybean rust associated with leaf area index in soybean cultivars of different maturity groups. *Plant Disease*, 99(9), 1216-1226.

Moreira, V.S., Candido, L.A., Mota, M.C., Webler, G., Oliveira, E.P., Roberti, D.R. (2023). Impacts of climate change on water fluxes and soybean growth in southern Brazil. *Revista Ciência Agronômica*, 54, e20228398.

Moreira, V.S., Candido, L.A., Roberti, D.R., Webler, G., Diaz, M.B., Gonçalves, L.G.G., Pousa, R., Degrazia, G.A. (2018). Influence of soil properties in different management systems: Estimating soybean water changes in the Agro-IBIS model. *Earth Interactions*, 22(4), 1-19.

Mota, M.C. (2019). Análise de risco edafoclimático para a soja cultivada na região do Cone Sul de Rondônia: diagnóstico atual e em cenários futuros do clima. PhD Thesis, Instituto Nacional de Pesquisas da Amazônia (INPA), Brasil.

Muchow, R.C. (1985). An analysis of the effects of water deficits on grains legumes grown in a semi-arid tropical environment in terms of radiation interception and its efficiency of use. *Field Crops Research*, 11(4), 309-323.

Müller, A.G., Bergamaschi, H., Silva, M.I.G. (2001). Eficiências de interceptação, absorção e de uso da radiação fotossinteticamente ativa pelo milho (*Zea mays* L.), em diferentes disponibilidades hídricas. In: Congresso Brasileiro de Agrometeorologia, 12. e Reunião Latino-Americana de Agrometeorologia, 3. Fortaleza. Anais [...]. Fortaleza: Sociedade Brasileira de Agrometeorologia.

Mundstock, C.M., Thomas, A.L. (2005). Soja: fatores que afetam o crescimento e o rendimento de grãos. Porto Alegre: Departamento de plantas de lavoura da Universidade Federal do Rio Grande do Sul: Evangraf.

Nóia Júnior, R.S., Sentelhas, P.C. (2019). Soybean-maize sucession in Brazil: Impacts of sowing dates on climate variability, yields and economic profitability. *European Journal of Agronomy*, 103, 140-151.

Paredes, P., Rodrigues, G.C., Cameira, M.R., Torres, M.O., Pereira, L.S. (2017). Assessing yield, water productivity and farm economic returns of malt barley as influenced by the sowing dates and supplemental irrigation. *Agricultural Water Management*, 179, 132-143.

Pengelly, B.C., Blamey, F.P.C., Muchow, R.C. (1999). Radiation interception and accumulation of biomass and nitrogen by soybean and three tropical annual forage legumes. *Field Crops Research*, 63(2), 99-112.

Petter, F.A. (2016). Elevada densidade de semeadura aumenta a produtividade da soja? Respostas da radiação fotossinteticamente ativa. *Bragantia*, 75(2), 173-183.

Plénet, D., Mollier, A., Pellerin, S. (2000). Growth analysis of maize field crops under phosphorus deficiency. II.

Radiation-use efficiency, biomass accumulation and yield components. *Plant and Soil*, 224(2), 259-272.

Purcell, L.C., Ball, R.A., Reaper, J.D., Vories, E.D. (2002). *Crop Science*, 42(1), 172-177.

Sakamoto, T., Wardlow, B.D., Gitelson, A.A., Verma, S.B., Suyker, A.E., Arkebauer, T.A. (2010). Two-step filtering approach for detecting maize and soybean phenology with time-series MODIS data. *Remote Sensing of Environment*, 114(10), 2146-2159.

Salvagiotti, F., Cassman, K.G., Specht, J.E., Walters, D.T., Weiss, A., Dobermann, A. (2008). Nitrogen uptake, fixation and response to fertilizer N in soybeans: A review. *Field Crops Research*, 108(1), 1-13.

Santos, J.B., Procópio, S.O., Silva, A.A., Costa, L.C. (2003). Captação e aproveitamento da radiação solar pelas culturas da soja e do feijão e por plantas daninhas. *Bragantia*, 62(1), 147-153.

Schöffel, E.R., Volpe, C.A. (2001). Eficiência de conversão da radiação fotossinteticamente ativa interceptada pela soja para a produção de fitomassa. *Revista Brasileira de Agrometeorologia*, 9(2), 241-249.

Shibles, R.M., Weber, C.R. (1966). Interception of solar radiation and dry matter production by various soybean planting patterns. *Crop Science*, 6(1), 55-59.

Shibles, R.M., Weber, C.R. (1965). Leaf area, solar radiation and dry matter production by soybeans. *Crop Science*, 5(6), 575-577.

Souza, P.J.O.P., Ribeiro, A., Rocha, E.J.P., Farias, J.R.B., Loureiro, R.S., Bispo, C.C., Sampaio, L. (2009). Solar radiation use efficiency by soybean under field conditions in the Amazon region. *Pesquisa Agropecuária Brasileira*, 44(10), 1211-1218.

Srinivasan, V., Kumar, P., Long, S.P. (2017). Decreasing, not increasing, leaf area will raise crop yields under global atmospheric change. *Global Change Biology*, 23(4), 1626-1635.

Steinmetz, S., Siqueira, O.J.W. (1995). Eficiência de conversão em biomassa da radiação solar interceptada pela cultura do arroz irrigado submetida a níveis diferenciados de adubação nitrogenada. In: Congresso Brasileiro de Agrometeorologia, 9. Campina Grande. Anais [...]. Campina Grande: Sociedade Brasileira de Agrometeorologia.

Steinmetz, S.; Siqueira, O.J.W. (2001). Eficiência de conversão em biomassa da radiação solar interceptada nas distintas fases do ciclo de três tipos de planta de arroz irrigado. in: Congresso Brasileiro de Agrometeorologia, 12. e Reunião Latino-Americana de Agrometeorologia, 3., 2001, Fortaleza. Anais [...]. Fortaleza: Sociedade Brasileira de Agrometeorologia.

Tagliapietra, E.L., Streck, N.A., Rocha, T.S.M., Richter, G.L., Silva, M.R., Cera, J.C., Guedes, J.V.C., Zanon, A.J. (2018). Optimum leaf area index to reach soybean yield potential in subtropical environment. *Agronomy Journal*, 110(3), 932-938.

Taiz, L., Zeiger, E. (2004). Fisiologia vegetal. 3.ed. Porto Alegre: Artmed.

Thimijan, R.W., Heins, R.D. (1983). Photometric, radiometric, and quantum light units of measure: a review of procedures for interconversion. *HortScience*, 18(6), 818-822.

Webler, G., Cuadra, S.V., Moreira, V.S., Costa, M.H. (2012). Evaluation of a dynamic agroecosystem model (Agro-IBIS) for soybean in Southern Brazil. *Earth Interactions*, 16(12), 1-15.

Willmott, C.J. (1982). Some comments on the evaluation of model performance. *Bulletin of Meteorological Society*, 63(11), 1309-1313

Yokoyama, A.H., Balbinot Junior, A.A., Zucareli, C., Ribeiro, R.H. (2018). Índice da área foliar e SPAD durante o ciclo da soja em função da densidade de plantas e sua relação com a produtividade de grãos. *Revista de Ciências Agroveterinárias*, 17(4), 531-538.

Zdziarski, A.D., Todeschini, M.H., Milioli, A.S., Woyann, L.G., Madureira, A., Stoco, M.G., Benin, G. (2018). Key soybean maturity groups to increase grain yield in Brazil. *Crop Science*, 58(3), 1155-1165.

Italian Journal of Agrometeorology
Rivista Italiana di Agrometeorologia

Firenze University Press
https://riviste.fupress.net/index.php/IJAm

OPEN ACCESS

**Citation:** Fettam, D., Gherissi, R. & Otmane, A. (2025). Trend analysis of monthly rainfall data using the Innovative Polygon Trend Analysis (IPTA) in the Tafna Watershed (Northwestern Algeria). *Italian Journal of Agrometeorology* (1): 31-42. doi: 10.36253/ijam-3110

**Received:** November 14, 2024

**Accepted:** June 2, 2025

**Published:** August 27, 2025



**Data Availability Statement:** All relevant data are within the paper and its Supporting Information files.

**Competing Interests:** The Author(s) declare(s) no conflict of interest.

**ORCID:**
DF: 0009-0000-6766-0642
RG: 0000-0002-1248-8483
AO: 0000-0002-0646-3327

# Trend analysis of monthly rainfall data using the Innovative Polygon Trend Analysis (IPTA) in the Tafna Watershed (Northwestern Algeria)

Djillali Fettam[1,2,*], Radia Gherissi[1,2], Abdelkader Otmane[2,3]

[1] *Department of Hydraulics, Institute of Science and Technology, University Centre of Maghnia, 13300 Tlemcen, Algeria*
[2] *Laboratory n° 25, Promotion of the Water Resources, Mines and Pedological. Legislation of the Environment and Technological Choices, University of Tlemcen, 13300 Tlemcen, Algeria*
[3] *Faculty of Natural Sciences and Life, Ibn Khaldoun Tiaret University, Karman, BP14000, Tiaret, Algeria*
*Corresponding author. Email: d.fettam@cu-maghnia.dz

**Abstract.** Trend analysis of hydroclimatic data is essential for assessing climate variability. Precipitation is an important parameter affected by climate change in the Mediterranean climate, particularly in sensitive regions like the Tafna watershed in Northwestern Algeria. This study used the Innovate Polygon Trend Analysis (IPTA) to study the change between two successive months. Additionally, the Mann-Kendall (MK) test was compared to the IPTA method in detecting trends. Total monthly rainfall data was collected from 14 stations in the Tafna watershed over 50 years from the hydrological year 1970-71 to 2019-20. The maximum trend length using the IPTA method was found in the transition May-June for most stations. The MK test does not indicate any significant trend (increase and decrease) in most of the months at all stations. In contrast, the IPTA method shows an increasing trend in October and January in all stations; August, September, November, and December show an increasing trend in most stations. A decreasing trend was found in February and March at all stations and in May at most stations. The results showed that the MK test detected a significant trend in 6.5% of the total months analyzed in this study, whereas the IPTA method identified a trend in 88.7% of the total months. The findings revealed that the IPTA method was more sensitive to detecting trends in precipitation data than the MK test, which suggests the IPTA method could be a valuable tool for assessing trends of precipitations in the Tafna watershed.

**Keywords:** rainfall, trend, Mann-Kendall test, IPTA, Tafna Watershed.

## 1. INTRODUCTION

Precipitation is one of the most important components of the hydrological cycle and the environment, particularly in regions with a Mediterranean climate, where it is significantly affected by climate change (Şan et al., 2024). Several precipitation variability and trends studies have been conducted in the Mediterranean basin to understand this effect better (Khomsi

et al., 2015; Longobardi & Villani, 2010; Martínez et al., 2007; Mehta & Yang, 2008; Nouaceur & Murărescu, 2016; Philandras et al., 2011; Tramblay et al., 2013). In Algeria, many researchers have studied spatiotemporal trends of precipitation in many parts of the country, such as Meddi and Meddi (2009), Meddi et al. (2010), Ghenim and Megnounif (2016), Taibi et al. (2017), Bessaklia et al. (2018), Otmane et al. (2018), Merniz et al. (2019), and Gherissi et al. (2021).

One of the classical methods to detect trends in hydrometeorological data is the Mann-Kendall (MK) test (Kendall, 1975; Mann, 1945). In Algeria, the MK test was used to indicate the trend of rainfall at different time scales in many studies, such as in the North-East (Merniz et al., 2019; Mrad et al., 2018), in the northern part of Algeria (Ghenim & Megnounif, 2016; Ghorbani et al., 2021), in the North-West of Algeria, such as in two watersheds Coastal-Oran and Macta (Oufrigh et al., 2023), in the Macta watershed (Benzater et al., 2024). One of the latest graphical methods developed for detecting trends, especially at the monthly scale, is the Innovate Polygon Trend Analysis (IPTA) method developed by Şen et al. (2019). It was recently used to detect the trend in some regions in Algeria, such as in the Wadi Sly Basin (Achite et al., 2021), in the North Coast Algerian (Boudiaf et al., 2022), and in the Wadi Mina Basin (Hallouz et al., 2024).

Many studies around the world compared the IPTA method with the MK test, such as Hallouz et al. (2024) in Algeria; Akçay et al. (2022), Hırca et al. (2022), Esit (2023), and Esit et al. (2024) in Turkey; and Şan et al. (2021) in Vietnam. All these researchers found that the IPTA method was more sensitive in detecting trends with precipitation data than the MK test.

In the Tafna watershed, Bougara et al. (2020) used the MK test to identify the trend in precipitations for nine stations from 1979–2011. The findings showed an increasing trend in rainfall in September and October, meaning the increase was found in autumn. Bouklikha et al. (2021) used the Innovate Trend Analysis (ITA) method to identify the trend in rainfall time series for 17 stations over the period 1970-2016; the results showed a decreasing trend in February, March, April, and May in all stations, June and July for the majority of stations.

This study aims to analyze monthly precipitation trends in the Tafna watershed using data from 14 rainfall stations over a 50-year period (1970-71 to 2019-20). To achieve this, both the Mann-Kendall (MK) test and the Innovate Polygon Trend Analysis (IPTA) method are employed to examine monthly rainfall trends. Notably, the IPTA method uniquely allows for the analysis of trend patterns between two consecutive months. The study is structured around two main objectives: (1) investigating trends between consecutive months using the IPTA method, and (2) comparing the effectiveness of the MK test and IPTA in detecting monthly precipitation trends.

## 2. STUDY AREA AND DATA

The research area is located in the Tafna watershed in (Northwestern Algeria), covering an area of 7200 km$^2$. It is situated between latitude North 34°3' and 35°9' and longitude West 1° and 2°, and its altitude is between 0 and 1773 m (Figure. 1). Monthly precipitation data of 14 rainfall stations from 1970-71 to 2019-20 was collected from the National Hydraulic Resources Agency (ANRH) (https://anrh.dz/). The names of the stations, their IDs, coordinates (longitude, latitude), and elevation are presented in Table 1. The selection of stations was based on the duration of the time series and their spatial distribution, ensuring comprehensive coverage of the study area. The analysis period for the selected stations extended over 50 years, started with the hydrological year 1970–1971, which begins in September and closes in August. The selected data demonstrates a highly uniform distribution within the research area.

## 3. METHODOLOGY

### *3.1 IPTA method*

The Innovate Polygon Trend Analysis (IPTA) method developed by Şen et al. (2019) was modified recently

**Table 1.** The rainfall stations utilized in this study

| Station | Name | ID | Longitude (DD) | Latitude (DD) | Elevation (m) |
|---|---|---|---|---|---|
| S1 | Maghnia | 160302 | -1.80254 | 34.79900 | 395 |
| S2 | Sebdou | 160401 | -1.32548 | 34.65515 | 875 |
| S3 | Beni Bahdel | 160403 | -1.50369 | 34.71165 | 660 |
| S4 | Sidi Medjahed | 160407 | -1.64262 | 34.77520 | 360 |
| S5 | Sebra | 160502 | -1.52886 | 34.82671 | 600 |
| S6 | Hennaya | 160516 | -1.38812 | 34.92100 | 515 |
| S7 | Zaouia Ben Amar | 160517 | -1.65752 | 35.03999 | 370 |
| S8 | Djebel Chouachi | 160518 | -1.49698 | 35.05436 | 110 |
| S9 | Oued Lakhdar | 160601 | -1.13454 | 34.86408 | 700 |
| S10 | Meurbah | 160602 | -1.17134 | 34.74197 | 1100 |
| S11 | Ouled Mimoun | 160607 | -1.03406 | 34.90429 | 705 |
| S12 | Mefrouche | 160701 | -1.28586 | 34.84734 | 1110 |
| S13 | Lalla Setti | 160705 | -1.30650 | 34.86604 | 1020 |
| S14 | Pierre Du Chat | 160802 | -1.43970 | 35.14572 | 80 |

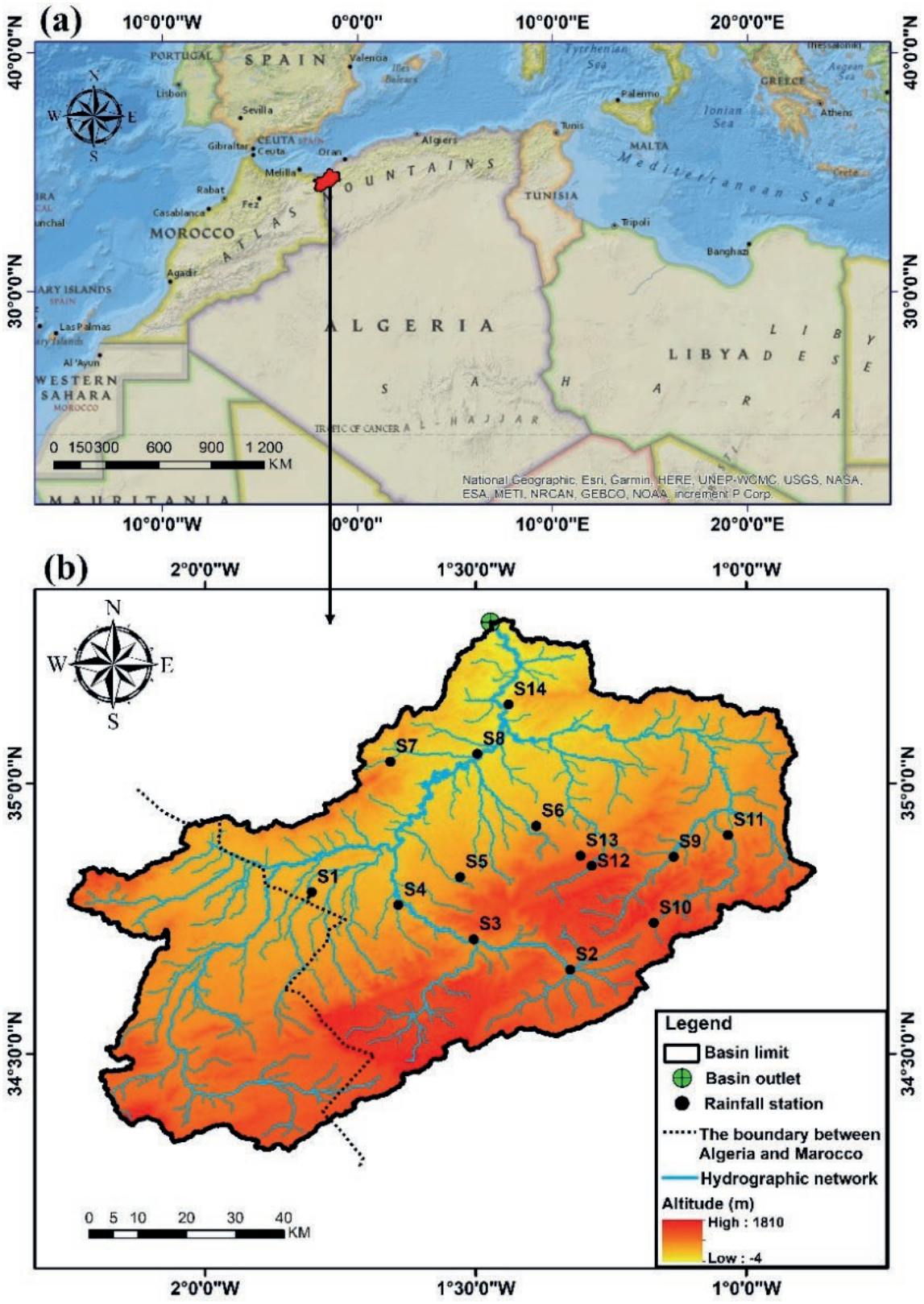


**Figure 1.** Study area: (a) location of the Tafna watershed in Algeria, (b) DEM, Hydrographic Network, and location of rainfall stations used in this study.

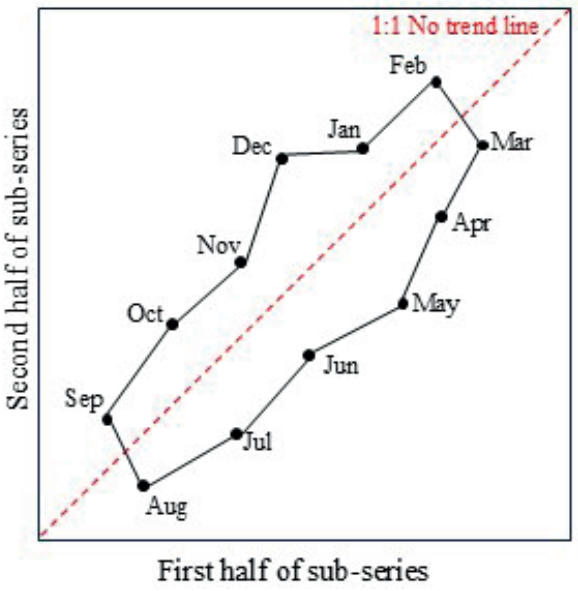


**Figure 2.** IPTA template for monthly records.

from the Innovate Trend analysis (ITA) created by Şen (2012). This study applied the IPTA method to monthly precipitation data following seven processing steps. Step (1): the monthly precipitation data was divided into two equal periods. Step (2): the monthly mean for each month is calculated in both periods. Step (3): the first and second periods are placed on the horizontal and vertical axis in a cartesian coordinate system. Step (4): the points of consecutive months are joined by straight lines that result in a polygon (Figure. 2).

Step (5): the trend length (TL) and the trend slope (TS) between consecutive points were calculated as follows:

$$|TL| = \sqrt{(x_2 - x_1)^2 + (y_2 - y_1)^2} \quad (1)$$

$$TS = \frac{y_2 - y_1}{x_2 - x_1} \quad (2)$$

Where TL and TS are trend length and trend slope, x1 and x2 are two consecutive months in the first period, and y1 and y2 are two consecutive months in the second period. The TL indicates the magnitude of change in precipitation (mm) between two consecutive months, while the TS reflects the direction and rate of this change. Step (6): Draw the no-trend line (1:1 line) at 45° in the cartesian coordinate system. Step (7): The months above the no-trend line indicate an increasing trend, whereas the months below the no-trend line indicate a decreasing trend, while the months found on the no-trend line do not show any trend. According to Boudiaf et al. (2022), the trend length can be classified into four categories as follows.

1) weak for 0 < TL < 30 mm,
2) medium for 30 mm < TL < 50 mm,
3) strong for 50 mm < TL < 75 mm,
4) very strong for TL > 75 mm.

Although the TS is computed as part of the IPTA method, it is not a central focus of the present study. The interpretation of monthly trends relies primarily on the TL and its visual positioning relative to the no-trend line. These thresholds are empirical and not based on statistical significance testing. Unlike the Mann-Kendall test, the IPTA method does not offer a formal statistical framework, which represents a known limitation of this graphical technique. However, it provides a valuable visual and comparative assessment of monthly changes that complements statistical approaches.

### *3.2 Mann-Kendall (MK) trend test*

One of the non-parametric tests used to detect trends is the MK test (Kendall, 1975; Mann, 1945), which is particularly useful for meteorological, climatological, and hydrological time series. The following equations give the MK test statistic (S):

$$S = \sum_{i=1}^{n-1} \sum_{j=i+1}^{n} sgn(x_j - x_i) \quad (3)$$

$$sgn(\mathrm{x_j} - \mathrm{x_i}) = \begin{cases} +1 & if\ (\mathrm{x_j} - \mathrm{x_i}) > 0 \\ 0 & if (\mathrm{x_j} - \mathrm{x_i}) = 0 \\ -1 & if (\mathrm{x_j} - \mathrm{x_i}) < 0 \end{cases} \quad (4)$$

Where xi and xj represent the data points in periods i and j, while the amount of data series is larger than or equivalent to ten (n ≥ 10), since n ≥ 10, the MK test is then categorised by a standard distribution with the mean E(S) = 0 and variance Var(S) given as:

$$Var(S) = \frac{n(n-1)(2n+5) - \sum_{k=1}^{m} t_k(t_k-1)(2t_k+5)}{18} \quad (5)$$

Where m is the number of the tied groups in the time series and $t_k$ is the number of ties in the $k_{th}$ tied group. From this, the test Z statistics is obtained using an approximation as follows:

$$Z = \begin{cases} \frac{\mathrm{s}-1}{\sqrt{\mathrm{Var(S)}}} & if \quad S > 0 \\ 0 & if \quad S = 0 \\ \frac{\mathrm{s}+1}{\sqrt{\mathrm{Var(S)}}} & if \quad S < 0 \end{cases} \quad (6)$$

In a Z test, the null hypothesis ($H_0$) indicates no trend in the time series, the alternative hypothesis ($H_a$) indicates a significant change. At the 5% significance level, negative values indicate decreasing trends, and positive values indicate an increasing trend. If $|Z| > 1.96$, $H_0$ is rejected (Sneyers, 1990).

## 4. RESULTS AND DISCUSSION

### *4.1 IPTA results*

IPTA graphics are shown in Figure 3 for Maghnia, Sebdou, Beni Bahdel, Sidi Medjahed, Sebra, Hennaya stations, in Figure 4 for Zaouia Ben Amar, Djebel Chouachi, Oued Lakhder, Meurbah, Ouled Mimoun, and Mefrouche stations, and in Figure 5 for Lalla Setti, and Pierre Du Chat stations. The rainiest month during the first half of 1970-71/1994-95 is March in all stations, with an average of 54.1 mm for Sidi Medjahed, Djebel Chouachi, Ouled Mimoun, Pierre Du Chat, and Maghnia Stations, an average of 70.5 mm for Sebdou, Meurbah, and Sebra stations, an average of 79.7 mm for Zaouia Ben Amar, Oued Lakhdar, Beni Bahdel, and Hennaya stations. The highest values were found in Lalla Setti (103.7 mm) and Mefrouche stations (121.5 mm). The driest month during the first half of 1970-71/1994-95 is July in Maghnia, Sebdou, Hennaya, Djebel Chouachi, and Pierre du chat stations, with values not exceeding 4.5 mm; for the other stations, the driest month is August with values not exceeding 4.9 mm. The rainiest month during the second half of 1995-96/2019-20 in November for the half of stations such as Maghnia, Sidi Medjahed, and Djebel Chouachi stations with an average of 45.6 mm, Hennaya and Sebra stations with an average of 59.4 mm, the highest values were found in Lalla Setti (76.8 mm) and Mefrouche stations (85 mm). for the other half of stations January is the rainiest month. The driest month during the second half of 1995-96/2019-20 is July in all stations, with values not exceeding 6.4 mm.

Table 2 shows statistical values (trend length and trend slope) of arithmetic mean for each station. The maximum trend slopes were observed in the transition July-August, with values of 21.62, -8.0, -32.28, -32.39, -7.13, 2.79, -7.85, -14.94, and 9.68 for the Maghnia, Beni Bahdel, Sidi Medjahed, Sebra, Zaouia Ben Amar, Djebel Chouachi, Meurbah, Ouled Mimoun, and Pierre Du Chat stations, respectively. Additionally, trend slopes of 10.66, -8.37, and 4.38 were recorded in the transition April-May for the Sebdou, Mefrouche, and Lalla Setti stations, respectively. A trend slope of 2.77 was observed in the transition November-December for the Hennaya station and -13.3 in the transition December-January for the Oued Lakhdar station.

The trend length is weak in all stations in the transition of November-December, December-January, January-February, June-July, July-August, and August-September. The trend length is medium in the transition September-October in Mefrouche and Pierre du chat stations, in the transition October-November in Beni Bahdel, Hennaya, Zaouia Ben Amar, Oued Lakhdar, and Lalla Setti stations, in the transition February-March in Mefrouche and Lalla Setti stations, in the transition March-April in Beni Bahdel, Zaouia Ben Amar, and Lalla Setti stations, in the transition April-May Mefrouche station only, in the transition May-June for most of stations such as Maghnia, Sebdou, Beni Bahdel, Sidi Medjahed, Sebra, Hennaya, Zaouia Ben Amar, Oued Lakhdar, Meurbah, and Ouled Mimoun stations. The trend length is strong in the transition of October-November, March-April, and May-June in Mefrouche station. The transition May-June also shows another strong trend length in Lalla Setti station. The maximum trend length was found in the transition May-June (ranging between 31.09 mm and 69.66 mm) for most stations, and these strongest values explain the change between the two seasons, from Spring to Summer.

### *4.2 Comparison between the IPTA method and the MK test*

Table 3 shows the results of the MK test on monthly rainfall data for all stations. It clearly appears that there is no significant trend in most months for all stations. An increasing trend is found in September at Beni Bahdel and Meurbah stations, in October at Beni Bahdel and Sidi Medjahed stations. Whereas, a decreasing trend appears in February at Sebra and Hennaya stations, in March at Pierre Du Chat station, in June and July at Maghnia and Ouled Mimoun stations.

Bougara et al. (2020) studied the trend analysis in the Tafna watershed using the MK test for a period of data from 1979 to 2011 with some stations can found in this study such as Sebdou, Beni Bahdel, Djbel Chouachi, Hennaya, Oued Lakhder (ex-Chouly), Meurbah, and Ouled Mimoun stations. The results showed a significant increasing trend for rainfall in two months only (September and October) for most of stations, the other months do not show any trend except August at Meurbah station, wich indicated an increasing trend. The variations observed among stations and throughout different months underline the complexity of precipitation trends in this region. The study's extended timeframe and inclusion of more stations improve the understanding of the spatial and temporal variability in precipita-

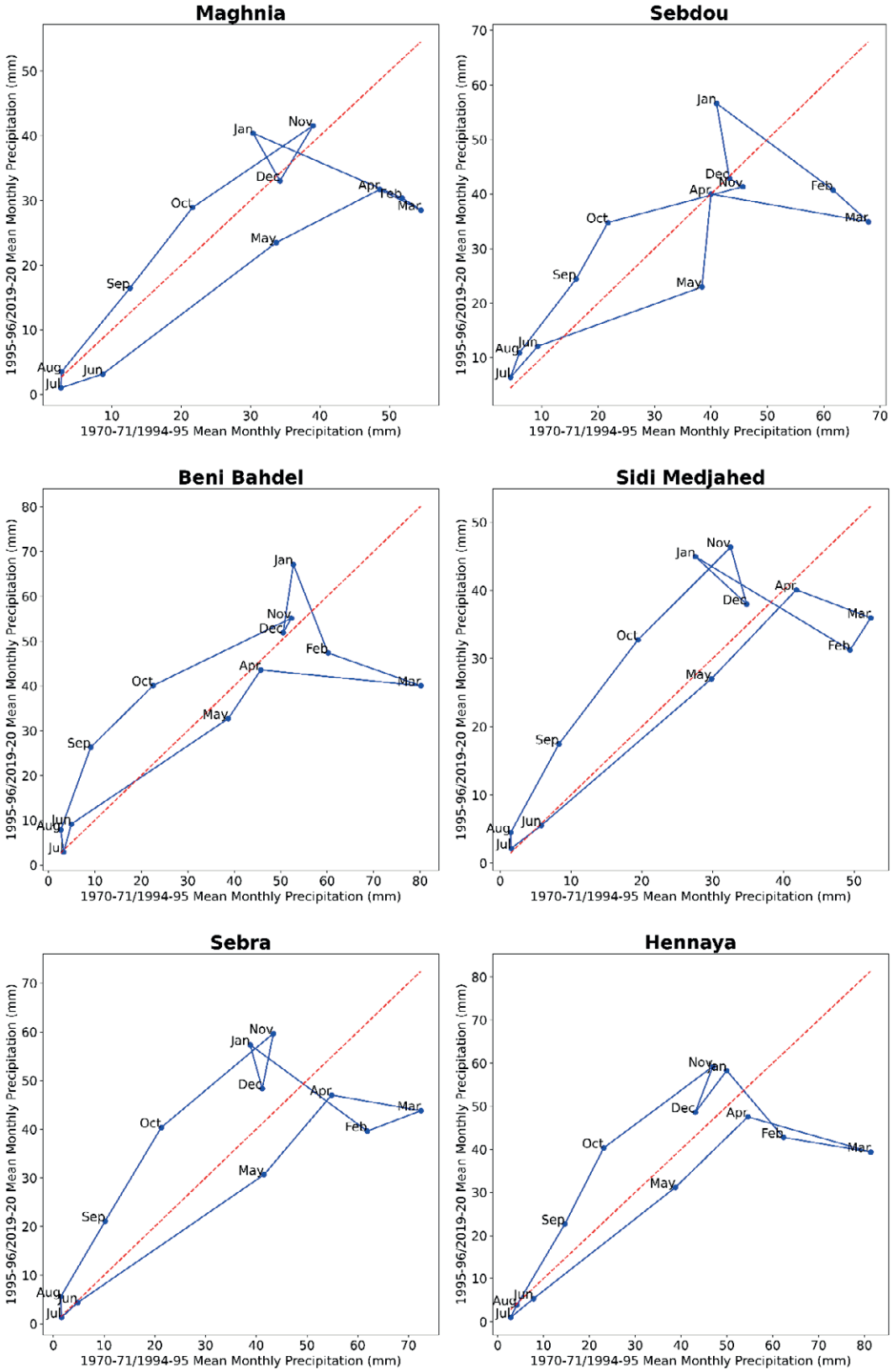


**Figure 3.** IPTA graphics for Maghnia, Sebdou, Beni Bahdel, Sidi Medjahed, Sebra, Hennaya stations.

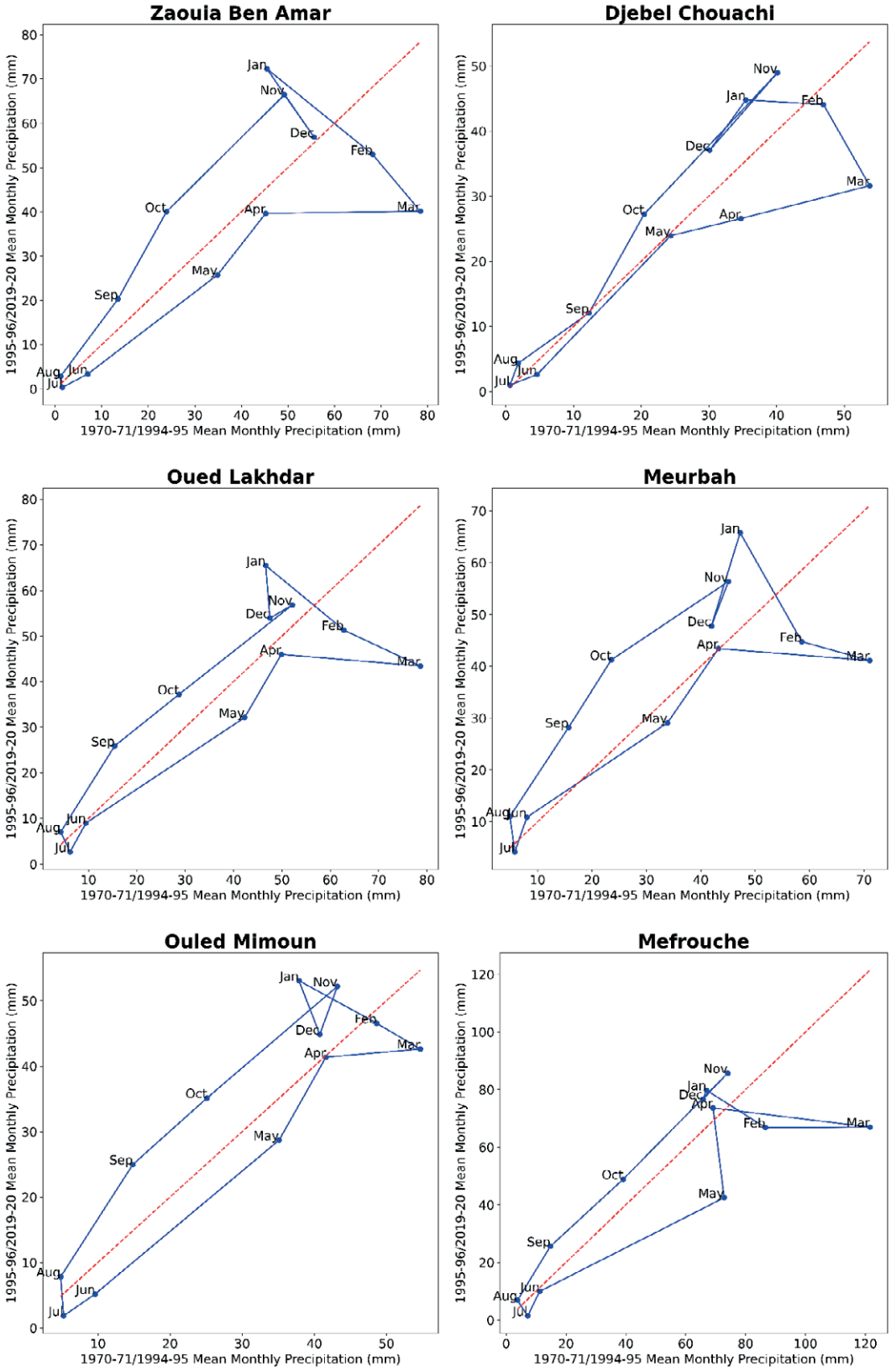


**Figure 4.** IPTA graphics for Zaouia Ben Amar, Djebel Chouachi, Oued Lakhder, Meurbah, Ouled Mimoun, and Mefrouche stations.

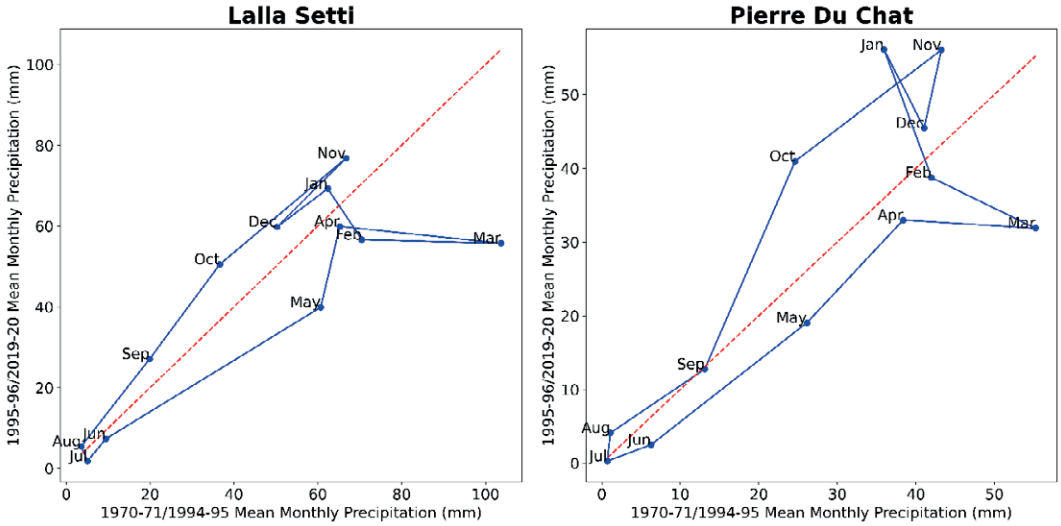


**Figure 5.** IPTA graphics for Lalla Setti, and Pierre Du Chat stations.

**Table 2.** Statistical values of arithmetic mean for each station.

| | | Sep-Oct | Oct-Nov | Nov-Dec | Dec-Jan | Jan-Feb | Feb-Mar | Mar-Apr | Apr-May | May-Jun | Jun-Jul | Jul-Aug | Aug-Sep |
|---|---|---|---|---|---|---|---|---|---|---|---|---|---|
| S1 | TL (mm) | 15.38 | 21.46 | 9.75 | 8.31 | 23.67 | 3.31 | 6.72 | 17.03 | 32.22 | 6.43 | 2.51 | 16.26 |
| | TS | 1.38 | 0.73 | 1.79 | -1.90 | -0.47 | -0.69 | -0.54 | 0.55 | 0.81 | 0.36 | 21.62 | 1.31 |
| S2 | TL (mm) | 11.76 | 24.84 | 2.83 | 13.94 | 26.05 | 8.59 | 28.38 | 17.09 | 31.09 | 7.45 | 4.76 | 16.86 |
| | TS | 1.84 | 0.28 | -0.64 | -5.97 | -0.77 | -0.93 | -0.18 | 10.66 | 0.37 | 1.17 | 2.85 | 1.34 |
| S3 | TL (mm) | 19.29 | 33.31 | 3.67 | 15.43 | 21.17 | 21.28 | 34.64 | 12.94 | 41.18 | 6.48 | 5.00 | 19.53 |
| | TS | 1.03 | 0.51 | 1.84 | 6.97 | -2.64 | -0.37 | -0.10 | 1.55 | 0.70 | 3.80 | -8.00 | 2.87 |
| S4 | TL (mm) | 18.93 | 18.85 | 8.65 | 10.03 | 25.75 | 5.54 | 11.29 | 17.71 | 32.25 | 5.43 | 2.33 | 14.66 |
| | TS | 1.37 | 1.04 | -3.70 | -0.96 | -0.63 | 1.61 | -0.39 | 1.09 | 0.89 | 0.79 | -32.28 | 1.90 |
| S5 | TL (mm) | 22.21 | 29.32 | 11.55 | 9.33 | 29.11 | 11.37 | 17.89 | 21.08 | 45.16 | 4.42 | 4.28 | 17.80 |
| | TS | 1.74 | 0.87 | 5.18 | -3.77 | -0.77 | 0.40 | -0.18 | 1.23 | 0.72 | 0.96 | -32.39 | 1.77 |
| S6 | TL (mm) | 19.58 | 30.37 | 11.27 | 11.89 | 19.86 | 19.34 | 28.03 | 22.75 | 40.35 | 6.61 | 3.20 | 21.50 |
| | TS | 2.08 | 0.79 | 2.77 | 1.41 | -1.25 | -0.18 | -0.31 | 1.04 | 0.83 | 0.88 | 2.11 | 1.80 |
| S7 | TL (mm) | 22.28 | 36.63 | 11.55 | 18.46 | 29.80 | 16.41 | 33.24 | 17.31 | 35.74 | 6.26 | 2.56 | 21.33 |
| | TS | 1.89 | 1.04 | -1.50 | -1.52 | -0.85 | -1.25 | 0.02 | 1.34 | 0.80 | 0.56 | -7.13 | 1.42 |
| S8 | TL (mm) | 17.24 | 29.33 | 15.55 | 9.41 | 11.50 | 14.21 | 19.70 | 10.71 | 29.07 | 4.31 | 3.54 | 13.02 |
| | TS | 1.86 | 1.10 | 1.19 | 1.45 | -0.06 | -1.83 | 0.27 | 0.25 | 1.08 | 0.40 | 2.79 | 0.74 |
| S9 | TL (mm) | 17.50 | 30.53 | 5.46 | 11.58 | 21.46 | 17.69 | 28.86 | 15.80 | 40.14 | 7.14 | 4.80 | 21.88 |
| | TS | 0.85 | 0.84 | 0.63 | -13.30 | -0.88 | -0.50 | -0.09 | 1.82 | 0.70 | 1.93 | -2.28 | 1.69 |
| S10 | TL (mm) | 15.23 | 26.30 | 9.16 | 18.78 | 23.89 | 12.98 | 27.89 | 17.13 | 31.63 | 7.05 | 6.90 | 20.29 |
| | TS | 1.66 | 0.70 | 2.74 | 3.41 | -1.85 | -0.29 | -0.08 | 1.53 | 0.70 | 3.00 | -7.85 | 1.59 |
| S11 | TL (mm) | 14.44 | 24.85 | 7.74 | 8.70 | 12.58 | 7.21 | 13.14 | 14.24 | 34.66 | 5.52 | 5.99 | 19.86 |
| | TS | 0.99 | 0.94 | 3.00 | -2.84 | -0.60 | -0.65 | 0.10 | 1.95 | 0.92 | 0.76 | -14.94 | 1.71 |
| S12 | TL (mm) | 33.69 | 50.72 | 12.20 | 3.28 | 23.63 | 34.90 | 52.85 | 31.40 | 69.66 | 9.39 | 6.38 | 21.72 |
| | TS | 0.96 | 1.06 | 1.09 | 2.77 | -0.66 | 0.00 | -0.13 | -8.37 | 0.53 | 2.11 | -1.60 | 1.71 |
| S13 | TL (mm) | 28.71 | 40.01 | 23.68 | 15.38 | 15.02 | 33.20 | 38.66 | 20.53 | 60.69 | 7.09 | 3.95 | 27.11 |
| | TS | 1.40 | 0.87 | 1.03 | 0.78 | -1.56 | -0.03 | -0.11 | 4.38 | 0.64 | 1.26 | -2.51 | 1.33 |
| S14 | TL (mm) | 30.47 | 23.98 | 10.84 | 11.82 | 18.41 | 14.91 | 16.89 | 18.55 | 25.85 | 6.00 | 3.85 | 14.80 |
| | TS | 2.45 | 0.81 | 4.82 | -2.09 | -2.87 | -0.52 | -0.07 | 1.14 | 0.83 | 0.40 | 9.68 | 0.72 |

**Table 3.** Results of the MK test on monthly rainfall data for all stations (significant values in bold at ≤ 0.05 level of significance)

| | Sep | Oct | Nov | Dec | Jan | Feb | Mar | Apr | May | Jun | Jul | Aug |
|---|---|---|---|---|---|---|---|---|---|---|---|---|
| S1 | 0.737 | 1.398 | 0.318 | 0.000 | 0.703 | -1.782 | -1.815 | -1.430 | -0.778 | **-2.182** | **-2.004** | -1.004 |
| S2 | 1.733 | 1.449 | -0.527 | -0.418 | 0.100 | -1.397 | -1.372 | 0.084 | -1.481 | 0.151 | 1.000 | 0.604 |
| S3 | **2.988** | **1.974** | 0.125 | -0.184 | 0.477 | -1.163 | -1.280 | -0.368 | -0.125 | 1.155 | 0.569 | 1.384 |
| S4 | 1.398 | **2.085** | 1.882 | 0.485 | 1.138 | -1.832 | -1.021 | -0.159 | 0.142 | 0.200 | 1.219 | 2.313 |
| S5 | 1.801 | 1.518 | 1.732 | 0.134 | 1.096 | **-2.267** | -1.573 | -0.995 | -0.343 | -0.353 | 0.435 | 1.888 |
| S6 | 0.854 | 1.514 | 1.397 | 0.042 | 0.736 | **-1.974** | -1.857 | -0.318 | -0.611 | -1.307 | -0.511 | -0.979 |
| S7 | 1.811 | 1.842 | 1.497 | -0.611 | 1.757 | -1.314 | -1.958 | -0.636 | -0.627 | -0.103 | -0.646 | 1.516 |
| S8 | 0.394 | 0.988 | 0.728 | 0.176 | 0.636 | -0.870 | -1.865 | -1.297 | 0.376 | -0.526 | 0.000 | 1.140 |
| S9 | 1.189 | 0.569 | -0.176 | 0.184 | 1.071 | -0.803 | -1.631 | -0.410 | -0.326 | -0.354 | -0.329 | 1.290 |
| S10 | **2.394** | 1.372 | 0.845 | -0.477 | 0.996 | -0.820 | -1.949 | 0.402 | 0.033 | 0.862 | 1.344 | 1.567 |
| S11 | 1.080 | 0.662 | 1.548 | -0.728 | 0.929 | -0.318 | -0.862 | 0.067 | -0.502 | **-2.443** | **-2.701** | -0.511 |
| S12 | 1.691 | 0.310 | 0.527 | 0.075 | 0.552 | -1.339 | -1.899 | 0.042 | -1.514 | -1.561 | -1.254 | 0.654 |
| S13 | 1.708 | 0.929 | 0.435 | -0.393 | -0.243 | -0.669 | -1.840 | -0.435 | -1.305 | -1.454 | -0.822 | 0.086 |
| S14 | 0.452 | 0.736 | 1.372 | -0.360 | 1.489 | -0.419 | **-2.459** | -0.803 | -0.502 | -1.182 | -0.510 | 1.864 |

tion patterns. This emphasises the need of conducting detailed analyses at the station level to precisely evaluate the effects of climate change in the Tafna watershed.

The IPTA method shows an increasing trend in October and January at all stations; November also shows an increasing trend at all stations except Sebdou station, which indicates a decreasing trend; September and December show an increasing trend at most of the stations (12 and 11 stations, respectively), August shows an increasing trend in all stations except Maghnia and Hennaya stations. A decreasing trend is found in February, March, and May in all stations except Djebel Chouachi station, which shows no significant trend in May. Ten stations in April show a decreasing trend. June indicates a decreasing trend at seven stations, while the other stations, such as Sebdou, Beni Bahdel, and Meurbah stations, show an increasing trend; the rest do not show any trend. Jule indicates a decreasing trend in 8 stations; only Sebdou station shows an increasing trend this month, and the other stations do now show any significant trend.

Table 4 presents the trends detected by the MK test and IPTA method for monthly precipitation data for all stations. The MK test indicates a significant trend (increase and decrease) in 11 of 168 months (12 months × 14 stations), representing 6.5% of the total months analyzed in this study. However, the IPTA method identifies a significant trend in 149 of 168 months, accounting for 88.7% of the total months. It can be concluded that the IPTA method is more sensitive than the MK test in detecting rainfall trends. However, this increased sensitivity may lead to an over-identification of trends, as the IPTA method does not incorporate any statistical significance threshold . The appearance of Table 4 would change if a stricter significance level (e.g., 0.01 instead of 0.05) or a larger one were applied to MK results, thereby highlighting differences in methodological sensitivity and interpretability. Many studies in different countries can support these findings, such as Hallouz et al. (2024) in Algeria; Akçay et al. (2022), Hırca et al. (2022), Esit (2023), and Esit et al. (2024) in Turkey; and Şan et al. (2021) in Vietnam.

## 5. CONCLUSIONS

In this study, the IPTA method was applied to monthly total rainfall data from 14 stations in the Tafna watershed over a 50-year period (1970-71 to 2019-20). The trend length and slope were calculated for consecutive months, and IPTA graphs were created for all stations. Additionally, a comparison was made between the IPTA method and the MK test in detecting monthly rainfall trends. The main findings are as follows:

- The rainiest month in the first half of the period (1970-71 to 1994-95) was March across all stations, whereas in the second half (1995-96 to 2019-20), November was the rainiest month in half of the stations, while January was for the others. The driest month in the first half was July for five stations, while it was August for the rest.
- The trend length was weak in all stations for the transitions of November-December, December-January, January-February, June-July, July-August, and August-September. The maximum trend length occurred in the transition May-June (ranging from

**Table 4.** comparison between MK and IPTA for monthly precipitation for all stations.


31.09 mm to 69.66 mm) in most stations, reflecting the seasonal shift from spring to summer.

- The MK test indicates a significant trend (increase and decrease) in 11 of 168 months (12 months × 14 stations), representing 6.5 % of the total months analyzed in this study. However, the IPTA method identifies a significant trend in 149 of 168 months, accounting for 88.7% of the total months.
- The MK test indicated a significant trend (increase or decrease) in only 11 of 168 months (12 months × 14 stations), or 6.5% of all months analyzed. In contrast, the IPTA method identified significant trends in 149 of 168 months, representing 88.7% of the total.

In conclusion, the IPTA method proved more sensitive in detecting monthly rainfall trends than the MK test, suggesting its potential as a valuable tool for assessing rainfall trends in regions affected by climate variability, particularly in Mediterranean climates like that of the Tafna watershed.

ACKNOWLEDGMENTS

The authors thank the national hydraulic resources agency (ANRH) for providing the data necessary to prepare this research work.

REFERENCES

Achite, M., Ceribasi, G., Ceyhunlu, A. I., Wałęga, A., & Caloiero, T. (2021). The Innovative Polygon Trend Analysis (IPTA) as a Simple Qualitative Method to Detect Changes in Environment—Example Detecting Trends of the Total Monthly Precipitation in Semiarid Area. *Sustainability*, *13*(22), 12674. https://doi.org/10.3390/su132212674

Akçay, F., Kankal, M., & Şan, M. (2022). Innovative approaches to the trend assessment of streamflows in the Eastern Black Sea basin, Turkey. *Hydrological Sci-*

*ences Journal*, *67*(2), 222-247. https://doi.org/10.1080/02626667.2021.1998509

Benzater, B., Elouissi, A., Fellah, S., & Hachemaoui, A. (2024). Spatio-temporal analysis of trends in annual maximum rainfall in the North-West of Algeria : Comparative analysis of recent and old non-parametric methods. *Water and Environment Journal*, *38*(1), 121-138. https://doi.org/10.1111/wej.12905

Bessaklia, H., Ghenim, A. N., Megnounif, A., & Martin-Vide, J. (2018). Spatial variability of concentration and aggressiveness of precipitation in North-East of Algeria. *Journal of Water and Land Development*, *36*(1), 3-15. https://doi.org/10.2478/jwld-2018-0001

Boudiaf, B., Şen, Z., & Boutaghane, H. (2022). North coast Algerian rainfall monthly trend analysis using innovative polygon trend analysis (IPTA). *Arabian Journal of Geosciences*, *15*(21), 1626. https://doi.org/10.1007/s12517-022-10907-8

Bougara, H., Hamed, K. B., Borgemeister, C., Tischbein, B., & Kumar, N. (2020). Analyzing Trend and Variability of Rainfall in The Tafna Basin (Northwestern Algeria). *Atmosphere*, *11*(4), 347. https://doi.org/10.3390/atmos11040347

Bouklikha, A., Habi, M., Elouissi, A., & Hamoudi, S. (2021). Annual, seasonal and monthly rainfall trend analysis in the Tafna watershed, Algeria. *Applied Water Science*, *11*(4), 77. https://doi.org/10.1007/s13201-021-01404-6

Esit, M. (2023). Investigation of innovative trend approaches (ITA with significance test and IPTA) comparing to the classical trend method of monthly and annual hydrometeorological variables : A case study of Ankara region, Turkey. *Journal of Water and Climate Change*, *14*(1), 305-329. https://doi.org/10.2166/wcc.2022.356

Esit, M., Yuce, M. I., Deger, İ. H., & Yasa, I. (2024). Trend and variability analysis in rainfall and temperature records over Van Province, Türkiye. *Theoretical and Applied Climatology*, *155*(1), 451-472. https://doi.org/10.1007/s00704-023-04644-5

Ghenim, A. N., & Megnounif, A. (2016). Variability and Trend of Annual Maximum Daily Rainfall in Northern Algeria. *International Journal of Geophysics*, *2016*, 1-11. https://doi.org/10.1155/2016/6820397

Gherissi, R., Baba-Hamed, K., & Bouanani, A. (2021). Highlighting drought in the Wadi Lakhdar Watershed Tafna, Northwestern Algeria. *Arabian Journal of Geosciences*, *14*(11), 984. https://doi.org/10.1007/s12517-021-07094-3

Ghorbani, M. A., Kahya, E., Roshni, T., Kashani, M. H., Malik, A., & Heddam, S. (2021). Entropy analysis and pattern recognition in rainfall data, north Algeria. *Theoretical and Applied Climatology*, *144*(1), 317-326. https://doi.org/10.1007/s00704-021-03542-y

Hallouz, F., Meddi, M., Ali Rahmani, S. E., & Abdi, I. (2024). Innovative versus traditional statistical methods in hydropluviometric : A detailed analysis of trends in the Wadi Mina Basin (Northwest of Algeria). *Theoretical and Applied Climatology*, *155*(8), 8263-8286. https://doi.org/10.1007/s00704-024-05127-x

Hırca, T., Eryılmaz Türkkan, G., & Niazkar, M. (2022). Applications of innovative polygonal trend analyses to precipitation series of Eastern Black Sea Basin, Turkey. *Theoretical and Applied Climatology*, *147*(1-2), 651-667. https://doi.org/10.1007/s00704-021-03837-0

Kendall, M. G. (1975). *Rank correlation methods. Griffin, London.*

Khomsi, K., Mahe, G., Tramblay, Y., Sinan, M., & Snoussi, M. (2015). *Trends in rainfall and temperature extremes in Morocco*. https://doi.org/10.5194/nhess-sd-3-1175-2015

Longobardi, A., & Villani, P. (2010). Trend analysis of annual and seasonal rainfall time series in the Mediterranean area. *International Journal of Climatology*, *30*(10), 1538-1546. https://doi.org/10.1002/joc.2001

Mann, H. B. (1945). Nonparametric Tests Against Trend. *Econometrica*, *13*(3), 245-259. https://doi.org/10.2307/1907187

Martínez, M. D., Lana, X., Burgueño, A., & Serra, C. (2007). Spatial and temporal daily rainfall regime in Catalonia (NE Spain) derived from four precipitation indices, years 1950–2000. *International Journal of Climatology*, *27*(1), 123-138. https://doi.org/10.1002/joc.1369

Meddi, H., & Meddi, M. (2009). Variabilité des précipitations annuelles du Nord-Ouest de l'Algérie. *Sécheresse*, *20*(1), 057-065. https://doi.org/10.1684/sec.2009.0169

Meddi, M. M., Assani, A. A., & Meddi, H. (2010). Temporal Variability of Annual Rainfall in the Macta and Tafna Catchments, Northwestern Algeria. *Water Resources Management*, *24*(14), 3817-3833. https://doi.org/10.1007/s11269-010-9635-7

Mehta, A. V., & Yang, S. (2008). Precipitation climatology over Mediterranean Basin from ten years of TRMM measurements. *Advances in Geosciences*, *17*, 87-91. https://doi.org/10.5194/adgeo-17-87-2008

Merniz, N., Tahar, A., & Benmehaia, A. M. (2019). Statistical assessment of rainfall variability and trends in northeastern Algeria. *Journal of Water and Land Development*, *40*(1), 87-96. https://doi.org/10.2478/jwld-2019-0009

Mrad, D., Djebbar, Y., & Hammar, Y. (2018). Analysis of trend rainfall : Case of North-Eastern Algeria. *Journal of Water and Land Development*, *36*(1), 105-115. https://doi.org/10.2478/jwld-2018-0011

Nouaceur, Z., & Murărescu, O. (2016). Rainfall Variability and Trend Analysis of Annual Rainfall in North Africa. *International Journal of Atmospheric Sciences*, *2016*, 1-12. https://doi.org/10.1155/2016/7230450

Otmane, A., Baba-Hamed, K., Bouanani, A., & Kebir, L. W. (2018). Mise en évidence de la sécheresse par l'étude de la variabilité climatique dans le bassin versant de l'oued Mekerra (Nord-Ouest algérien). *Techniques Sciences Méthodes*, *9*, 23-37. https://doi.org/10.1051/tsm/201809023

Oufrigh, O., Elouissi, A., & Benzater, B. (2023). Trend Assessment by the Mann-Kendall Test and the Innovative Trend Analysis Method (North-West Algeria). *GeoScience Engineering*, *69*(2), 186-233. https://doi.org/10.35180/gse-2023-0099

Philandras, C. M., Nastos, P. T., Kapsomenakis, J., Douvis, K. C., Tselioudis, G., & Zerefos, C. S. (2011). Long term precipitation trends and variability within the Mediterranean region. *Natural Hazards and Earth System Sciences*, *11*(12), 3235-3250. https://doi.org/10.5194/nhess-11-3235-2011

Şan, M., Akçay, F., Linh, N. T. T., Kankal, M., & Pham, Q. B. (2021). Innovative and polygonal trend analyses applications for rainfall data in Vietnam. *Theoretical and Applied Climatology*, *144*(3-4), 809-822. https://doi.org/10.1007/s00704-021-03574-4

Şan, M., Nacar, S., Kankal, M., & Bayram, A. (2024). Spatiotemporal analysis of transition probabilities of wet and dry days under SSPs scenarios in the semi-arid Susurluk Basin, Türkiye. *Science of The Total Environment*, *912*, 168641. https://doi.org/10.1016/j.scitotenv.2023.168641

Şen, Z., Şişman, E., & Dabanli, I. (2019). Innovative Polygon Trend Analysis (IPTA) and applications. *Journal of Hydrology*, *575*, 202-210. https://doi.org/10.1016/j.jhydrol.2019.05.028

Sneyers, R. (1990). *On the Statistical Analysis of Series of Observations. Technical Note No. 143, WMO No. 415, World Meteorological Organization, Geneva, 192 p.*

Taibi, S., Meddi, M., Mahé, G., & Assani, A. (2017). Relationships between atmospheric circulation indices and rainfall in Northern Algeria and comparison of observed and RCM-generated rainfall. *Theoretical and Applied Climatology*, *127*(1), 241-257. https://doi.org/10.1007/s00704-015-1626-4

Tramblay, Y., El Adlouni, S., & Servat, E. (2013). Trends and variability in extreme precipitation indices over Maghreb countries. *Natural Hazards and Earth System Sciences*, *13*(12), 3235-3248. https://doi.org/10.5194/nhess-13-3235-2013

Italian Journal of Agrometeorology
Rivista Italiana di Agrometeorologia

Firenze University Press
https://riviste.fupress.net/index.php/IJAm

OPEN ACCESS

**Citation:** Quiloango-Chimarro, C. A., Coelho, R. D., Gundim, A. S. & Costa, J. O. (2025). Water use efficiency and yield response factor of common bean subjected to deficit irrigation strategies: a case study in Brazil. *Italian Journal of Agrometeorology* (1): 43-50. doi: 10.36253/ijam-2396

**Received:** November 28, 2023

**Accepted:** May 29, 2025

**Published:** August 27, 2025



**Data Availability Statement:** All relevant data are within the paper and its Supporting Information files.

**Competing Interests:** The Author(s) declare(s) no conflict of interest.

# Water use efficiency and yield response factor of common bean subjected to deficit irrigation strategies: a case study in Brazil

Carlos Alberto Quiloango-Chimarro[1,*], Rubens Duarte Coelho[1], Alice da Silva Gundim[1], Jéfferson de Oliveira Costa[2]

[1] *University of São Paulo/USP-ESALQ, Biosystems Engineering Department, C.P. 09, 13418-900 Piracicaba, SP, Brazil*
[2] *Minas Gerais Agricultural Research Agency/EPAMIG, Experimental Field of Gorutuba, 39525-000 Nova Porteirinha, MG, Brazil*
*Corresponding author. Email: caquiloango@usp.br

**Abstract.** Water-saving strategies are important to cope with water shortages that affect irrigated agriculture. To determine the water use efficiency (WUE) and yield response factor (Ky) of common bean (*Phaseolus vulgaris* L.) grown under different deficit irrigation strategies, a rain shelter experiment was conducted. Common bean was subjected to five water replacement levels: 100% of field capacity (FC) throughout the growing season (M1; the reference treatment); 75% (M2) and 50% (M3) FC, starting at 20 days after sowing until the end of the growing season; and 75% (M4) and 50% (M5) FC at flowering. Grain yield (GY), yield components, WUE, and Ky were evaluated. Water use efficiency under M3 and M4 was comparable to M1, the highest WUE obtained (1.55 kg·m$^{-3}$). However, M3 significantly reduced GY (42%), which was mainly caused by the decrease in the number of pods and grains per plant. Therefore, limiting water at 75% FC during flowering (M4) could be viable to avoid yield gaps and maintain higher WUE in water scarce regions. Yield response factor of common bean revealed that the greatest water savings were obtained with the M3 irrigation strategy, reducing crop evapotranspiration by approximately 70%.

**Keywords:** grain yield, irrigation water applied, *Phaseolus vulgaris*, water saving.

## HIGHLIGHTS

1. Deficit irrigation strategies at different phenological stages of common beans were evaluated;
2. Water use efficiency and yield response factor of common bean were included;
3. Mild water stress of short duration did not reduce water use efficiency or grain yield;
4. The relationship between irrigation water applied and grain yield showed that water stress reduces productivity independently of phenological stage;

5. Yield response factor of common bean revealed the possibility of obtaining reasonable grain yield and water savings.

## 1. INTRODUCTION

Many regions where common bean (*Phaseolus vulgaris* L.) is produced are rainfed systems which are susceptible to drought stress (Darkwa et al., 2016). Brazil, which is the largest world edible producer of this crop, has 93% of the total area under rainfed conditions (FAOSTAT, 2024). It is estimated that 60% of common bean production occurs under the risk of intermittent or flowering drought stress (Beebe et al., 2013). These conditions cause yield reductions of common bean by up to 80% (Rosales et al., 2012; Lanna et al., 2016).

Irrigation is the best option for reducing yield gaps in agricultural crops by enabling the supply of water in the appropriate quantity for each phase of the growing season (Kang et al., 2021). However, water shortages as part of climate change are reducing the availability of water for agriculture (Darkwa et al., 2016). Deficit irrigation plays a positive role in regions where water is scarce, saving water as well as ensuring yield per unit of planted area (Geerts and Raes, 2009). Previous research has focused on deficit irrigation at specific growth stages (Sánchez-Reinoso et al., 2020) and is scarce on the water replacement levels at which common bean is most efficient in water use. In addition, "all-stage" adaptation to drought is required for cultivation in dry environments, but in common bean this strategy has been poorly studied. Therefore, different deficit strategies both in duration and intensity are expected to help develop water-saving strategies in this crop.

One of the alternatives for evaluating drought response is water use efficiency (WUE), which is defined as the ratio of dry matter production to water use (Geerts and Raes, 2009). Improved WUE in common beans is important for leading to a rational use of resources without adverse effects on production (Webber et al., 2006; Quiloango-Chimarro et al., 2022). The approach to increasing WUE could be made by adopting technologies that increase the proportion of water that is transpired by the crop, and increasing the crop's capacity to produce biomass and yield per unit of water transpired (Mathobo et al., 2017). An additional approach to consider involves examining the impact of drought by assessing yield response factor (Ky) derived from the correlation between relative yield (compared to yield potential) and relative evapotranspiration (compared to maximum evapotranspiration - no stress), as outlined by Doorenbos and Kassan (1979). In the context of deficit irrigation, exploring both WUE and yield response factor (Ky) can provide a comprehensive understanding of water saving in common beans.

It was hypothesized that water deficit strategies reduce the water use of common bean without significant reductions in grain yield. Therefore, the objectives of this study were to determine the water use efficiency and yield response factor of common bean under mild and moderate water deficit strategies, considering both the entire growing season and specific growth stages (vegetative and flowering).

## 2. MATERIAL AND METHODS

### *2.1 Study site, field preparation, and treatment description*

The experiment was carried out under rain shelter conditions in Piracicaba, São Paulo State, Brazil (22°46'39" S, 47°17'45" W, altitude of 570 m) from March to June 2020. The experimental area is specifically designed for water use efficiency experimentation (França et al., 2024; Quiloango-Chimarro et al., 2021) and consisted of a shelter with a ceiling height of 5.2 m, a transparent plastic cover shielded against UV rays, and a black screen on the sides that intercepted 50% of the incident radiation.

TAA Dama, a common bean cultivar, was sown in a single row per plot with an inter-row spacing of 0.1 m (10 plants·plot$^{-1}$). Each plot consisted of a large waterproofed container with an area of 0.43 m$^2$ and dimensions of 1.04 x 0.41 x 0.76 m (length, width, and depth) filled with soil characterized as Oxisol Typic Ustox with a sandy-loam texture, which was hydro-physically and chemically characterized before the beginning of the experiment. Soil characteristics in the 0-0.4 m layer were: pH ($CaCl_2$) = 5.4; Ca (mg·kg$^{-1}$) = 560.4; Mg (mg·kg$^{-1}$) = 84.7; K (mg·kg$^{-1}$) = 23.4; H + Al (mg·kg$^{-1}$) = 175.5; P (mg·kg$^{-1}$) = 21.4; S (mg·kg$^{-1}$) = 23.3, organic matter (g·kg$^{-1}$) = 9, dry bulk density (kg·m$^{-3}$) = 1600, field capacity (m$^3$·m$^{-3}$) = 0.22, permanent wilting point (m$^3$·m$^{-3}$) = 0.16, sand (%) = 72.2, clay (%) = 19.7 and silt (%) = 8.0. Fertilization was conducted following the guidelines for São Paulo state (van Raij et al., 1997). Phosphate and potassium fertilizer were applied at rates of 70 kg·ha$^{-1}$ of $P_2O_5$ and 45 kg·ha$^{-1}$ of $K_2O$, respectively. All the phosphate was applied in the sowing furrow, while potassium was divided into two soil cover applications (sowing and beginning of flowering). Pesticide applications were made when necessary and weed control was conducted manually throughout the growing season.

Air temperature, relative humidity, and global solar radiation were recorded inside the shelter area at 2 m

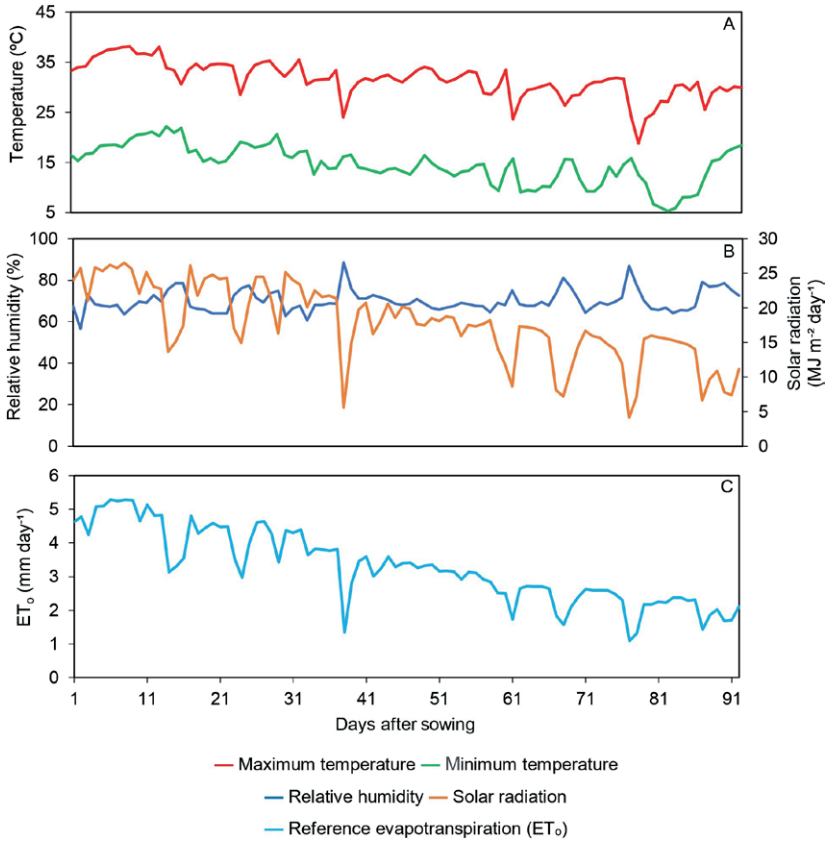


**Figure 1.** Maximum and minimum air temperature (A), relative humidity and solar radiation (B), and reference evapotranspiration ($ET_o$) (C) in the experimental area throughout the growing season.

height and the reference evapotranspiration ($ET_o$) was calculated using the Penman-Monteith method (Allen et al., 1998) (Figure 1).

During the experiment, the minimum daily temperature ranged from 5.9°C at 82 days after sowing (DAS) to 22.2°C at 14 DAS. In turn, the maximum temperature varied between 18.8°C and 38.1°C at 78 DAS and 13 DAS, respectively. In general, during the experimental period, the temperature remained within the ideal temperature range for common bean cultivation. The average value for global solar radiation recorded during the experimental period was 16.7 $MJ \cdot m^{-2} \cdot day^{-1}$, with extremes of 26.5 and 4.1 $MJ \cdot m^{-2} \cdot day^{-1}$ at 9 and 77 DAS, respectively. The average relative humidity during the period was 71.7%, reaching a maximum value of 88.6% at 38 DAS and a minimum value of 56.6% at 2 DAS. The $ET_o$ varied between 1.1 and 5.3 $mm \cdot day^{-1}$ at 77 DAS and 9 DAS, respectively.

The irrigation treatments consisted of five water replacement levels with five replications distributed completely at random and included: irrigation at field capacity (FC) throughout the growing season (M1); 75 and 50% FC from 20 DAS until the end of the growing season, denominated M2 and M3, respectively; and 75 and 50% FC at flowering (from 40 to 61 DAS), denominated M4 and M5, respectively. In this trial, 75% and 50% FC were considered as mild and moderate drought stress, respectively (Figure 2).

### *2.2 Irrigation management*

Irrigation water was provided through a drip irrigation system. A small drip line (1 m length) with six emitters was installed in each plot. The emitters were spaced 0.15 m apart and had a flow rate of 0.6 $L \cdot h^{-1}$, resulting in a flow rate of 3.6 $L \cdot h^{-1}$ per plot. All plots were controlled individually with micro-registers from a control panel. In each replication of the M1 (full irrigation treatment), a set of three tensiometers was installed at 0.1, 0.3, and 0.5 m depths, providing soil matric potential records for the soil layers 0.0-0.2, 0.2-0.4, and 0.4-0.6 m, respectively, which were monitored every other day. Irrigation for M1 was computed by applying water to bring the soil


**Figure 2.** Experimental area (A) and experimental design used in this study (B). M1 - 100% of field capacity (FC) throughout the growing season; M2 - 75% FC from 20 days after sowing until the end of the growing season; M3 - 50% FC from 20 days after sowing until the end of the growing season; M4 - 75% FC at flowering; M5 - 50% FC at flowering; DAS - days after sowing; b - border.

water to FC the first two layers, while the third layer was used for drainage control. Irrigation was triggered when the soil water potential reached -20 kPa at 0.1 m depth. Volumetric soil water content for each layer before irrigation was estimated from matric potential readings using the van Genuchten approach (van Genuchten, 1980). The other treatments (M2, M3, M4 and M5) received a fraction of the water applied to M1. Plants were irrigated to FC until 20 DAS using the Penman-Monteith approach ($K_c$ initial = 0.35) as described by Allen et al. (1998), when seedlings were well established.

### *2.3 Yield measurement and calculation of WUE and Ky*

At physiological maturity, plants from the central part of the row were harvested (5 plants) and were dried in a forced-ventilation oven at 60°C for 72 h. The number of pods per plant (PP), total number of grains per plant (TNG), number of grains per pod (NGP) and grain yield (GY) (kg·ha$^{-1}$) were obtained. WUE (kg·m$^{-3}$) was calculated for each treatment as the ratio of the GY (kg·ha$^{-1}$) to the total volume of irrigation water applied (IWU) (mm), using equation 1:

$$\mathrm{WUE} = \frac{\mathrm{GY}}{\mathrm{IWU}\cdot 10} \quad (1)$$

Ky was calculated for each treatment as the ratio of the relative yield (1 – ($Y_a$·$Y_m^{-1}$)) to the relative evapotranspiration (1 – ($ET_a$·$ET_m^{-1}$)), using equation 2:

$$\mathrm{Ky} = \frac{1 - (\mathrm{Ya}\cdot \mathrm{Ym}^{-1})}{1 - (\mathrm{ETa}\cdot \mathrm{ETm}^{-1})} \quad (2)$$

where $Y_a$ is the actual yield, $Y_m$ is the maximum yield, $ET_a$ is the actual evapotranspiration and $ET_m$ is the maximum evapotranspiration. A Ky value greater than 1 indicates that yield loss exceeds the proportional reduction in water availability; a Ky value less than 1 suggests that yield loss is less severe than the water deficit; and a Ky value equal to 1 means that yield reduction is directly proportional to the water deficit. In this study, the yield and evapotranspiration of treatment M1 (100% of FC throughout the growing season) were considered to be equal to $Y_m$ and $ET_m$, respectively, and the yield and evapotranspiration of the other treatments to be $Y_a$ and $ET_a$. Actual evapotranspiration represents the amount of water used by the crop, which in deficit irrigation treatments is typically equal to the water supplied (Djaman and Irmak, 2012).

### *2.4 Statistical analysis*

All the statistical analyses were performed with R Studio (R Project for Statistical Computing, version 4.1.2). One-way analysis of variance (ANOVA) was performed after testing the homogeneity of variances and normality of the residuals by the Levene and Shapiro-Wilk tests, respectively. The means were compared with the Fisher Least Significant Difference (LSD) at 5% probability.

## 3. RESULTS AND DISCUSSION

### *3.1 Irrigation water applied (IWU)*

The total amount of IWU to the experimental common bean differed depending on the strategies irrigation treatments (Figure 3). 451, 357, 263, 403 and 355 mm of irrigation water were applied throughout the growing season in treatments M1, M2, M3, M4 and M5, respectively. At the seedling establishment stage (0 to 20 DAS) all treatments received 74 mm of irrigation water. In the vegetative stage (21 to 39 DAS) the IWU in treatments M1, M4 and M5 was 89 mm and in treatments M2 and M3 it was 67 and 44 mm. During flowering (40 to 61 DAS) the crop received the highest amount of irrigation water, 190, 143, 95,143 and 95 mm for treatments M1, M2, M3, M4 and M5, respectively. During grain-filling to physiological maturity (62 to 92 DAS) the IWU was 97, 73, 49, 97 and 97 mm for treatments M1, M2, M3, M4 and M5.

### *3.2 Grain yield and grain yield components*

Grain yield decreased as drought stress increased, except for M4, which was similar to M1 (Table 1). Under field conditions, Calvache et al. (1997) reported significant

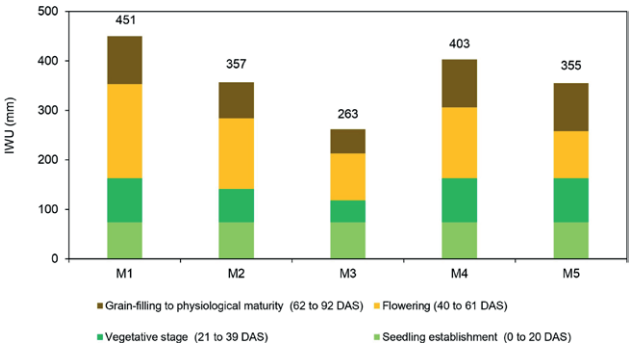


**Figure 3.** Irrigation water applied (mm) in the different phases of the growing season of common bean subjected to deficit irrigation strategies. M1 - 100% of field capacity (FC) throughout the growing season; M2 - 75% FC from 20 days after sowing until the end of the growing season; M3 - 50% FC from 20 days after sowing until the end of the growing season; M4 - 75% FC at flowering; M5 - 50% FC at flowering; DAS - days after sowing.

yield decreases when water limiting was applied during all the growing season as well as at flowering. The yield penalty in common bean is variable due to differences in the timing and intensity of drought stress (Heinemann et al., 2016; Galvão et al., 2019; do Nascimento Silva et al., 2020). Therefore, the non-significant yield reduction of M4 could be associated with the high frequency of irrigation and the water replacement level used.

The grain yield penalty due to drought stress was mostly caused by the reduction in the number of pods per plant (PP) and the low number of grains per plant (TNG). All deficit irrigation treatments showed significant reductions in PP and TNG compared to M1, except

**Table 1.** Effect of deficit irrigation strategies on yield and yield components of common bean.

| Treatment | Grain yield ($kg \cdot ha^{-1}$) | Pods per plant | Grains per pod | Grains per plant |
|---|---|---|---|---|
| M1 | 4625 ± 759 a | 19.9 ± 3.8 a | 4.6 ± 0.3 | 92 ± 15.3 a |
| M2 | 3145 ± 685 bc | 14.4 ± 2.6 bc | 4.5 ± 0.8 | 64 ± 9.7 bc |
| M3 | 2693 ± 404 c | 11.9 ± 1.5 c | 4.6 ± 0.2 | 56 ± 6.3 c |
| M4 | 3883 ± 849 ab | 17.3 ± 3.8 ab | 4.7 ± 0.6 | 83 ± 24.1 ab |
| M5 | 3202 ± 607 bc | 15.9 ± 3.4 b | 4.5 ± 0.3 | 68 ± 11.1 bc |
| LSD (0.05) | 1071 | 4.7 | ns | 22 |

Each value represents the mean ± standard deviation. Treatments with the same letters within a column do not differ from each other at the 5% probability level by the LSD test ($p < 0.05$). M1 = 100% of field capacity (FC) throughout the growing season; M2 = 75% FC from 20 days after sowing until the end of the growing season; M3 = 50% FC from 20 days after sowing until the end of the growing season; M4 = 75% FC at flowering; M5 = 50% FC at flowering. ns, no significant.

M4. This was expected because previous studies showed that the yield component most affected by drought stress is PP (Nuñez Barrios et al., 2005; de Oliveira Neto et al., 2022), mainly by flower senescence and flower abortion (Mathobo et al., 2017). The number of grains per pod (NGP) was similar for all irrigation treatments, with an average of 4.5 grains per pod. Previous studies confirm that NGP is not susceptible to drought stress (Acosta Gallegos & Shibata, 1989; Galvão et al., 2019), suggesting that limited water in common bean does not disrupt the supply of assimilates to the pods.

### *3.3 Water use efficiency (WUE)*

Water use efficiency in this study ranged from 1.03 to 0.90 kg·m$^{-3}$ (Figure 4). The WUE of M3 and M4 was similar to that of M1, whereas it was reduced for M2 and M5. This could be because common bean invests photosynthetic resources for root production per unit water used to extract more water under drought conditions, but this strategy is insufficient to increase WUE for biomass and grain (Webber et al., 2006). Considering that the yield penalty was significant for M3, the WUE of M4 could be considered the best option to save water (a water reduction of 48 mm) while maintaining a substantial yield (3.9 Mg·ha$^{-1}$). These results are also relevant because future drought stress patterns for central Brazil suggest stress on the reproductive stage (Heinemann et al., 2016).

### *3.4 Yield response factor (Ky)*

The analysis of yield response factor in the context of different irrigation strategies revealed distinct performances, focusing only on the impact of soil moisture while keeping all other production variables constant (Table 2). Treatment M2 and M5 resulted in higher Ky values > 2.00, showing similar reductions not only for GY but also for evapotranspiration. Treatments M3 and M4 showed a Ky of approximately 1.71 but were affected by different patterns of grain yield reduction and evapotranspiration.

According to Smith and Steduto (2012), common beans are categorized as very sensitive to water stress (with Ky values of 1.15). This is consistent with this study where all deficit irrigation resulted in Ky values >1.70. Among the tested strategies, the least impact in Ky was observed in M3 and M4. It is important to note, however, that water stress during flowering in common beans should be avoided, as a 10% reduction in evapotranspiration resulted in a 17.2% decrease in yield.

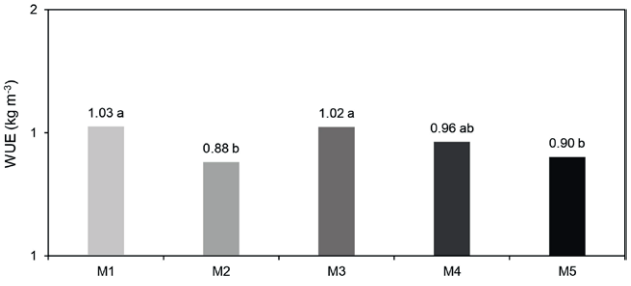


**Figure 4.** Effect of deficit irrigation strategies on water use efficiency (WUE) of common bean. Treatments with the same letters do not differ from each other at the 5% probability level by the LSD test ($p < 0.05$). M1 = 100% of field capacity (FC) throughout the growing season; M2 = 75% FC from 20 days after sowing until the end of the growing season; M3 = 50% FC from 20 days after sowing until the end of the growing season; M4 = 75% FC at flowering; M5 = 50% FC at flowering.

**Table 2.** Effect of deficit irrigation strategies on yield response factor (Ky) of common bean.

| Treatment | Relative yield ($1 - (Y_a \cdot Y_m^{-1})$) | Relative evapotranspiration ($1 - (ET_a \cdot ET_m^{-1})$) | Yield response factor (Ky) |
|---|---|---|---|
| M1 | 0 | 0 | - |
| M2 | 0.47 | 0.21 | 2.23 |
| M3 | 0.72 | 0.42 | 1.71 |
| M4 | 0.19 | 0.11 | 1.72 |
| M5 | 0.44 | 0.22 | 2.00 |

M1 - 100% of field capacity (FC) throughout the growing season; M2 - 75% FC from 20 days after sowing until the end of the growing season; M3 - 50% FC from 20 days after sowing until the end of the growing season; M4 - 75% FC at flowering; M5 - 50% FC at flowering; $Y_a$ - actual yield; $Y_m$ – maximum yield; $ET_a$ - actual evapotranspiration; $ET_m$ - maximum evapotranspiration.

## 4. CONCLUSIONS

Water use efficiency (WUE) and yield response factor (Ky) can support decision-making when implementing deficit irrigation strategies in common bean. By analyzing both indicators, it was observed that the adoption of 50% field capacity (FC) throughout the growing season (M3) and 75% FC during flowering (M5) maintained WUE comparable to that of full irrigation (M1), while also resulting in a low Ky. However, since this study was conducted over a single cropping season, further research across multiple seasons is required to better understand the effects of deficit irrigation strategies in common bean.

ACKNOWLEDGEMENTS

The first author would like to thank the Coordenação de Aperfeiçoamento de Pessoal de Nível Superior (CAPES) for the support of this study through a MSc scholarship. All authors would like to thank the Fundação de Amparo a Pesquisa do Estado de São Paulo (FAPESP) for the support of this research (Process Nº 2018/09729-7).

REFERENCES

Acosta Gallegos J.A., Kohashi Shibata J. (1989). Effect of water stress on growth and yield of indeterminate dry-bean (*Phaseolus vulgaris*) cultivars. *Field Crops Research*, 20: 81–93.

Allen R.G., Pereira L.S., Raes D., Smith M. (1998). Crop Evapotranspiration-Guidelines for Computing Crop Water Requirements. *FAO Irrigation and Drainage Paper 56*.

Androcioli L.G., Zeffa D.M., Alves D.S., Tomaz J.P., Moda-Cirino V. (2020). Effect of water deficit on morphoagronomic and physiological traits of common bean genotypes with contrasting drought tolerance. *Water (Switzerland)*, 12: 1–13.

Beebe S.E., Rao I.M., Blair M.W., Acosta-Gallegos J.A. (2013). Phenotyping common beans for adaptation to drought. *Frontiers in Physiology*, 4: 35.

Calvache M., Reichardt K., Bacchi O.O.S., Dourado-Neto D. (1997). Deficit irrigation at different growth stages of the common bean (Phaseolus vulgaris L., cv. Imbabello). *Scientia Agricola*, 54: 1–16.

Castañeda-Saucedo M.C., Córdova-Téllez L., González-Hernández V.A., Delgado-Alvarado A., Santacruz-Varela A., Los Santos G.G. De (2009). Physiological performance, yield, and quality of dry bean seeds under drought stress. *Interciencia*, 34: 748–54.

Darkwa K., Ambachew D., Mohammed H., Asfaw A., Blair M.W. (2016). Evaluation of common bean (Phaseolus vulgaris L.) genotypes for drought stress adaptation in Ethiopia. *The Crop Journal*, 4: 367–76.

Dipp C.C., Marchese J.A., Woyann L.G., Bosse M.A., Roman M.H., Gobatto D.R., Paludo F., Fedrigo K., Kovali K.K., Finatto T. (2017). Drought stress tolerance in common bean: what about highly cultivated Brazilian genotypes?. *Euphytica*, 213: 1–16.

Djaman, K., Irmak, S. (2012). Soil water extraction patterns and crop, irrigation, and evapotranspiration water use efficiency of maize under full and limited irrigation and rainfed settings. *Transactions of the ASABE*, *55*: 1223–1238.

Doorenbos, J., Kassan, A.H. Yield response to water. Rome: FAO, 1979. 193p. (FAO. Irrigation and Drainage Paper, 33).

FAOSTAT. (2024). *Data - dataset - Crops, National Production*. Food and Agriculture Organization of the United Nations (FAOSTAT). https://www.fao.org/faostat/en/#data/QCL

Flexas J., Medrano H. (2002). Drought-inhibition of Photosynthesis in C3 Plants: Stomatal and Non-stomatal Limitations Revisited. *Annals of Botany*, 89: 183–9.

França, A. C. F., Coelho, R. D., da Silva Gundim, A., de Oliveira Costa, J., & Quiloango-Chimarro, C. A. (2024). Effects of different irrigation scheduling methods on physiology, yield, and irrigation water productivity of soybean varieties. *Agricultural Water Management*, *293*, 108709.

Galvão Í.M., dos Santos O.F., de Souza M.L.C., de Jesus Guimarães J., Kühn I.E., Broetto F. (2019). Biostimulants action in common bean crop submitted to water deficit. *Agricultural Water Management*, 225: 105762.

Geerts S., Raes D. (2009). Deficit irrigation as an on-farm strategy to maximize crop water productivity in dry areas. *Agricultural Water Management*, 96: 1275–84.

van Genuchten M.T. (1980). A Closed-form Equation for Predicting the Hydraulic Conductivity of Unsaturated Soils. *Soil Science Society of America Journal*, 44: 892–8.

Heinemann A.B., Ramirez-Villegas J., Souza T.L.P.O., Didonet A.D., di Stefano J.G., Boote K.J., Jarvis A. (2016). Drought impact on rainfed common bean production areas in Brazil. *Agricultural and Forest Meteorology*, 225: 57–74.

Kang J., Hao X., Zhou H., Ding R. (2021). An integrated strategy for improving water use efficiency by understanding physiological mechanisms of crops responding to water deficit: Present and prospect. *Agricultural Water Management*, 255: 107008.

Lanna A.C., Mitsuzono S.T., Gledson T., Terra R., Vianello R.P., Alves M., Carvalho D.F. (2016). Physiological characterization of common bean ("Phaseolus vulgaris" L.) genotypes, water-stress induced with contrasting response towards drought. *Australian Journal of Crop Science*, 10: 1–6.

Mathobo R., Marais D., Steyn J.M. (2017). The effect of drought stress on yield, leaf gaseous exchange and chlorophyll fluorescence of dry beans (Phaseolus vulgaris L.). *Agricultural Water Management*, 180: 118–25.

Medrano H., Tomás M., Martorell S., Flexas J., Hernández E., Rosselló J., Pou A., Escalona J.M., Bota J. (2015). From leaf to whole-plant water use efficien-

cy (WUE) in complex canopies: Limitations of leaf WUE as a selection target. *Crop Journal*, 3: 220–8.

do Nascimento Silva A., Ramos M.L.G., Júnior W.Q.R., de Alencar E.R., da Silva P.C., de Lima C.A., Vinson C.C., Silva M.A.V. (2020). Water stress alters physical and chemical quality in grains of common bean, triticale and wheat. *Agricultural Water Management*, 231: 106023.

Nuñez Barrios A., Hoogenboom G., Dennis ;, Nesmith S. (2005). Drought Stress and the Distribution of Vegetative and Reproductive Traits of a Bean Cultivar Stress Hídrico E a Distribuição De Características Vegetativas E Reprodutivas De Um Cultivar De Feijão. *Sci Agric*, 18–22.

de Oliveira Neto S.S., Pereira F.F.S., Zoz T., Oliveira C.E. da S., Moda Cirino V. (2022). Effect of water deficit on morphoagronomic traits of black common bean genotypes (Phaseolus vulgaris L.) with contrasting drought tolerance. *Journal of Agronomy and Crop Science*.

Quiloango-Chimarro C.A., Coelho R.D., costa, J. O., Gomez-Arrieta, R. (2021). CROP water stress index for predicting yield loss in common bean. *Revista IRRIGA (Brazilian Journal of Irrigation & Drainage)*.

Quiloango-Chimarro C.A., Coelho R.D., Heinemann A.B., Arrieta R.G., da Silva Gundim A., França A.C.F. (2022). Physiology, yield, and water use efficiency of drip-irrigated upland rice cultivars subjected to water stress at and after flowering. *Experimental Agriculture*, 58.

van Raij B., Cantarella H., Quaggio J.A., Furlani a. M.C. (1997). Recomendacoes da adubacao e calagem para o Estado de Sao Paulo: 1–88.

Rosales M.A., Ocampo E., Rodríguez-Valentín R., Olvera-Carrillo Y., Acosta-Gallegos J., Covarrubias A.A. (2012). Physiological analysis of common bean (Phaseolus vulgaris L.) cultivars uncovers characteristics related to terminal drought resistance. *Plant Physiology and Biochemistry*, 56: 24–34.

Sánchez-Reinoso A.D., Ligarreto-Moreno G.A., Restrepo-Díaz H. (2020). Evaluation of drought indices to identify tolerant genotypes in common bean bush (Phaseolus vulgaris L.). *Journal of Integrative Agriculture*, 19: 99–107.

Smith, M., Steduto, P. (2012). Yield response to water: the original FAO water production function. *FAO Irrigation and Drainage Paper*, 66: 6–13.

Webber H.A., Madramootoo C.A., Bourgault M., Horst M.G., Stulina G., Smith D.L. (2006). Water use efficiency of common bean and green gram grown using alternate furrow and deficit irrigation. *Agricultural Water Management*, 86: 259–268.

Italian Journal of Agrometeorology
Rivista Italiana di Agrometeorologia

Firenze University Press
https://riviste.fupress.net/index.php/IJAm

OPEN ACCESS

**Citation:** Adam, A. M., Hamad, A. A. A. & Zheng, Y. (2025). Solar radiation prediction in semi-arid regions: A machine learning approach and comprehensive evaluation in Gadarif, Sudan. *Italian Journal of Agrometeorology* (1): 51-67. doi: 10.36253/ijam-2815

**Received:** June 9, 2024

**Accepted:** May 19, 2025

**Published:** August 27, 2025



**Data Availability Statement:** All relevant data are within the paper and its Supporting Information files.

**Competing Interests:** The Author(s) declare(s) no conflict of interest.

**ORCID:**
AMA: 0009-0003-7723-3101
AAAH: 0000-0001-7990-048X
YZ: 0000-0002-4991-0190

# Solar radiation prediction in semi-arid regions: A machine learning approach and comprehensive evaluation in Gadarif, Sudan

Abdelkarem M. Adam[1,2], Amar Ali Adam Hamad[1,*], Yuan Zheng[3]

[1] *College of Resources and Environment, Shanxi Agricultural University, Taiyuan, 030031, China*
[2] *College of Water Conservancy and Hydropower Engineering, Hohai University, Nanjing, 210098, China*
[3] *Renewable Energy Power Generation Engineering Research, MOE; School of Water Resources and Hydropower, Hohai University, 210098 Nanjing, China*
*Corresponding author. Email: abdoadam7878@gmail.com

**Abstract**. Solar radiation (H) is a critical factor in Earth's surface processes, influencing climate, ecosystems, agriculture, and energy fluxes. Accurate prediction of daily H is essential for advancing solar power as a sustainable energy source. This study evaluates the effectiveness of machine learning (ML) models-support vector regression (SVR), extreme gradient boosting (XGBoost), boosted regression forest (BRF), and k-nearest neighbors (K-NN)-in predicting daily H in Gadarif, Sudan, a semi-arid region with limited prior research on solar radiation. The models were developed using daily climatic variables, including temperature and a binary precipitation variable ($P_t$) to account for cloud cover effects. The dataset was split into training (80%) and testing (20%) subsets, with model performance evaluated using key metrics: coefficient of determination ($R^2$), root mean square error (RMSE), and mean absolute error (MAE). BRF achieved the best performance with an $R^2$ of 0.963 and RMSE of 4.38 (MJ $m^{-2}$ $d^{-1}$) during training. However, model performance decreased during testing, with XGBoost and K-NN showing higher error margins. Including Pt improved the models' ability to account for cloud cover effects, particularly on overcast days. Despite these improvements, challenges remained in predicting H under extreme climatic conditions, highlighting the need for more advanced approaches. These findings suggest that ML models can be effectively adapted for H prediction in other semi-arid and arid regions. The results underscore the importance of considering precipitation and cloud cover in H predictions, which is crucial for optimizing solar energy systems and enhancing agricultural planning.

**Keywords:** solar radiation, machine learning, renewable energy, semi-arid climate, comprehensive evaluation.

## HIGHLIGHTS

- Machine learning models, including SVR, XGBoost, BRF, and K-NN, were applied to predict daily solar radiation (H).

- BRF outperformed the other models, achieving the highest performance with an $R^2$ of 0.963 and RMSE of 4.38 (MJ $m^{-2}$ $d^{-1}$) during training.
- Incorporating a precipitation variable ($P_t$) improved the models' accuracy by accounting for cloud cover effects.
- Testing showed a performance drop, though BRF maintained strong generalization, needing refinement for extreme conditions.
- The methodology, applied in Gadarif, Sudan, can be adapted for other semi-arid and arid regions for solar energy optimization.

## NOMENCLATURE

### *Parameters*

| | |
|---|---|
| C | penalty parameter of the error |
| H | global solar radiation (MJ $m^{-2}$ $day^{-1}$) |
| $H_0$ | extra-terrestrial solar radiation (MJ $m^{-2}$ $day^{-1}$) |
| K | kernel function |
| I | loss function |
| n | number of observations |
| N | sunshine duration |
| ΔT | diurnal temperature range (°C) |
| Pt | transformed precipitation |
| $T_{max}$ | daily maximum temperature (°C) |
| $T_{min}$ | daily minimum temperature (°C) |
| $X_{min}$ | minimum observed value in the dataset |
| $X_{max}$ | maximum observed value in the dataset |
| $X_{mean}$ | mean observed value in the dataset |
| $C_s$ | Skewness coefficient |
| SD | Stander deviation |
| $C_k$ | Kurtosis coefficient |
| φ | higher-dimensional feature space |
| ω | weights vector |
| ε | tube size |
| λ | regularization parameter |
| γ | minimum loss |
| Ω | regularization term |

### *Constants*

a, b, and c empirical coefficients

### *Abbreviation*

| | |
|---|---|
| ANN | Artificial Neural Networks |
| MLP | Multi-layer Perceptron |
| SVM | Support Vector Machine |
| XGBoost | Extreme Gradient Boosting |
| ANFIS | adaptive neuro-fuzzy inference system |
| RF | Random Forest |
| AI | Artificial Intelligence |
| BRF | Boosted Regression Forests |
| ML | Machine Learning |

## 1. INTRODUCTION

Solar radiation (H) plays a crucial role in Earth's surface processes, influencing climate systems, hydrology, and ecosystems (Caldwell, M.M., Bornman, J.F., Ballaré, 2007). Its accurate estimation is particularly critical in semi-arid regions where environmental and agricultural systems heavily depend on it. Solar radiation directly impacts photosynthesis, making it a vital variable in crop modeling, where agronomic applications are essential for optimizing yield predictions (Holzman et al., 2018). Precise H forecasts are essential for improving agricultural planning and water resource management, especially in regions with limited resources.

This study addresses the gap in H prediction for semi-arid regions, focusing on Gadarif, Sudan, by employing advanced machine learning (ML) techniques support vector machines (SVM), extreme gradient boosting (XGBoost), boosted regression forest (BRF), and k-nearest neighbors (K-NN). While traditional studies have focused on temperate climates using statistical models, this research applies ML models to capture complex, non-linear interactions in semi-arid conditions. SVM and XGBoost were selected for their robustness and ability to generalize well across varying datasets, BRF for its ensemble method, which reduces bias and variance, and K-NN for its effectiveness in modeling local relationships. By utilizing a daily temporal scale, this study provides precise short-term H forecasts, enhancing prediction accuracy for agricultural applications in resource-challenged regions like Gadarif.

ML approaches have been increasingly applied to estimate H in various climates. (Wang et al., 2016) conducted a comparative study in China, estimating daily H using models such as multilayer perceptron (MLP), radial basis function (RBF), and generalized regression neural networks (GRNN). The study found that GRNN underperformed compared to MLP and RBF, highlighting the need for more robust models in H prediction. Similarly, (Belmahdi et al., 2020) forecasted daily H one month ahead using ARIMA and ARMA models, with ARIMA demonstrating superior accuracy over a persistence model.

Most previous studies focused on a specific timescale or component of H. For instance, (Belmahdi et al., 2022) introduced a new optimization method to predict hourly H, comparing several models, including feed-forward backpropagation (FFBP), ARIMA, k-NN, and SVM. FFBP and ARIMA models exhibited the highest accuracy, as confirmed by regression plots under clear-sky conditions.

Fan et al. (2018a) employed SVM and extreme gradient boosting (EGB) models to predict H in humid regions with limited data. They found that SVM outper-

formed EGB and traditional empirical models in terms of prediction stability. Similarly, (Belaid and Mellit, 2016) explored the use of SVM and artificial neural networks (ANN) for predicting daily and monthly H, concluding that SVM produced better correlations between predicted and observed values at both timescales.

Geographical and meteorological data have also been extensively utilized in H modeling. For example, (Sözen et al., 2008) employed an artificial neural network (ANN) model to estimate H in Turkey, achieving highly accurate predictions. In Algeria, (Mellit et al., 2008) applied both ANN and adaptive neuro-fuzzy inference system (ANFIS) models, also producing reliable results for H estimation. (Chen et al., 2011) found that SVM were dependable model for H predictions across multiple stations, while (Ahmed and Adam, 2013) demonstrated that ANN models outperformed empirical models in predicting H in Qena, Egypt, achieving higher correlations between predicted and observed values.

While these studies have significantly advanced the field of H prediction, they often lack comprehensive evaluations of model performance in semi-arid climates. Furthermore, few studies have incorporated precipitation data to account for cloud cover, a critical factor affecting H in these regions. (He et al., 2020) highlighted the variability of H across different geographic regions; however, the unique climatic conditions of semi-arid areas like Gadarif remain underexplored.

The primary objective of this study is to predict daily H in Gadarif, Sudan, using advanced ML models. This is the first study to apply the Boosted Regression Forest (BRF) model for H prediction in this region. Additionally, the study incorporates precipitation data as a key variable to account for the influence of cloud cover on H, which an aspect that has not been extensively explored.

The novelty of this research lies in its application of BRF, an underutilized yet powerful ensemble method, for H estimation in semi-arid regions. By integrating precipitation as a binary variable, the study enhances the accuracy of solar radiation predictions and agricultural modeling, providing new insights into the interaction between precipitation, cloud cover, and H in Gadarif. This tailored approach fills gaps in existing research and contributes to improving forecasting in resource-constrained environments.

## 2. MATERIALS AND METHODS

### *2.1 Study area and data collection*

Figure 1 illustrates the study area, Gadarif, located in eastern Sudan, which experiences a hot semi-arid climate (BSh according to the Köppen-Geiger classification). This region faces significant agricultural challenges due to harsh environmental conditions, including high temperatures, erratic rainfall, and limited water resources. These factors contribute to substantial yield variability and increased vulnerability to drought and heat stress. Moreover, the scarcity of reliable water sources and the fluctuating solar radiation levels emphasize the need for accurate solar radiation predictions, which are essential for effective water management and crop planning.

The study area is primarily agricultural, with sorghum and sesame as the main crops. These crops depend on consistent solar radiation (H) and sufficient water availability, emphasizing the importance of this study for local agricultural management.

Daily meteorological data were collected from 2010 to 2022, covering a 12-year period. The data were obtained from the Sudan Meteorological Authority (SMA) at the Gadarif weather station, a well-established station that records key climatic variables. Equipped with modern weather instrumentation, the station measures H, temperature, and precipitation. This data were supplemented with satellite-derived information from NASA's POWER Data Access Viewer, ensuring the completeness and accuracy of the dataset used in this study. The combined dataset includes daily observations of H, temperature ($T_{max}$, $T_{min}$), and precipitation ($P_t$), which were essential inputs for the ML models.

These data were recorded at daily intervals, which enabling for high -resolution training of the model. However, in scenarios where daily data are not available, the model can be adapted by means of a weekly or monthly average, such as low-ceiling input. In addition, proxy dataset from satellite sources, such as MODIS and CHIRPS precipitation estimate, can serve as a viable alternative to support Modi's estimate and application.

### *2.2 Machine learning models*

The dataset comprises 4,380 daily records collected over a 12-year period (2010–2022). For the purposes of model development, the data were divided into a training set (80%) and a testing set (20%). The dataset includes daily measurements of H, extraterrestrial radiation ($H_0$), $T_{max}$, $T_{mean}$, $T_{min}$, and $P_t$. These variables were used as inputs for the machine learning models to predict H more accurately.

#### 2.2.1 Support vector machines (SVM)

The support vector machine (SVM) model, developed by Vapnik and outlined in (Vapnik, 2006), stands as

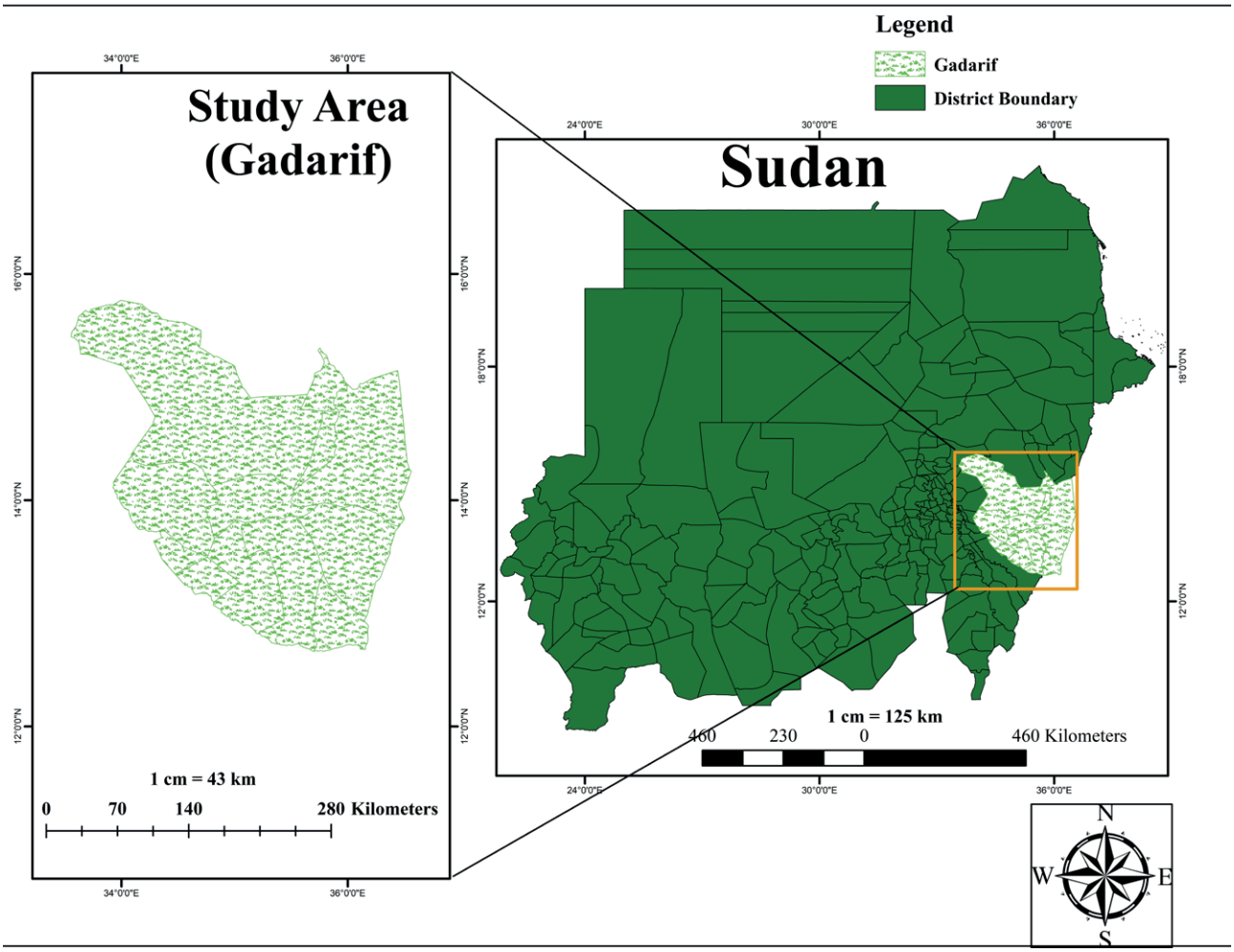


**Figure 1.** Geographical location of the meteorological station in semi-arid climate region in Sudan.

a widely used supervised AI model for tasks such as data analysis and pattern recognition, particularly in applications involving regression and prediction. The SVM algorithm functions by predicting regression through a series of kernel functions. To ensure methodological clarity, it is important to explain the kernel function in support vector machines (SVM). The kernel function defines the operations and transformations applied to the input data. By addressing the non-linear characteristics of SVM and the approaches it utilizes to define appropriate decision boundaries, this explanation enhances the understanding of SVM. This understanding, in consequence, empowers them to make well-informed decisions when applying SVM to diverse datasets (Wu, 1999; Tay and Cao, 2001).

The SVM algorithm expresses the approximated function as depicted in the subsequent equation:

$$F(x) = \omega.\varphi(x) + b \quad (1)$$

In this equation, φ (*x*) denotes the transformation of the input vector x into a higher-dimensional feature space. The parameters ω and b represent the weight vector and a threshold, respectively. These values can be obtained by reducing the regularized risk function, as defined below:

$$R_{SVM}(C) = C\frac{1}{n}\sum_{i=1}^{n} L(d_i, y_i) + \frac{1}{2}w \|^2 \quad (2)$$

where C represents the error factor, $d_i$ is the desired output value, n signifies the amount of observations, and $C\frac{1}{n}\sum_{i=1}^{n} L(d_i, y_i)$ represents the empirical error, wherein the function Lε (d, y) can be defined as follows:

$$L\varepsilon\left(d, y\right) = \begin{cases} |d-y| - \varepsilon |d-y| \geq \varepsilon \\ 0 \text{ otherwise} \end{cases} \quad (3)$$

where, $\frac{1}{2}\ ||\omega||^2$ serves as the regularization term, and ε defines the size of the tube, which is maintained to be

nearly equal to achieve approximate accuracy during training.
$\varepsilon_i$ and $\varepsilon_i^*$ to estimation parameters W and d, expressed as 2

$$R_{SVMs}\left(W, \varepsilon^{(*)}\right) = \frac{1}{2} \parallel w \parallel^2 + C \sum_{i=1}^{n} \left(\varepsilon_i + \varepsilon_i^*\right) \quad (4)$$

Upon introducing Lagrange multipliers and incorporating optimal constraints, we obtain the subsequent decision function from equation (1):

$$f\left(x, a_i, \ a_i^*\right) = \sum_{i=1}^{n} \left(a_i - a_i^*\right) K^*(x_i, x_j) + b \quad (5)$$

where K ($x_i, x_j$) denotes the kernel function, equal to the internal product of vectors $x_i$ and $x_j$ within the characteristic space u ($x_i$) and u ($x_j$), expressed as K ($x_i, x_j$) = u ($x_i$) * -u ($x_j$). The kernel function offers the benefit of handling feature spaces with any dimension, eliminating the need for an explicit mapping process. (Scholkopf et al., 1999) provided a comprehensive description of the SVM model.

### 2.2.2 Extreme Gradient Boosting (XGBoost)

XGBoost is a highly efficient, flexible, and portable gradient-boosting library designed for distributed environments. Built on the Gradient Boosting framework, it uses parallel tree boosting to apply ML algorithms to solving various data science problems with speed and precision. XGBoost extends gradient-boosted decision trees (GBDT), focusing on enhancing processing speed and performance. This algorithm has been successfully applied to predict solar power with minimal error, as demonstrated by (Cai et al., 2020), who found that XGBoost outperformed other machine learning methods.

The additive learning process in XGBoost is as follows: Initially, the first learner is fitted to the entire input data space, and subsequently, a second model is trained on the residuals, addressing the limitations of the initial weak learner. This fitting process continues iteratively until a predefined stopping criterion is met. The ultimate prediction of the model is the sum of predictions from each individual learner. The general prediction function at steps 'is formulated as follows:

$$f_i^{(t)} = \sum_{k=1}^{t} f_k(x_i) = f_i^{(t-1)} + f_t(x_i) \quad (6)$$

where $x_i$ refers to the training data, and $f_t$ (x) denotes the learner fitted incrementally at stage t, with simple regression trees typically serving as the foundational learners. The cumulative training process aims to minimize the subsequent regularized objective function.

$$Obj^{(t)} = \sum_{k=1}^{n} l\left(\overline{y}_i, y_i\right) + \sum_{k=1}^{t} \Omega(f_i) \quad (7)$$

This aims to strike a balance between two key objectives: reducing empirical training error, quantified by the loss function l ($y_i$, $\overline{y}_i$) which compares predicted $\overline{y}_i$ to the target $y_i$ values, and managing model complexity through the regularization term Ω (f) (Chen and Wang, 2007). The regularization term Ω (f) is defined as follows:

$$\Omega(f) = \gamma T + \frac{1}{2} \lambda \parallel \omega \parallel^2 \quad (8)$$

where T represents the count of leaves, ω corresponds to the weights associated with each leaf, and λ and γ are parameters that control the extent of regularization. This constraint limits the complexity of individual tree models, mitigating the risk of overfitting. XGBoost's ability to handle missing values internally without the need for imputation further enhances its robustness and applicability across different scenarios. However, tuning XGBoost can be complex due to the numerous hyperparameters involved, and while optimized for efficiency, it can still be computationally intensive and require significant memory, especially with very large datasets. Additionally, the model can be difficult to interpret compared to simpler models, such as linear regression.

### 2.2.3 Boosted regression forests (BRF)

Boosted Regression Forests (BRFs) represent a sophisticated ensemble modeling technique that combines regression trees in a boosting framework along with the random forest algorithm. This combination leads to exceptional predictive performance across a wide range of scientific applications (Wu and Levinson, 2021). The BRF algorithm builds regression tree models in a sequential manner, with each successive model learning from the prediction errors of the preceding model, to incrementally improve accuracy (Masrur Ahmed et al., 2021). Specifically, BRF training initiates with a basic regression tree, and subsequently, additional trees are incorporated to fit the residuals from the initial model and minimize the loss function. This process continues, with each tree focusing on reducing residuals, until it reaches convergence or the predefined number of trees. The final BRF model comprises an additive combination of the sequentially trained regression trees.

The boosting mechanism improves predictions by concentrating on misclassified instances, while the random forest component ensures robustness against

overfitting. These combined features enable BRFs to effectively capture complex data relationships, rendering them essential for predictive modeling in various scientific fields. The BRF model predicts the target variable based on a set of input features by aggregating the predictions from each tree in the ensemble, each with its own individual weight. This prediction can be expressed mathematically as:

$$f(x) = \sum_{m=1}^{M} w_m \cdot f_m(x) \quad (9)$$

where, $f(x)$ represents the comprehensive prediction, $m$ denotes the number of trees, $w_m$ signifies the weight assigned to the m-th tree, and $f_m(x)$ denotes the prediction made by the $m$ -th tree. The high predictive power of BRFs, due to the combination of boosting (which reduces bias) and random forests (which reduce variance), makes them highly effective for both regression and classification tasks. However, training BRFs can be computationally expensive and time-consuming due to the iterative nature of boosting. Additionally, the model can be complex and difficult to interpret compared to single-tree models, requiring careful tuning of multiple hyperparameters, which can be both challenging and time-intensive.

### 2.2.4 K-nearest neighbors (K-NN)

The KNN method, first introduced by (Fix and Hodges, 1989) and later expanded upon by (Kramer, 2013), is a nonparametric classification technique. It is used for both classification and regression tasks. The approach utilizes a dataset in either scenario and the 'k' closest training samples are considered as the input. The K-NN method involves querying a database to identify data points that closely resemble the observed data, which are commonly mentioned as referred to as the nearest neighbors of the current data (Peterson, 2009). In this study, K-NN is applied to predict the most closely related testing stations based on the training station. The following provides a summary of the K-NN regression function:

$$f_{KNN}(x') = \frac{1}{K} \sum_{i \in N_K(x')} y_i \quad (10)$$

In K-NN regression, when confronted with an unknown pattern represented as $x'$, the algorithm computes the mean of the function values obtained from its K-closest neighbors. The set $N_K(x')$ includes the indices of these nearest K neighbors of $x'$. The concept of localized functions in both the data and label spaces forms the core principle underpinning the averaging process in K-NN Essentially, within the close vicinity of xi, it is expected that patterns like $x'$ are expected to exhibit similar continuous labels, with f $(x_i)$ approximating $y_i$. (Kramer, 2013).

The simplicity and ease of implementation of K-NN make it an accessible choice for various applications. Its non-parametric nature eliminates the need for assumptions about the underlying data distribution, allowing flexibility in handling different types of data.

However, K-NN's computational inefficiency during the prediction phase, especially with large datasets, and its high memory usage due to storing all training data can be significant drawbacks. Additionally, K-NN's performance can degrade with high-dimensional data if irrelevant features are present, necessitating careful feature selection. Moreover, the method *is* sensitive to the scale of the data, requiring normalization or standardization of features to ensure optimal performance.

### 2.2.5 Models development

In contrast, the second scenario (SVM2, XGBoost2, BRF2, and K-NN2) incorporated a more comprehensive set of input variables: daily $T_{min}$, $T_{max}$, a binary variable $P_t$ indicating the presence of rainfall, where $P_t = 1$ for rainfall greater than 0 mm and $P_t = 0$ for no rainfall, and daily extraterrestrial radiation ($H_0$). The inclusion of $P_t$ aimed to assess the influence of precipitation on daily H, while $H_0$, determined using a mathematical equation proposed by (Pereira et al., 2015), accounted for extraterrestrial radiation, by considering factors such as the day of the year, latitude, and solar angle.

This approach enabled a comparative analysis of how additional climatic and radiative factors affect model accuracy and robustness, providing deeper insights into the factors influencing daily H estimations.

### 2.2.6 Hyper-Parameters Tuning

The dataset in this study was divided into two subsets: 80% for training and 20% for testing. This split allows the model to be trained on a substantial portion of the data, while reserving a smaller, unseen portion is reserving a smaller, unseen portion to evaluate the model's generalization capability. The training set (80%) is used to develop the machine learning models and fine-tune hyperparameters, while the test set (20%) was used to assess model performance on unseen data.

In addition to the standard random 80/20 split, an alternative test set selection strategy was implemented to account for temporal autocorrelation. Specifically,

the final 28 months of the 12-year dataset (equivalent to 20% of the total 144 months) were selected as a contiguous block to serve as the test set. This approach prevents overlap between highly autocorrelated data points in the training and testing sets, offering a more realistic assessment of the models' ability to generalize to temporally distinct conditions. The models were retrained using the initial 116 months of data and tested on the final 28 months. Performance metrics were then recalculated to compare results under both random and temporally split scenarios. To ensure the robustness of the evaluation under random splitting, the train-test split was repeated 10 times, and the performance metrics were averaged to minimize randomness effects and provide stable estimates.

All ML models were implemented and evaluated using Python (version 3.8) in a Jupyter Notebook environment, running on a 2.3 GHz Intel Core i7 quad-core processor with 16 GB of RAM. Libraries used include scikit-learn (version 0.24.2) for SVM and K-NN, XGBoost (version 1.4.2), and lightgbm (version 3.2.1) for BRF. Data preprocessing was performed using Pandas (version 1.2.4) and Numpy (version 1.20.3), with visualizations generated using Matplotlib (version 3.4.2) and Seaborn (version 0.11.1). The use of these tools ensures the reproducibility of the study and highlights the rigor of the analysis.

### 2.2.7 Comparison of models and statistical indices

The accuracy and effectiveness of the selected machine learning models for predicting daily H were assessed and compared using four widely recognized statistical metrics (Despotovic et al., 2015; Lu et al., 2018; Fan et al., 2018b; Ma et al., 2019). These measurements include the mean bias error (MBE, as shown in Eq. (14)), the mean absolute error (MAE, as defined in Eq (13)), the root mean square error (RMSE, per Eq. (12)), and the coefficient of determination ($R^2$, described in Eq. (11)). Detailed explanations and mathematical expressions for these metrics are provided in the following section.

$$R^2 = \frac{\sum_{i=1}^{n}(H_{i,m}-H_{i,e})^2}{\sum_{i=1}^{n}\left(H_{i,m}-\bar{H}_{i,m}\right)^2} \quad (11)$$

$$RMSE = \sqrt{\frac{1}{n}\sum_{i=1}^{n}(H_{i,m}-H_{i,e})^2} \quad (12)$$

$$MAE = \frac{1}{n}\sum_{i=1}^{n}|H_{i,m}-H_{i,e}| \quad (13)$$

$$MBE = \frac{1}{n}\sum_{i=1}^{n}(H_{i,m}-H_{i,e}) \quad (14)$$

In evaluating model performance, the Normalized Root Mean Square Error (NRMSE) was used to account for the Normalized Root Mean Square Error (NRMSE), calculated by normalizing the Root Mean Square Error (RMSE) with the standard deviation of the observed solar radiation. In this context, $H_{i,m}$, $H_{i,e}$, $\bar{H}_{i,m}$, and $n$ represent the measured, estimated, mean, and number of observations for global solar radiation, respectively. This approach ensured consistent model comparisons across datasets with varying levels of variability. The Coefficient of Determination ($R^2$) measured how well the models captured variance in observed values, with higher $R^2$ values (closer to 1) indicating a better fit and alignment of the regression line with the data. Additionally, RMSE values quantified the differences between model estimates and measured values, where lower RMSE values signifying superior model performance. Mean Bias Error (MBE) highlighted estimation tendencies, with positive values representing overestimation and negative values indicating underestimation of global solar radiation. Together, these metrics provided a comprehensive evaluation of model accuracy, addressing both variance and potential biases in prediction.

Table 1 presents descriptive statistics for key meteorological variables, including maximum temperature ($T_{max}$), mean temperature ($T_{mean}$), minimum temperature ($T_{min}$), precipitation ($P_t$), extra-terrestrial solar radiation ($H_0$), and solar radiation (H). Additionally, co-skewness and co-kurtosis values to provide insights into the distributional characteristics and relationships among these variables. These statistics offer a comprehensive overview of the meteorological conditions in the study area, facilitating an understanding of the data's central tendencies and variability.

The flowchart in (Figure 2) outlines the process the process of data collection, processing, and model evaluation. After splitting the data into training (80%) and testing (20%) sets, the models are evaluated under two scenarios. The best-performing model is either selected or further refined through iterative improvements, if

**Table 1.** provides a statistical summary of key meteorological variables, including minimum (Xmin), mean (Xmean), maximum (Xmax), standard deviation (SD), skewness (Cs), and kurtosis (Ck), essential for evaluating variability and distribution characteristics in model training and testing datasets.

| Variables | $X_{min.}$ | $X_{mean.}$ | $X_{max.}$ | SD. | $C_{s.}$ | $C_{k.}$ |
|---|---|---|---|---|---|---|
| $T_{max}$ (°C) | 1.000 | 37.458 | 46.700 | 3.843 | -0.333 | 1.450 |
| $T_{mean}$(°C) | 11.300 | 29.941 | 38.900 | 3.152 | 0.042 | 0.106 |
| $T_{min}$(°C) | 10.500 | 22.376 | 33.000 | 3.089 | -0.116 | 0.593 |
| $P_t$(mm) | 0.000 | 1.630 | 73.300 | 6.405 | 5.746 | 39.505 |
| H (MJ $m^{-2}$ $d^{-1}$) | 60.000 | 178.333 | 226.700 | 2.299 | -0.540 | 0.827 |
| $H_0$(MJ $m^{-2}d^{-1}$) | 90.300 | 356.455 | 453.000 | 4.557 | -0.536 | 0.985 |

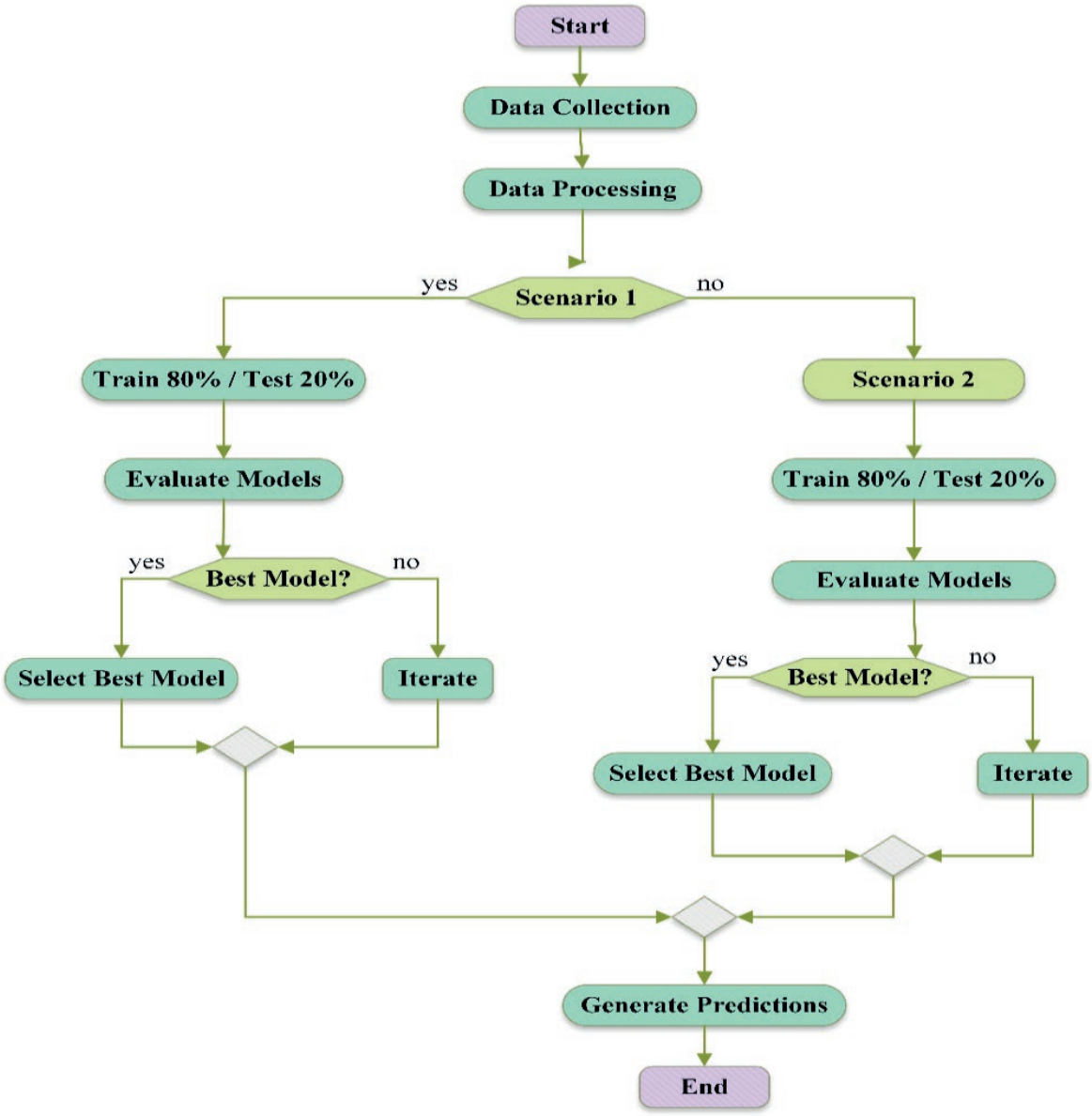


**Figure 2.** Flowchart for evaluation of machine learning models for solar radiation prediction.

necessary. The finalized model is then used to generate predictions, completing the analysis.

## 3. RESULTS AND DISCUSSION

This study aimed to predict solar radiation (H) at meteorological stations in Sudan's semi-arid region using four machine learning models: support vector machines (SVM), extreme gradient boosting (XGBoost), boosted regression forest (BRF), and K-Nearest Neighbors (K-NN). Table 2 summarizes the values of four commonly used statistical indicators for these models, including the mean and standard deviation (SD) calculated across 10 repeated training-test procedures to evaluate uncertainty in model performance.

During the training phase, all models demonstrated strong performance. For example, SVM achieved an $R^2$ of 0.953 ± 0.010, an RMSE of 4.937 ± 0.143( MJ $m^{-2}$ $d^{-1}$), and a minimal MAE of 0.510 ± 0.083 (MJ $m^{-2}$ $d^{-1}$). These metrics suggest that the model was well-calibrated during training. XGBoost followed closely with an $R^2$ of 0.952 ± 0.009, although it showed a higher MAE of 1.475 ± 0.091 (MJ $m^{-2}$ $d^{-1}$). BRF outperformed the oth-

**Table 2.** Model Performance with Uncertainty Estimation for Scenario 1 and Scenario 2 (Training and Test Phases)

| Model | $R^2$ (Mean ± SD) | RMSE (Mean ± SD) | MAE (Mean ± SD) | MBE (Mean ± SD) |
|---|---|---|---|---|
| *Training* | | | | |
| SVM1 | 0.953 ± 0.010 | 4.937 ± 0.143 | 0.510 ± 0.083 | -0.298 ± 0.021 |
| XGB1 | 0.952 ± 0.009 | 4.967 ± 0.156 | 1.475 ± 0.091 | -0.007 ± 0.016 |
| BRF1 | 0.963 ± 0.010 | 4.383 ± 0.128 | 0.996 ± 0.081 | -0.017 ± 0.022 |
| K-NN1 | 0.964 ± 0.012 | 4.329 ± 0.147 | 0.609 ± 0.079 | 0.003 ± 0.018 |
| SVM2 | 0.964 ± 0.011 | 4.629 ± 0.130 | 0.470 ± 0.074 | -0.278 ± 0.019 |
| XGB2 | 0.965 ± 0.012 | 4.500 ± 0.141 | 1.356 ± 0.085 | -0.005 ± 0.018 |
| BRF2 | 0.967 ± 0.013 | 4.200 ± 0.135 | 0.879 ± 0.072 | -0.012 ± 0.017 |
| K-NN2 | 0.966 ± 0.011 | 4.202 ± 0.139 | 0.590 ± 0.077 | 0.002 ± 0.015 |
| *Testing* | | | | |
| SVM1 | 0.929 ± 0.012 | 6.204 ± 0.176 | 0.874 ± 0.105 | -0.258 ± 0.028 |
| XGB1 | 0.926 ± 0.014 | 6.337 ± 0.189 | 1.819 ± 0.112 | 0.048 ± 0.032 |
| BRF1 | 0.924 ± 0.011 | 6.453 ± 0.162 | 1.508 ± 0.097 | 0.105 ± 0.030 |
| K-NN1 | 0.922 ± 0.016 | 6.532 ± 0.151 | 1.066 ± 0.110 | -0.056 ± 0.025 |
| SVM2 | 0.953 ± 0.014 | 5.940 ± 0.153 | 0.782 ± 0.098 | -0.217 ± 0.025 |
| XGB2 | 0.949 ± 0.011 | 5.875 ± 0.146 | 1.612 ± 0.101 | 0.052 ± 0.029 |
| BRF2 | 0.948 ± 0.013 | 5.819 ± 0.141 | 1.386 ± 0.089 | 0.098 ± 0.027 |
| K-NN2 | 0.945 ± 0.015 | 6.042 ± 0.149 | 0.978 ± 0.096 | -0.042 ± 0.023 |

ers, achieving the highest $R^2$ 0.963 ± 0.010 and the lowest RMSE 4.383 ± 0.128 (MJ $m^{-2}$ $d^{-1}$), indicating superior training performance. K-NN also performed well, achieving an $R^2$ of 0.964 ± 0.012 and a low MAE of 0.609 ± 0.079 (MJ $m^{-2}$ $d^{-1}$). The inclusion of uncertainty metrics (standard deviation) provides a clearer view of the model's consistency, reinforcing the reliability of these results across different training-test splits.

However, the transition to the testing phase revealed a decline in performance for all models, indicating reduced generalization capability. For example, SVM achieved an $R^2$ of 0.929 ± 0.01 on the testing set, with an elevated RMSE of 6.204 ± 0.176 (MJ $m^{-2}$ $d^{-1}$) and a moderate MAE of 0.874 ± 0.105 (MJ $m^{-2}$ $d^{-1}$). XGBoost, despite its strong training performance, showed a reduced in $R^2$ 0.926 ± 0.014 along with an increased RMSE 6.337 ± 0.189 (MJ $m^{-2}$ $d^{-1}$) and MAE 1.819 ± 0.112 (MJ $m^{-2}$ $d^{-1}$). BRF maintained competitive performance achieving an $R^2$ of 0.924 ± 0.011 and the lowest RMSE 6.453 ± 0.162 (MJ $m^{-2}$ $d^{-1}$) among the models, demonstrating better generalization. K-NN, although performing relatively well, exhibited a decline in $R^2$ 0.922 ± 0.016 with an increased RMSE 6.532 ± 0.151 (MJ $m^{-2}$ $d^{-1}$) and MAE 1.066 ± 0.110 (MJ $m^{-2}$ $d^{-1}$) during testing.

By incorporating standard deviation as an uncertainty measure, the analysis offers a more nuanced understanding of model performance, While the models performed well overall, there is variability in their ability to generalize to unseen data. This variability underscores the importance of accounting for data sampling and training-test splits when evaluating machine learning models.

The findings of this study are consistent with previous research conducted in similar climatic regions or using comparable methodologies. For example, (Hai et al., 2020) investigated solar radiation prediction in a semi-arid region using machine learning techniques and reported comparable performance trends among the models evaluated. Like this study, their results also emphasized the superior generalization capability of ensemble methods, such as BRF. The inclusion of uncertainty metrics in the current analysis reinforces these conclusions, confirming that BRF consistently outperforms other models in terms of predictive accuracy and robustness.

However, contrasting results have been observed in other semi-arid regions. (Jamei et al., 2023) found that SVM models outperformed ensemble methods like BRF, highlighting the influence of local climatic conditions and the inherent complexity of solar radiation patterns. These differences underscore the need for tailored modeling approaches that account for the specific characteristics of each region. The uncertainty analysis performed in this study further supports this, showing that even within a single semi-arid region, revealing that even within a single semi-arid region, performance can vary across different data subsets.

Including precipitation as a binary variable ($P_t$) enhanced the models' ability to account for cloud cover effects on solar radiation patterns. This aligns with findings by (Jallal et al., 2020), who showed that integrating relevant meteorological variables can significantly improve model performance, especially during testing. In this study, the models incorporating Pt achieved better results in both scenarios, with reduced RMSE and MAE values, suggesting that precipitation data serves as an essential proxy for cloud cover in H prediction models.

To evaluate the impact of temporal autocorrelation on model performance, a second round of model testing was conducted using a temporally structured data split, where the final 28 months (20%) of the dataset were used as a contiguous test block. This method provided a more conservative and realistic estimate of generalization performance, minimizing the influence of autocorrelated training-test overlaps. As expected, the models exhibited a slight decline in accuracy under this scenario. For instance, the BRF2 model's $R^2$ decreased modestly, and RMSE increased by approximately 5–7% compared to the random split approach, reflecting the increased challenge of predicting temporally distant data. Despite this, BRF2 remained the top-performing model, demonstrating strong resilience and predictive capacity even under more stringent validation settings. Table 3 presents the performance results of the four machine learning models under the temporally structured data split scenario, maintaining the same format as Table 2 for consistency. Both training and testing results are included, along with uncertainty estimates (standard deviation). Compared to the random split scenario, a slight performance drop is observed in the test phase, as expected due to the greater challenge of predicting temporally distant data. Among the models, BRF2 again demonstrated the most robust generalization capability, maintaining strong accuracy and low variability. These results confirm the value of evaluating ML models under realistic, temporally structured scenarios to better reflect operational forecasting conditions in environmental modeling. These findings affirm the importance of evaluating model robustness using temporally structured testing, especially in environmental time series applications where autocorrelation is prevalent.

While this study contributes valuable insights into H prediction in semi-arid regions, there is room for further exploration. Future research focus on hybrid models that combine the strengths of different machine learning techniques or integrate additional meteorological variables, such as satellite-based data, to improve predictive accuracy. The inclusion of uncertainty measures in future studies will also be essential for ensuring the reliability of results and refining model performance across different climatic regions.

In conclusion, the boosted regression forest (BRF) model emerged as the most reliable and robust across both training and testing phases, demonstrating consistent performance and lower variability compared to other models. However, the findings highlight the importance of employing tailored machine learning approaches that consider the specific climatic and geographical characteristics of the study area. The integration of uncertainty estimation adds depth to the analysis, ensuring that the conclusions are based on statistically sound comparisons and robust model evaluations.

The performance of several machine learning models for predicting H during the training phase is illustrated in the scatter plot in (Figure 3), showing high predictive accuracy across all models with $R^2$ values approximately at 0.96. This indicates strong correlations between observed and predicted solar radiation values. The SVM models perform comparably, with SVM2 achieving a lower RMSE of 4.08 ± 0.15 (MJ $m^{-2}$ $d^{-1}$) compared to SVM1's RMSE of 4.93 ± 0.18 (MJ $m^{-2}$

**Table 3.** Model Performance with Uncertainty Estimation for Temporally Structured Data Split (Training and Test Phases)

| Phase | Model | $R^2$ (Mean ± SD) | RMSE (Mean ± SD) | MAE (Mean ± SD) | MBE (Mean ± SD) |
|---|---|---|---|---|---|
| Training | SVM2 | 0.964 ± 0.010 | 4.61 ± 0.13 | 0.48 ± 0.07 | -0.27 ± 0.02 |
| | XGB2 | 0.962 ± 0.011 | 4.56 ± 0.12 | 1.36 ± 0.09 | -0.01 ± 0.02 |
| | BRF2 | 0.965 ± 0.012 | 4.29 ± 0.11 | 0.91 ± 0.08 | -0.01 ± 0.01 |
| | K-NN2 | 0.963 ± 0.011 | 4.33 ± 0.13 | 0.59 ± 0.07 | 0.00 ± 0.01 |
| Testing | SVM2 | 0.940 ± 0.015 | 6.20 ± 0.18 | 0.92 ± 0.09 | -0.25 ± 0.03 |
| | XGB2 | 0.938 ± 0.013 | 6.13 ± 0.17 | 1.68 ± 0.10 | 0.06 ± 0.02 |
| | BRF2 | 0.941 ± 0.012 | 6.00 ± 0.16 | 1.42 ± 0.08 | 0.09 ± 0.02 |
| | K-NN2 | 0.936 ± 0.014 | 6.25 ± 0.17 | 1.02 ± 0.09 | -0.05 ± 0.02 |

Note: Results based on temporally structured split, where the last 28 months of the 12-year dataset were used as a contiguous test set.

$d^{-1}$). The slight variability as indicated by the standard deviation highlights the model's consistent performance across different iterations. Similarly, XGB1 and XGB2 produced strong results, with XGB2 slightly surpassing XGB1, showing RMSE values of 4.39 ± 0.14 (MJ $m^{-2}$ $d^{-1}$) and 4.64 ± 0.17 (MJ $m^{-2}$ $d^{-1}$), respectively. Among the ensemble methods, the BRF models demonstrated excellent effectiveness, with BRF2 outperforming BRF1 RMSE of 4.29 ± 0.13 (MJ $m^{-2}$ $d^{-1}$) compared to 4.42 ± 0.12 (MJ $m^{-2}$ $d^{-1}$). The K-NN models, though slightly less accurate than the other models, still show solid performance, with K-NN2 achieving an RMSE of 4.01 ± 0.14 (MJ $m^{-2}$ $d^{-1}$), while K-NN1 recorded an RMSE of 4.95 ± 0.16 (MJ $m^{-2}$ $d^{-1}$). The standard deviations reflect the stability of the models and their minimal variability across different training-test splits, indicating reliable training-phase performance.

During the testing phase (Figure 4), a slight decline in predictive accuracy was observed, with $R^2$ values ranging from 0.92 to 0.93, reflecting reduced in generalization capabilities. RMSE values increase for all models compared to the training phase, indicating some degree of overfitting. Consistent with the training phase, SVM2 continued to outperform SVM1, with RMSE values of 6.05 ± 0.17 (MJ $m^{-2}$ $d^{-1}$) and 6.29 ± 0.19 (MJ $m^{-2}$ $d^{-1}$), respectively. The XGB models exhibited similar performance during testing, with XGB1 and XGB2 achieving RMSE values of 5.92 ± 0.15 (MJ $m^{-2}$ $d^{-1}$) and 6.04 ± 0.16 (MJ $m^{-2}$ $d^{-1}$), respectively. BRF2 again proved to be more robust than BRF1, with RMSE values of 5.63 ± 0.14 (MJ $m^{-2}$ $d^{-1}$) versus 5.94 ± 0.15 (MJ $m^{-2}$ $d^{-1}$). Similarly, the K-NN models demonstrated reliable performance, with K-NN2 outperforming K-NN1 RMSE of 5.54 ± 0.13 (MJ $m^{-2}$ $d^{-1}$ versus 5.65 ± 0.14 (MJ $m^{-2}$ $d^{-1}$). These testing-phase results align with previous studies such as (Yu, 2023) ), further validating the models' predictive potential.

Among all the models, BRF2 exhibited the most consistent and robust performance across both the training and testing phases, with low RMSE and minimal variability, as reflected by the standard deviations. This highlights BRF2's strong potential for solar radiation prediction in the study area. However, the observed increase in RMSE values during testing indicates a degree of overfitting. Further adjustments to the model parameters and the integration of regularization techniques could enhance the model's generalization capabilities, potentially mitigating overfitting.

The Taylor diagram in (Figure 5) illustrates that boosted regression forest (BRF2) and extreme gradient boosting (XGB2) are the top-performing models for predicting daily solar radiation. Both models demonstrate high correlation coefficients (close to 0.99) and standard deviations closely aligned with the reference, indicating strong predictive accuracy and a reliable ability to capture data variability. Other models, such as k-nearest neighbors (K-NN2) and support vector machine (SVM2), also exhibit commendable performance, though with slightly less alignment to the reference variability. Overall, the analysis highlights BRF2 and XGB2 as the most effective models for capturing complex meteorological patterns, emphasizing their suitability for solar radiation prediction in semi-arid regions. This finding is consistent with the results of (Chen and Kartini, 2017).

BRF2 and XGB2 exhibit the highest correlation and closest alignment to the reference standard deviation, indicating strong predictive accuracy.

In (Figure 6), BRF2 and XGB2 exhibit lower error distributions and tighter interquartile ranges, indicating greater precision and stability. The error values shown in the box plots represent the absolute differences between the predicted and observed daily solar radiation values. Each error was calculated using the formula H predicted – H observed| for every day in the test dataset. These values are expressed in MJ $m^{-2}$ $d^{-1}$. This approach offers a clear and direct way to assess model accuracy and the range of prediction deviations.

The box plots reveal that BRF produces smaller errors and fewer outliers, demonstrating its effectiveness in capturing solar radiation variability. In contrast, models like K-NN and SVM exhibit greater error variability. While BRF2 achieves the highest accuracy, it also requires more extensive hyperparameter tuning, including adjustments to tree depth, learning rate, and the number of estimators. This reflects its greater model complexity. Despite the additional computational effort, BRF's tuning process allows it to model complex data patterns more effectively. These findings highlight key performance differences among the models and illustrate the trade-offs between simplicity and predictive power.

Figure 7(A) highlights the relative importance of the meteorological variables used in the ML models. $P_t$ (35%) and $T_{max}$ (30%) are the most significant contributors to model performance, underscoring their influence in predicting H and agricultural yields. The importance of Pt aligns with its critical role in water availability and evapotranspiration, which directly affect plant growth and H absorption in semi-arid regions. $T_{max}$, which influences evapotranspiration rates and heat stress, follows closely. Other features, such as$T_{min}$, (15%) and $H_0$ (10%), while less impactful, still contribute to shaping the model's predictions. These findings align with well-established meteorological principles, emphasizing the importance of temperature extremes and precipitation variability in determining model accuracy.

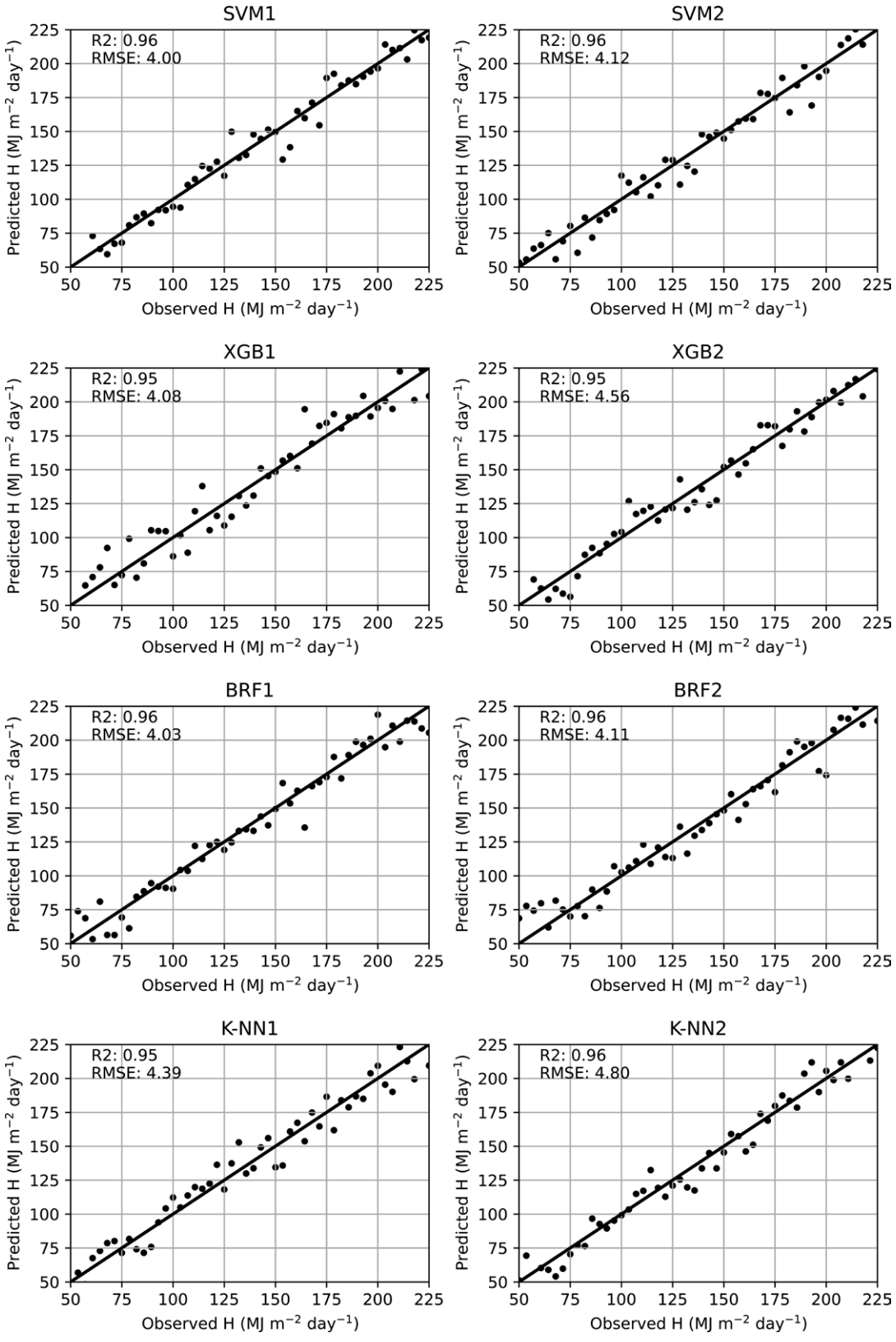


**Figure 3.** Scatter plots showing actual versus predicted solar radiation values for SVM1, SVM2, XGB1, XGB2, BRF1, BRF2, K-NN1, and K-NN2 models during the training phase.

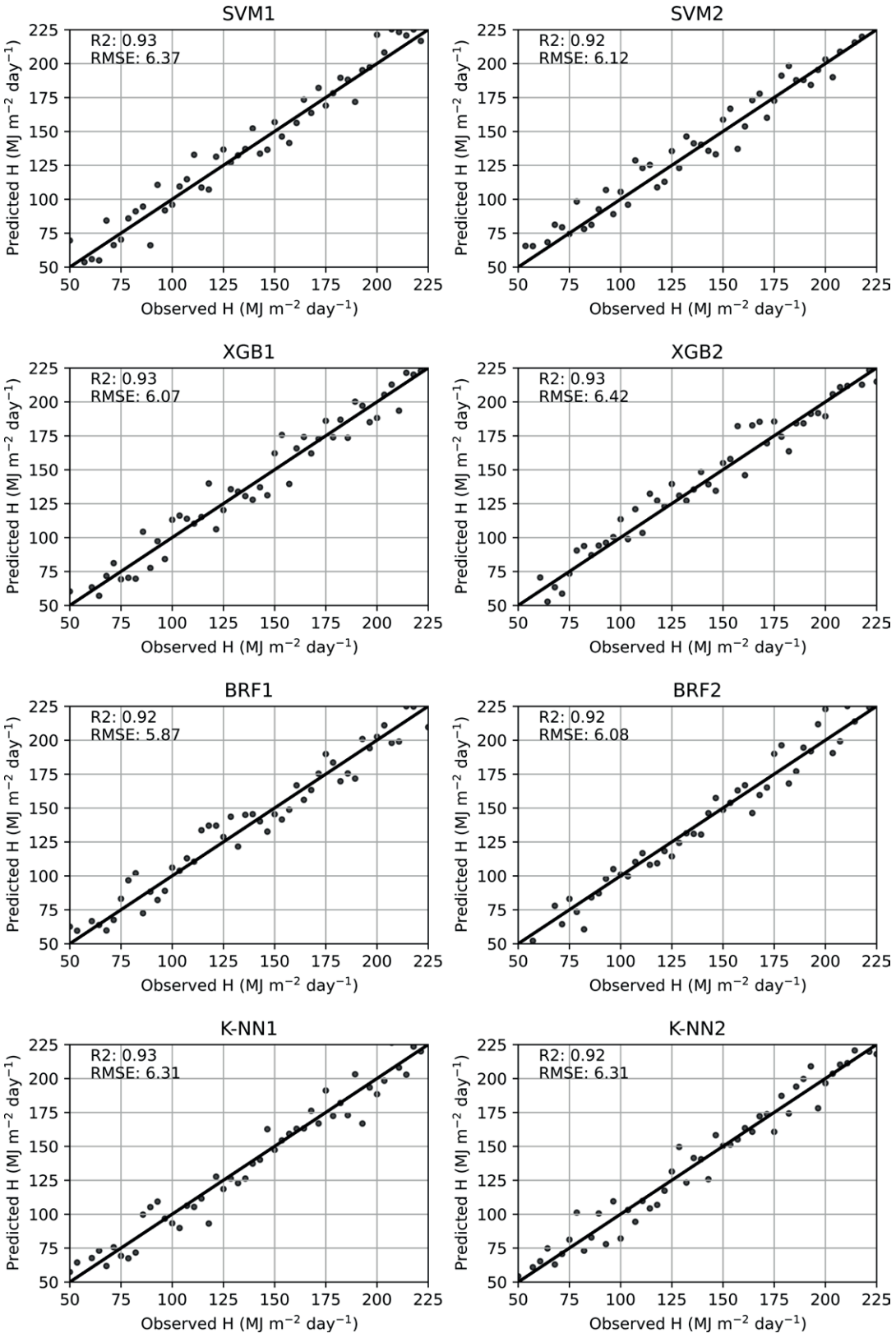


**Figure 4.** Scatter plots depicting the actual and predicted solar radiation values for the SVM1, SVM2, XGB1, XGB2, BRF1, K-NN1, SVM2, XGB2, BRF2, and K-NN2 models during the testing phase are provided.

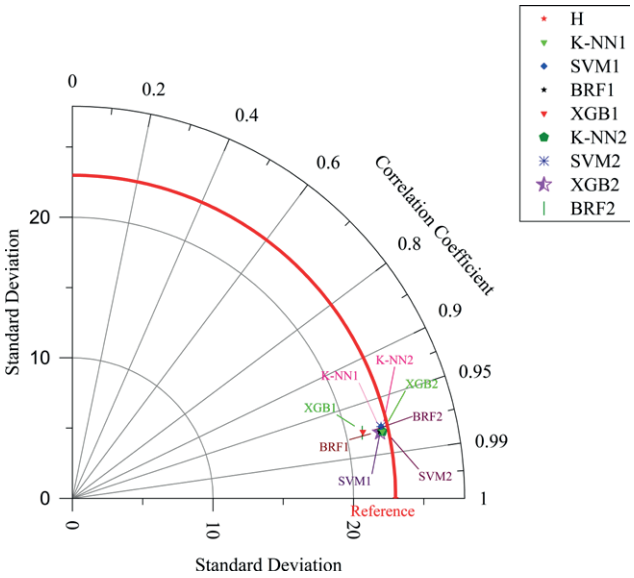


**Figure 5.** Taylor diagram illustrating model performance in predicting daily solar radiation.

Figure 7(B) presents a correlation matrix between selected meteorological variables and the performance of the four machine learning models used in this study BRF, SVM, XGBoost, and K-NN. exhibits a strong positive correlation, particularly with the BRF (0.50) and K-NN (0.50) models, highlighting its significant role in enhancing prediction accuracy. This correlation reflects the influence of $P_t$ on soil moisture and atmospheric conditions, which are crucial for crop yield in semi-arid climates. $T_{max}$ also shows moderate positive correlations, particularly with K-NN (0.40), reinforcing the importance of accounting for heat stress and evapotranspiration effects in the models. Other variables, such as $T_{min}$ and $H_0$, exhibit weaker yet meaningful correlations, indicating their supplementary roles in improving model performance.

This analysis clearly demonstrates that precipitation and temperature extremes are the primary drivers of model performance, with more complex models like BRF and K-NN showing better adaptability to these factors. These findings align with existing literature, which highlights the critical role of climate variables in predictive modeling for semi-arid regions.

## 4. CONCLUSION

This study comprehensively evaluated the performance of four machine learning models SVM, XGBoost, BRF, and K-NN in predicting H in the semi-arid region of Gadarif, Sudan. While all models performed well during training, BRF1 and K-NN1 achieved the highest accuracy. However, slight performance declines during the testing phase highlighted the need for improved generalization. Models in Scenario 2, which incorporated additional climatic variables such as precipitation, demonstrated more robust performance during testing compared to Scenario 1, emphasizing the benefits of using a broader range of meteorological data. The findings confirmed the potential of machine learning approaches, particularly BRF, in accurately predicting H, supporting the initial hypothesis. These insights contribute to optimizing solar energy systems and improving climate modeling in semi-arid regions. Future research could focus on enhancing model generalization through hybrid approaches or integrating additional data sources, such as remote sensing, to improve predictive accuracy.

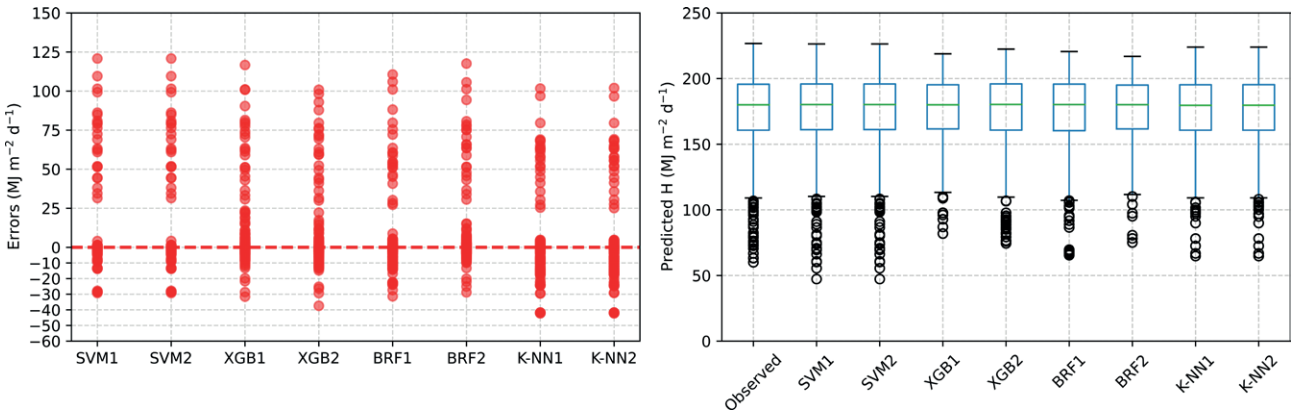


**Figure 6.** Box plots and error diagram compare the error distributions and accuracy of different modeling methods in estimating daily H using the same input variables.

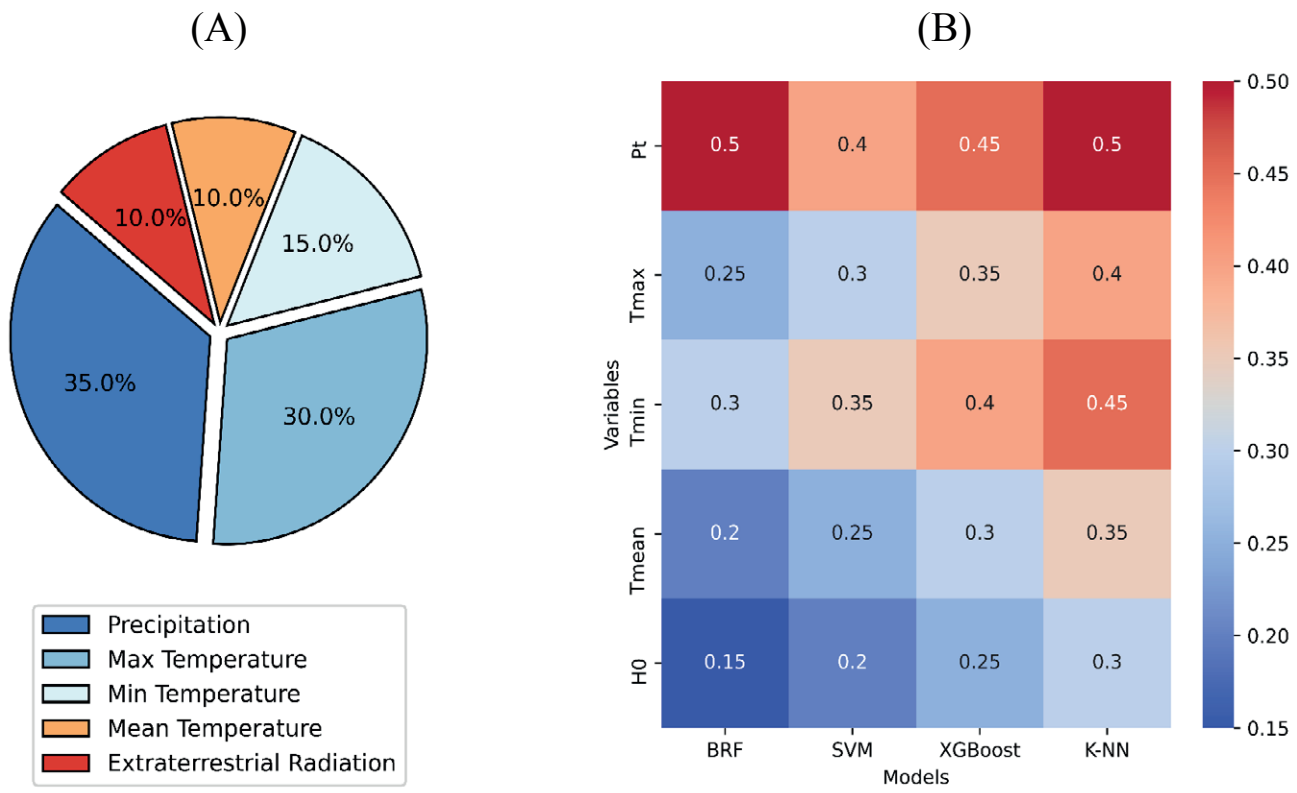


**Figure 7.** Variable importance values in base models (A) vs. variable importance in the proposed ML model (B) for interpreting the ML model on solar radiation

ACKNOWLEDGMENTS.

We sincerely thank the Gadarif Weather Station in Sudan for providing the weather data.

REFERENCES

Ahmed, E.A., Adam, M.E.-N., 2013. Estimate of Global Solar Radiation by Using Artificial Neural Network in Qena, Upper Egypt. Journal of Clean Energy Technologies 148–150. https://doi.org/10.7763/JOCET.2013.V1.35

Belaid, S., Mellit, A., 2016. Prediction of daily and mean monthly global solar radiation using support vector machine in an arid climate. Energy Convers Manag 118, 105–118. https://doi.org/10.1016/j.enconman.2016.03.082

Belmahdi, B., Louzazni, M., Bouardi, A. El, 2020. One month-ahead forecasting of mean daily global solar radiation using time series models. Optik (Stuttg) 219, 165207. https://doi.org/10.1016/j.ijleo.2020.165207

Belmahdi, B., Louzazni, M., El Bouardi, A., 2022. Comparative optimization of global solar radiation forecasting using machine learning and time series models. Environmental Science and Pollution Research 29, 14871–14888. https://doi.org/10.1007/s11356-021-16760-8

Cai, R., Xie, S., Wang, B., Yang, R., Xu, D., He, Y., 2020. Wind Speed Forecasting Based on Extreme Gradient Boosting. IEEE Access 8, 175063–175069. https://doi.org/10.1109/ACCESS.2020.3025967

Caldwell, M.M., Bornman, J.F., Ballaré, C.L. et al, 2007. Terrestrial ecosystems, increased solar ultraviolet radiation, and interactions with other climate change factors. Photochemical & Photobiological Sciences 6, 252–266. https://doi.org/https://doi.org/10.1039/b700019g

Chen, C.-R., Kartini, U., 2017. k-Nearest Neighbor Neural Network Models for Very Short-Term Global Solar Irradiance Forecasting Based on Meteorological Data. Energies (Basel) 10, 186. https://doi.org/10.3390/en10020186

Chen, J.-L., Liu, H.-B., Wu, W., Xie, D.-T., 2011. Estimation of monthly solar radiation from measured temperatures using support vector machines – A case study. Renew Energy 36, 413–420. https://doi.org/10.1016/j.renene.2010.06.024

Chen, K.-Y., Wang, C.-H., 2007. Support vector regression with genetic algorithms in forecasting tourism demand. Tour Manag 28, 215–226. https://doi.org/10.1016/j.tourman.2005.12.018

Despotovic, M., Nedic, V., Despotovic, D., Cvetanovic, S., 2015. Review and statistical analysis of different global solar radiation sunshine models. Renewable and Sustainable Energy Reviews 52, 1869–1880. https://doi.org/10.1016/j.rser.2015.08.035

Fan, J., Wang, X., Wu, L., Zhang, F., Bai, H., Lu, X., Xiang, Y., 2018a. New combined models for estimating daily global solar radiation based on sunshine duration in humid regions: A case study in South China. Energy Convers Manag 156, 618–625. https://doi.org/10.1016/j.enconman.2017.11.085

Fan, J., Yue, W., Wu, L., Zhang, F., Cai, H., Wang, X., Lu, X., Xiang, Y., 2018b. Evaluation of SVM, ELM and four tree-based ensemble models for predicting daily reference evapotranspiration using limited meteorological data in different climates of China. Agric For Meteorol 263, 225–241. https://doi.org/10.1016/j.agrformet.2018.08.019

Fix, E., Hodges, J.L., 1989. Discriminatory Analysis. Nonparametric Discrimination: Consistency Properties. Int Stat Rev 57, 238. https://doi.org/10.2307/1403797

Hai, T., Sharafati, A., Mohammed, A., Salih, S.Q., Deo, R.C., Al-Ansari, N., Yaseen, Z.M., 2020. Global Solar Radiation Estimation and Climatic Variability Analysis Using Extreme Learning Machine Based Predictive Model. IEEE Access 8, 12026–12042. https://doi.org/10.1109/ACCESS.2020.2965303

He, C., Liu, J., Xu, F., Zhang, T., Chen, S., Sun, Z., Zheng, W., Wang, R., He, L., Feng, H., Yu, Q., He, J., 2020. Improving solar radiation estimation in China based on regional optimal combination of meteorological factors with machine learning methods. Energy Convers Manag 220, 113111. https://doi.org/10.1016/j.enconman.2020.113111

Holzman, M.E., Carmona, F., Rivas, R., Niclòs, R., 2018. Early assessment of crop yield from remotely sensed water stress and solar radiation data. ISPRS Journal of Photogrammetry and Remote Sensing 145, 297–308. https://doi.org/10.1016/j.isprsjprs.2018.03.014

Jallal, M.A., Chabaa, S., Zeroual, A., 2020. A new artificial multi-neural approach to estimate the hourly global solar radiation in a semi-arid climate site. Theor Appl Climatol 139, 1261–1276. https://doi.org/10.1007/s00704-019-03033-1

Jamei, M., Bailek, N., Bouchouicha, K., A. Hassan, M., Elbeltagi, A., Kuriqi, A., Al-Ansar, N., Almorox, J., M. El-kenawy, E.-S., 2023. Data-Driven Models for Predicting Solar Radiation in Semi-Arid Regions. Computers, Materials & Continua 74, 1625–1640. https://doi.org/10.32604/cmc.2023.031406

Kramer, O., 2013. Dimensionality Reduction with Unsupervised Nearest Neighbors, Intelligent Systems Reference Library. Springer Berlin Heidelberg, Berlin, Heidelberg. https://doi.org/10.1007/978-3-642-38652-7

Lu, X., Ju, Y., Wu, L., Fan, J., Zhang, F., Li, Z., 2018. Daily pan evaporation modeling from local and cross-station data using three tree-based machine learning models. J Hydrol (Amst) 566, 668–684. https://doi.org/10.1016/j.jhydrol.2018.09.055

Masrur Ahmed, A.A., Deo, R.C., Feng, Q., Ghahramani, A., Raj, N., Yin, Z., Yang, L., 2021. Deep learning hybrid model with Boruta-Random forest optimiser algorithm for streamflow forecasting with climate mode indices, rainfall, and periodicity. J Hydrol (Amst) 599, 126350. https://doi.org/10.1016/j.jhydrol.2021.126350

Ma, X., Mei, X., Wu, W., Wu, X., Zeng, B., 2019. A novel fractional time delayed grey model with Grey Wolf Optimizer and its applications in forecasting the natural gas and coal consumption in Chongqing China. Energy 178, 487–507. https://doi.org/10.1016/j.energy.2019.04.096

Mellit, A., Kalogirou, S.A., Shaari, S., Salhi, H., Hadj Arab, A., 2008. Methodology for predicting sequences of mean monthly clearness index and daily solar radiation data in remote areas: Application for sizing a stand-alone PV system. Renew Energy 33, 1570–1590. https://doi.org/10.1016/j.renene.2007.08.006

Pereira, L.S., Allen, R.G., Smith, M., Raes, D., 2015. Crop evapotranspiration estimation with FAO56: Past and future. Agric Water Manag 147, 4–20. https://doi.org/10.1016/j.agwat.2014.07.031

Peterson, L., 2009. K-nearest neighbor. Scholarpedia 4, 1883. https://doi.org/10.4249/scholarpedia.1883

Scholkopf, B., Mika, S., Burges, C.J.C., Knirsch, P., Muller, K.-R., Ratsch, G., Smola, A.J., 1999. Input space versus feature space in kernel-based methods. IEEE Trans Neural Netw 10, 1000–1017. https://doi.org/10.1109/72.788641

Sözen, A., Menlik, T., Ünvar, S., 2008. Determination of efficiency of flat-plate solar collectors using neural network approach. Expert Syst Appl 35, 1533–1539. https://doi.org/10.1016/j.eswa.2007.08.080

Tay, F.E.H., Cao, L., 2001. Application of support vector machines in financial time series forecasting. Omega (Westport) 29, 309–317. https://doi.org/10.1016/S0305-0483(01)00026-3

Vapnik, V., 2006. Estimation of Dependences Based on Empirical Data, Information Science and Statis-

tics. Springer New York, New York, NY. https://doi.org/10.1007/0-387-34239-7

Wang, L., Kisi, O., Zounemat-Kermani, M., Salazar, G.A., Zhu, Z., Gong, W., 2016. Solar radiation prediction using different techniques: model evaluation and comparison. Renewable and Sustainable Energy Reviews 61, 384–397. https://doi.org/10.1016/j.rser.2016.04.024

Wu, H., Levinson, D., 2021. The ensemble approach to forecasting: A review and synthesis. Transp Res Part C Emerg Technol 132. https://doi.org/10.1016/j.trc.2021.103357

Wu, Y., 1999. Statistical Learning Theory. Technometrics 41, 377–378. https://doi.org/10.1080/00401706.1999.10485951

Yu, X., 2023. Evaluating parallelized support vector regression and nearest neighbor regression with different input variations for estimating daily global solar radiation of the humid subtropical region in China. International Journal of Low-Carbon Technologies 18, 95–110. https://doi.org/10.1093/ijlct/ctad005

Finito di stampare da
Logo s.r.l. – Borgoricco (PD) – Italia

**RIGOROUS PEER REVIEW**
Each submission to IJAm is subject to a rigorous quality control and peer-review evaluation process before receiving a decision. The initial in-house quality control check deals with issues such as competing interests; ethical requirements for studies involving human participants or animals; financial disclosures; full compliance with IJAm's data availability policy, etc.
Submissions may be returned to authors for queries, and will not be seen by our Editorial Board or peer reviewers until they pass this quality control check.
Each paper is subjected to critical evaluation and review by Field Editors with specific expertise in the different areas of interest and by the members of the international Editorial Board.

**OPEN ACCESS POLICY**
The Italian Journal of Agrometeorology provides immediate open access to its content. Our publisher, Firenze University Press at the University of Florence, complies with the Budapest Open Access Initiative definition of Open Access: By "open access", we mean the free availability on the public internet, the permission for all users to read, download, copy, distribute, print, search, or link to the full text of the articles, crawl them for indexing, pass them as data to software, or use them for any other lawful purpose, without financial, legal, or technical barriers other than those inseparable from gaining access to the internet itself. The only constraint on reproduction and distribution, and the only role for copyright in this domain is to guarantee the original authors with control over the integrity of their work and the right to be properly acknowledged and cited. We support a greater global exchange of knowledge by making the research published in our journal open to the public and reusable under the terms of a Creative Commons Attribution 4.0 International Public License (CC-BY-4.0). Furthermore, we encourage authors to post their pre-publication manuscript in institutional repositories or on their websites prior to and during the submission process and to post the Publisher's final formatted PDF version after publication without embargo. These practices benefit authors with productive exchanges as well as earlier and greater citation of published work.

**COPYRIGHT NOTICE**
Authors who publish with IJAm agree to the following terms:
Authors retain the copyright and grant the journal right of first publication with the work simultaneously licensed under a Creative Commons Attribution 4.0 International Public License (CC-BY-4.0) that allows others to share the work with an acknowledgment of the work's authorship and initial publication in IJAm.
Authors are able to enter into separate, additional contractual arrangements for the non-exclusive distribution of the journal's published version of the work (e.g., post it to an institutional repository or publish it in a book), with an acknowledgment of its initial publication in this journal.
Authors are allowed and encouraged to post their work online (e.g., in institutional repositories or on their website) prior to and during the submission process, as it can lead to productive exchanges, as well as earlier and greater citation of published work (See The Effect of Open Access).

**PUBLICATION FEES**
Unlike many open-access journals, the Italian Journal of Agrometeorology does not charge any publication fee.

**WAIVER INFORMATION**
Fee waivers do not apply at Firenze University Press because our funding does not rely on author charges.

**PUBLICATION ETHICS**
Responsibilities of IJAm's editors, reviewers, and authors concerning publication ethics and publication malpractice are described in IJAm's Guidelines on Publication Ethics.

**CORRECTIONS AND RETRACTIONS**
In accordance with the generally accepted standards of scholarly publishing, IJAm does not alter articles after publication: "Articles that have been published should remain extant, exact and unaltered to the maximum extent possible". In cases of serious errors or (suspected) misconduct IJAm publishes corrections and retractions (expressions of concern).

Corrections
In cases of serious errors that affect or significantly impair the reader's understanding or evaluation of the article, IJAm publishes a correction note that is linked to the published article. The published article will be left unchanged.

Retractions
In accordance with the "Retraction Guidelines" by the Committee on Publication Ethics (COPE) IJAm will retract a published article if:
- there is clear evidence that the findings are unreliable, either as a result of misconduct (e.g. data fabrication) or honest error (e.g. miscalculation)
- the findings have previously been published elsewhere without proper crossreferencing, permission or justification (i.e. cases of redundant publication)
- it turns out to be an act of plagiarism
- it reports unethical research.
- An article is retracted by publishing a retraction notice that is linked to or replaces the retracted article. IJAm will make any effort to clearly identify a retracted article as such.

If an investigation is underway that might result in the retraction of an article IJAm may choose to alert readers by publishing an expression of concern.

**ARCHIVING**
IJAm and Firenze University Press are experimenting a National legal deposition and long-term digital preservation service.

**SUBMITTING TO IJAm**
Submissions to IJAm are made using FUP website. Registration and access are available at: https://riviste.fupress.net/index.php/IJAm/submission
For more information about the journal and guidance on how to submit, please see https://riviste.fupress.net/index.php/IJAm/index

Principal Contact
Simone Orlandini, University of Florence
simone.orlandini@unifi.it

Support Contact
Alessandro Pierno, Firenze University Press
alessandro.pierno@unifi.it

**GUIDE FOR AUTHORS**
1. Manuscript should refer to original researches, not yet published except in strictly preliminary form.
2. Articles of original researches findings are published in Italian Journal of Agrometeorology (IJAm), subsequent to critical review and approval by the Editorial Board. External referees could be engaged for particular topics.
3. Three types of paper can be submitted: original paper, review, technical note. Manuscript must be written in English. All pages and lines of the manuscript should be numbered.
4. First Name, Last Name, position, affiliation, mail address, telephone and fax number of all the Co-Authors are required. Corresponding Authors should be clearly identified.
5. The abstract should be no longer than 12 typed lines.
6. Full stop, not comma, must be used as decimal mark (e.g. 4.33 and not 4,33).
7. Figures, tables, graphs, photos and relative captions should be attached in separate files. All images must be vector or at least 300 effective ppi/dpi to ensure quality reproduction.
8. Captions should be written as: Fig. x – Caption title, Tab. x – Caption title. Images should be referred to in the text as (Fig. x), (Tab. x).
9. Proof of the paper (formatted according to the Journal style) will be sent to the Corresponding Author for proof reading just one time. Corrections can be made only to typographical errors.
10. All the references in the text must be reported in the "References" section and vice-versa. In the text, only the Author(s) last name must be present, without the name or the first letter of the name (e.g. "Rossi, 2003" and not "Federico Rossi, 2003" or "F. Rossi, 2003"). If two authors are present, refer to them as: "Bianchi and Rossi, 2003" in the text (do not use "&" between the surnames). If more than two Authors are present, refer to them as: "Bianchi et al., 2003" in the text.
For journals, references must be in the following form:
Bianchi R., Colombo B., Ferretti N., 2003. Title. Journal name, number: pages.
For books:
Bianchi R., Colombo B., Ferretti N., 2003. Book title. Publisher, publishing location, total number of pages pp.
Manuscripts "in press" can be cited.

**BECOME A REVIEWER**
Peer review is an integral part of the scholarly publishing process. By registering as a reviewer, you are supporting the academic community by providing constructive feedback on new research, helping to ensure both the quality and integrity of published work in your field. Once registered, you may be asked to undertake reviews of scholarly articles that match your research interests. Reviewers always have the option to decline an invitation to review and we take care not to overburden our reviewers with excessive requests.
You must login before you can become a reviewer.
If you don't want to be a reviewer anymore, you can change your roles by editing your profile.

**COMPETING INTERESTS**
You should not accept a review assignment if you have a potential competing interest, including the following:
- Prior or current collaborations with the author(s)
- You are a direct competitor
- You may have a known history of antipathy with the author(s)
- You might profit financially from the work

Please inform the editors or journal staff and recuse yourself if you feel that you are unable to offer an impartial review.
When submitting your review, you must indicate whether or not you have any competing interests.

# Italian Journal of Agrometeorology

Rivista Italiana di Agrometeorologia

**n. 1 – 2025**


## Table of contents